The Effect of a Missense Mutation at the *KCNQ1* Locus in Functional β-Cell Development

A Dissertation
Submitted in Partial Fulfilment of the
Requirements for the Degree of Doctor rerum naturalium (Dr. rer. nat.)

to the Department of Biology, Chemistry, Pharmacy
of Freie Universität Berlin

by
Zhimin Zhou

Berlin, 2020

Supervisor: Dr. Zsuzsanna Izsvák

Second examiner: Prof. Dr. Oliver Daumke

Date of defense: 31st. March 2021

Acknowledgment

Thanks to my supervisor Dr. Zsuzsanna Izsvák, she gives me this chance to study this exciting project in the Mobile DNA group. I appreciate Zsuzsa's patience with me on the development of my English. I very much appreciate Zsuzsa's guidance on the training of independent thinking ability. I appreciate a lot her support and advice on how to write the allowance for my project.

Many thanks to Prof. Dr. Maike Sander for allowing me to systematically learn the 3D differentiation of pancreatic β cells in her lab. Maike shares with me lots of the newest techniques and results when I am in San Diego and Berlin. Thanks to her guidance, I can follow the latest research. Thanks to superior membranes in Maike's lab, Dr. Chun Zeng, Dr. Han Zhu, Jinzhao Wang, Nichole Wetton, and other people. I appreciated their patience with me, showing me the details of the related experiments, and making it possible to do the β cell differentiation in Berlin.

Thanks to Prof. Dr. Kelmens Raile for sharing the patient's clinical information, which helps us to create a hypothesis of my project. Thanks to Dr. Maolian Gong for sharing the results of preliminary experiments.

Many thanks to all of my colleagues. Thanks to Prof. Dr. Jichang Wang and Dr. Huiqiang Cai for training me on hPSCs culturing. Thanks to Prof. Dr. Jichang Wang, teaching me how to use CRISPR-Cas9 in gene editing. Thanks to Yuliang Qu and Dr. Chuanbo Sun, guiding me to use the machines for Western Blot experiment. Thanks to Dr. Rabia Anwar show me how to use a kit for methylation analysis. Thanks to Dr. Amit Pande, Haiyue Liu (N. Rajewsky lab), and Himanshu Bhusan Samal, teaching me the process of gene expression analysis. Thanks to Dr. Christine Römer and Sandra Neuendorf for reviewing my thesis.

Thanks to Dr. Bettina Prufürst, generating the β-cell figures in the facility of the electron microscope. Thanks to Dr. Anca Margineanu, together with me, to create images for the analysis of Ca^{2+} influx. Thanks to Dr. Sebastian Diecke for generating hiPSCs.

Thanks to Prof. Dr. Oliver Daumke teaching me how to write thesis. Many thanks to Chinese Scholarship Council for supporting four-year scholarship.

Directory

1. Introduction

The pancreas contains exocrine glands and endocrine glands. The exocrine gland secretes digestive enzymes and bicarbonate, which drains into the intestine for absorption[1,2]. The pancreatic islet is an endocrine gland that is surrounded by exocrine gland[3]. The pancreatic islets comprise five distinct cell types synthesizing and secreting specific hormones: α-cells (glucagon), β-cells (insulin), δ-cells (somatostatin), PP cells (pancreatic polypeptide), and ε-cells (ghrelin) (Figure 1)[1,2,4,5]. The human pancreas contains nearly 1,000,000 islets that scatter throughout the pancreas[3]. Pancreatic islets contribute to blood glucose homeostasis by harmoniously secreting two antagonistic hormones, insulin and glucagon. Islet β cells secrete insulin to promote glucose uptake and liver glycogen production during food intake[6]. Additionally, islet α-cells secrete glucagon to promote glycogenolysis and glucose production from liver[6].

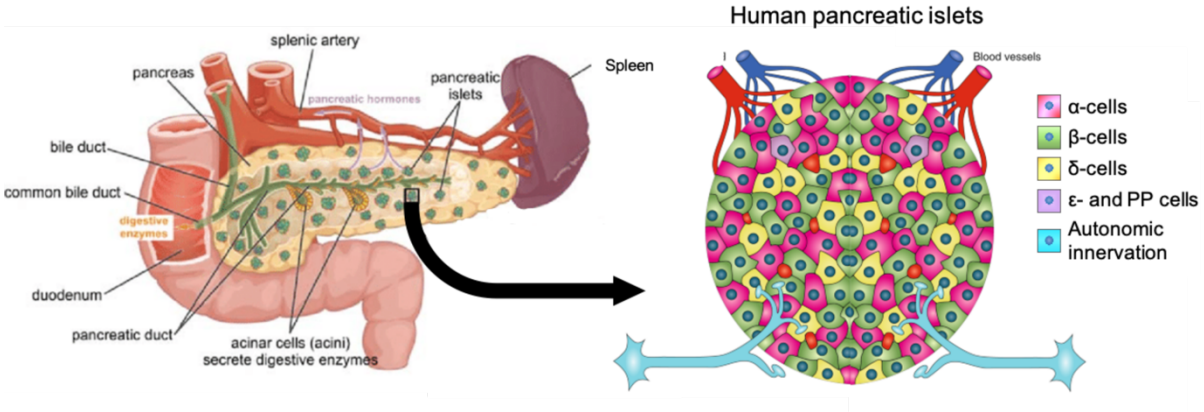

Figure 1. Overview of human pancreatic islets localization and composition. Figures were taken from chapter 17.9 figure1[4] and published figure 1[5].

Diabetes afflicts the endocrine pancreas[2]. Diabetes is a chronic metabolic and heterogeneous disease characterized by hyperglycemia due to inadequate production or utilization of insulin[7]. Over the last two decades, diabetes has become a significant health concern. Diabetes affects approximately 425 million people worldwide as one of the speedily growing diseases and triggers at least 727 billion dollars in health costs in 2017, according to the International Diabetes Federation[8]. In diabetes research and therapy, it has been the overarching goal to restore insulin production and maintain normoglycemia independently[9].

1.1 Diabetes and monogenic diabetes

The widely accepted classification of diabetes distinguishes between type 1 diabetes (T1D), type 2 diabetes (T2D), gestational diabetes mellitus (GDM), and other specific types of diabetes[7]. T1D attributes to a T-cell mediated autoimmune destruction of insulin-producing β cells[10]. Autoreactive T-cells and macrophages infiltrate into the islets, subsequently destroying β cells[10,11]. Previous studies have shown that T1D is characterized by the elevation of proinflammatory cytokine release, such as interleukin-1β (IL-1β), tumor necrosis factor-alpha (TNF-α) and interferon-alpha (IFN-α)[10,12]. However, an explanation for the diversity of phenotypic differentiation is the differential proinflammatory cytokine receptor density, signal transduction pathways, and gene expression profile[13]. The prevalence rate for T1D is increasing across the globe due to the interaction between considerable variation and natural selection[14].

Nevertheless, the majority of diabetic patients suffer predominantly from T2D, resulting from insulin resistance and relative insulin deficiency[7]. T2D is a consequence of a complicated interaction between genetic mutations and environment[15]. T2D most commonly occurs in older adults, but the occurrence nowadays become younger due to obesity and physical inactivity[8]. The prediabetic patients have insulin resistance developing from ectopic fat deposition. Therefore, β cells of prediabetes are forced to increase insulin production[8,16]. T2D consequently develops when β cells fail to produce inadequate insulin to keep up with demand due to endoplasmic reticulum (ER) stress[16,17]. Fat accumulation in the pancreas stimulates β-cell inflammation and dysfunction, which is recognized as a contributing factor for T2D[18,19]. The basis of T2D treatment is the maintenance of healthy body weight. Previous research finds that weight loss improves glucose homeostasis and insulin sensitivity of short-standing diabetes[20]. However, diabetes remission becomes difficult for long-standing diabetes[21], which suggests that timely T2D determination and treatment may globally decrease the prevalence of T2D. Unfortunately, the onset of T2D is usually slow with subtle metabolic disturbance, which is difficult to determine[8].

GDM is a development of glucose intolerance in the second or third trimester of pregnancy[7]. GDM should eliminate from preexisting diabetes, such as T2D, T1D, and monogenic diabetes, before diagnosis[22]. Patients with GDM have a high risk for the development of T2D after delivery; therefore, patients should receive lifelong prevention interventions[23,24].

Apoptosis acts as the central convergence between T1D and T2D with progressive β-cell failure[25]. The ER is a membranous tubule organelle for synthesis, folding, and transporting proteins in eukaryotic cells[26]. Redox homeostasis can maintain ER folding capacity through remitting reactive oxygen species (ROS)[27]. The impairment of ER redox status leads to the accumulation of unfolded or misfolded protein in the ER lumen[26]. If the ER cannot reestablish normal function via the unfolded protein response, the cell starts a death program, such as apoptosis[27].

Unlike T1D and T2D contributed from multiple genes and environmental factors, monogenic diabetes results from a single genetic mutation[8]. Monogenic diabetes is a rare type of diabetes and accounts for approximately 2% of diabetes patients[28]. Monogenic diabetes is caused by rare mutations in one single gene, and includes neonatal diabetes, mitochondrial diabetes, maturity-onset diabetes of the young (MODY), and so forth[29]. MODY is an autosomal dominant inheritable disease and is diagnosed before the age of 25[30]. Previous research has found 13 genes related to MODY through β-cell dysfunction, eventually causing hyperglycemia[31]. Patients with MODY present non-ketotic hyperglycemia without the requirement of insulin[30].

Neonatal diabetes mellitus is a monogenic diabetes that occurs in the first 180 days of life. Patients with neonatal diabetes are characterized with acute metabolic disorder and failure to thrive[32,33]. Neonatal diabetes patients usually lack islets, or their β-cell mass is decreased, presumably due to apoptosis, resulting in β-cell dysfunction[34]. Neonatal diabetes might be either transient or permanent, differing in the duration of insulin dependence[32]. Genetic analysis can predict whether neonatal diabetes mellitus is permanent or a transient disease[35]. Deciphering the underlying mechanisms of neonatal diabetes mellitus development might help identify individual genes that play a role in the polygenic forms of diabetes, such as T1D and T2D[34].

Diabetes complications include microvascular disease (nephropathy, neuropathy, and retinopathy) and macrovascular disease (acute coronary syndrome, chronic peripheral arterial syndrome, and stroke)[15,36]. These chronic complications of diabetes are a cause for an additional public health burden[15].

1.2 Human pluripotent stem cell therapy

As a potential treatment, cadaveric islet cell transplantation can maintain the recipient's glucose homeostasis without additional insulin administration for years[37,38]. However,

this approach is limited by the shortage of suitable organ donors and long-term immune suppression[2]. Due to ethical and practical issues, access to suitable cadaveric islet donations is currently a bottleneck. Therefore, there is a high medical need for other solutions to treat diabetes.

In the last decades, to overcome the shortage of suitable organ donations and to meet the enormous unmet patients' need, intensive pancreatic regeneration studies have been conducted[39]. Research-based on human pluripotent stem cells (hPSCs) has opened a new possibility to study disease mechanisms and potentially generate pancreatic tissue to replace the diseased tissue. Human somatic cells, including fibroblasts, peripheral blood mononuclear cells (PBMCs) can be reprogrammed into human induced pluripotent stem cells (hiPSCs)[40-42]. hiPSCs have a high potential in human disease modeling and cell-based therapies. However, using hiPSC reprogramming also has its limitations. Previous work showed that differentiated hiPSC lines do not have uniform gene expression levels, which may lead to variable differentiation efficiencies[43]. Rezania and his associates have indicated that although insulin$^+$ cells could be generated from hiPSCs, the efficiency of this process is low[44]. Moreover, the reproducibility of the protocol is considerably lower compared with human stem-cells (hESCs)[44].

Enhancing β-cell function is the primary strategy of diabetes treatment to meet insulin acquirement[6]. hESCs-derived functional pancreatic β cells emerged as a potential strategy to treat the disease and also for drug screening[45]. Several *in vitro* protocols have been established to differentiate hESCs into functional β cells[44-46]. The autoimmune attack is the bottleneck of pancreatic transplantation. To overcome this, the replacement cells are encapsulated into immunoprotective devices and implanted into non-endogenous sites[47]. Arturo and his associates have shown that it is possible to encapsulate hESC-derived functional β cells and induce glycemic correction without immunosuppression after implanting them into chemically induced type 1 diabetic mice model[48]. Hence, its possibility could be expected to use hESCs-derived functional pancreatic β cells in diabetes treatment.

1.3 β cells insulin secretion

The threshold of insulin secretion is at 3-4 mM glucose in human islets[49]. Even normoglycemia are species-specific, in humans, normoglycemia is around 5 mM[50].

The half-maxima and maxima of insulin secretion are at 7-8 mM glucose and above 20 mM glucose in human islets[51,52]. The association between glucose metabolism and insulin secretion is well established (Figure 2)[53]. In mouse β cells, glucose uptake is mediated by Glucose transporter 2 (GLUT2)[54]. Even though the deficiency of GLUT2 has been linked to developing transient neonatal diabetes[55], glucose transporter 1 (GLUT1) constitutes the predominant glucose transporter in human β cells[56]. The canonical process of glucose metabolism begins with the conversion of glucose to glucose-6-phosphate by glucokinase (GCK) after glucose uptake by β cells[3,10]. The metabolic substrate after entering glycolysis is pyruvate[10]. Pyruvate is oxidized to acetyl-CoA and enters the citric acid cycle by mitochondria[57]. The process of pyruvate oxidation produces ATP and NADPH, malonyl-CoA, and glutamate, crucial for K_{ATP} channel-dependent insulin secretion[10].

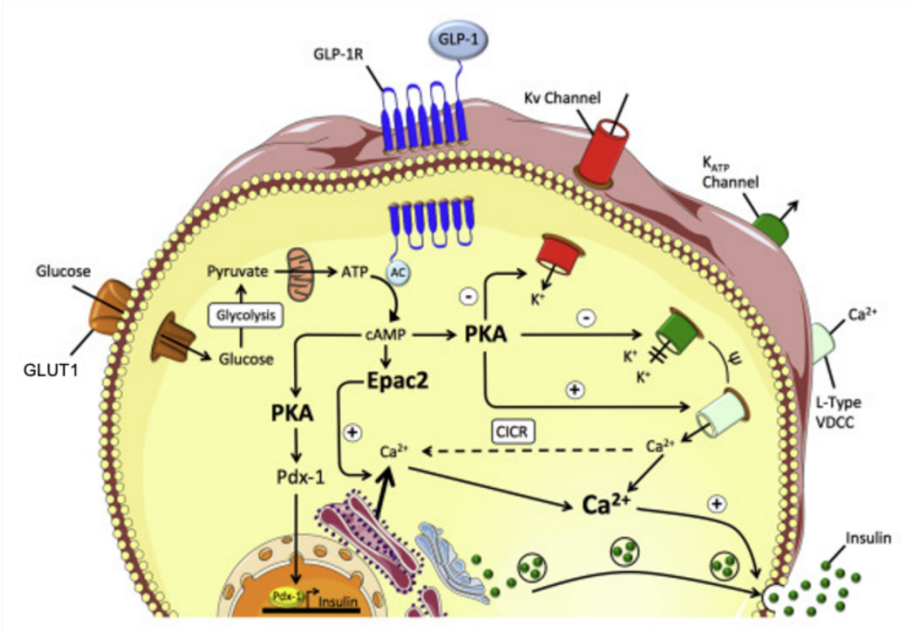

Figure 2. Schematic on glucose metabolism and insulin secretion. GLUT1 means glucose transporter 1, AC means adenylate cyclase, PKA means protein kinase A, Epac2 means exchange protein activated by cAMP, Pdx-1 means pancreatic and duodenal homeobox 1, CICR means calcium-induced calcium release. Figure was taken from published figure 5[53].

Insulin secretion is further regulated by 3',5'-cyclic adenosine monophosphate (cAMP), which is generated by glucagon-like peptide 1 (GLP-1) activated adenylate cyclase[58,59]. cAMP subsequently activate protein kinase A (PKA) and exchange protein directly activated by cAMP (Epac)[60,61]. The activation of PKA increases the expression of pancreatic duodenal homeobox-1 protein (PDX1), which binds to the promoter of insulin and initiates insulin expression in rat insulinoma cell line[62,63]. PKA increases

ATP binding to K_{ATP} channels by phosphorylation, and lead to the closure of K_{ATP} channels[53]. Closed K_{ATP} cause membrane depolarization, subsequently opens Ca_V channels, and causes Ca^{2+} influx[10,64]. β-cell ER is a main cytosolic Ca^{2+} store and regulates cytosolic Ca^{2+} level[65,66]. Epac2 increases cytosolic Ca^{2+} level via induced Ca^{2+} release from ER[67].

The rising of cytoplasmic Ca^{2+} triggers insulin secretion through granule exocytosis[64]. Insulin constitutes 5-10% of total protein in β cells, that is crystallized in secretory granules as a $(Zn^{2+})_2(Ca^{2+})Insulin_6$ hexamer[3,68]. Insulin granule is a large dense-core surrounded by a halo in a intracellular membrane[69]. The kinetics of insulin release is controlled by cytoplasmic free Ca^{2+} level in individual β cells. The cytoplasmic Ca^{2+} elevation activates Calmodulin (CaM) dependent kinase II[70,71]. CaM kinase II accelerates insulin granules transporting to plasma membrane by phosphorylated microtubule-associated proteins, especially Microtubule-associated protein 2 (MAP-2)[72,73]. In the next stage, cytosolic Ca^{2+} ions are required for the fusion between insulin granules and plasma membrane resulting in insulin secretion[74,75].

Interestingly, only 1% of insulin granules are immediately triggered to release by glucose in mice[76]. The insufficiency of insulin granules in the readily releasable pool is refilled from the reserve granules[10]. Both mouse and human islets have a first-phase and a second-phase of insulin release[3,77]. However, the glucose response of β cells within a rat islet is unsynchronized due to β-cell gap junction coupling[78,79].

1.4 β cells ion channels

Human β cells are equipped with various types of Ca_V channels, including T-type (CACNA1H), N-type (CACNA1B), P/Q-type (CACNA1A) and L-type (CACNA1C and CACNA1D)[3]. T-type Ca_V channels activate at -50 mV and contribute a particular role between -40 and -30 mV in human β cells[80]. Other Ca_V channels contribute to the regulation of whole human β-cell current between -20 and -10 mV[80]. Inhibition of L-type Ca_V channels reduces >90% of glucose-stimulated insulin secretion (GSIS) with isradipine treatment, while blockade all of other Ca_V channels only reduces 60-70% of GSIS[80]. β cells also express other types of Ca^{2+} channels in organelle membranes, especially the inositol trisphosphate receptor (InsP3R)[3]. InsP3R and sarcoplasmic reticulum Ca^{2+}-ATPase regulate cytosolic Ca^{2+} efflux and influx from ER affecting cytosolic Ca^{2+} homeostasis[81].

Besides, membrane depolarization activates Na_V channels together with Ca_V channels[3]. Blockade of Na_V channels by tetrodotoxin reduces insulin secretion with 5-6 mM glucose stimulation[82].

Recent studies in both human and mouse β cells have shown evidence for K_V channels stimulating GSIS[83,84]. K_V channels carry on a delayed outward K^+ current, which is referred to as the outward rectification[3]. The activation of K_V channels lasts only ~5 ms in human β cells[85]. The inhibition of K_V channels enhances GSIS via increasing action potential duration[86]. Human β cells are equipped with K_V1.6 (*KCNA6*), K_V2.2 (*KCNB2*), and three ether-a-go-go related genes (ERG) channels (*KCNH2*, *KCNH6*, and *KCNH7*)[3,87]. *KCNA5*, *KCNC3*, and *KCND3* have been discovered in human β cells[3].

KCNQ member 1 (*KCNQ1*) has an associated with T2D[88-90]. Previous research has shown that blockade of K_V7.1 channels increased glucose-stimulated insulin secretion by increasing action potentials firing and cytoplasmic Ca^{2+} concentration in rat islets[91]. However, it is controversial that K_V7.1 channels have an important role in modulating the action potential of β cells due to extremely low *KCNQ1* expression in human and mouse β cells[3].

1.5 Fibroblast growth factor signaling in β cells

Fibroblast growth factors (FGFs) are hormones and are known for their role in cell proliferation and differentiation by binding to fibroblast growth factor reporters (FGFRs)[92-95]. FGFs have been reported to regulate the metabolic of lipid and glucose[96,97]. Pharmacological administration or overexpression of FGFs increase metabolic rate and fatty acid oxidation in diabetic mice[97-99]. Over the past two decades, FGFs and FGFRs have been implicated as metabolic regulators in rats or mice β cells[100-102].

The mutation of FGFR1 impairs the expression of GLUT2 and prohormone convertases 1/3, which results in mouse β-cell dysfunction[102]. ChiPseq reveals that the nuclear isoform of FGFR1 targets PDX1 motifs and regulates PDX1 expression in neuron-committed cells[103]. However, in mouse PDX1 knock-out β-cells, the decreasing expression of FGFR1 implicates PDX1 is upstream of FGFR1[102]. Interestingly, the expression level of GLUT2 is determined by PDX1 in mouse β cells as well[104-106].

FGF21 treatment increases insulin content and secretion in islets isolated from diabetic rats, which is believed to protect the islets from glucolipotoxicity and apoptosis through

the activation of ERK1/2 and Akt-dependent signaling mechanisms[100]. However, FGF21 only increases insulin expression in healthy rats' islets[100].

FGFR-like 1 (FGFRL1) is a non-canonical FGFR, which lacks an intracellular kinase domain[107]. FGFRL1 binds and activates ERK1/2 based on the Src homology domain-2 binding motif[108]. FGFRL1 expresses at the cytoplasmic membrane and the insulin granules in β cells[108]. Overexpression of the fluorescent conjugated FGFRL1 increases insulin content and extracellular matrix adhesion in murine βTC3 cell[108]. In addition, FGFRL1 is co-expressed with FGFR1 formed heterocomplexes in response to FGF2 stimulation[109], suggesting that FGFRL1 is essential for FGFR1 activation.

1.6 Human β-like cells differentiation

Previous researches on pancreatic development have identified a multistage process of insulin$^+$-cell production derived from PSCs[44,45,110-112]. This includes definitive endoderm (DE, SOX17$^+$ / FOXA2$^+$), pancreatic endoderm (PE, PDX1$^+$ / NKX6.1$^+$), pancreatic endocrine precursors (EP, PDX1$^+$ / NKX6.1$^+$ / NEUROD1$^+$), immature β-cells (PDX1$^+$ / NKX6.1$^+$ / NEUROD1$^+$ / insulin$^+$ / glucagon$^+$) and maturing β-cells (PDX1$^+$ / NKX6.1$^+$ / NEUROD1$^+$ / insulin$^+$ / glucagon$^+$ / MAFA$^+$) (Figure 3)[44]. Obviously, understanding the signaling pathways related to organogenesis *in vivo* will help drive PSCs into insulin-producing cells with high percentages *in vitro*. Previous research have shown that TGFβ signals serve as vertebrate mesoderm and endoderm inducers[113,114]. Moreover, high grade of TGFβ signals member Nodal/Smad2 can promote endoderm differentiation in mouse[113]. Wnt/β-catenin pathway plays a role in foregut endoderm specification in an early stage, but in long term induces mesendoderm[115]. It has been shown that KGF promotes PDX1 expression by activation of PI3K/AKT signaling pathway[116]. These signaling pathways can enhance PDX1 expression and dedifferentiation of partial neonatal duct cells into insulin$^+$ cells[117].

To date, variety of growth factors and inhibitors, such as ACTIVIN A (AA, TGFβ family member), WNT3a (Wnt/β-catenin pathway member), KGF, SANT-1 (hedgehog pathway inhibitor), LDN193189 (BMP receptor inhibitor), TPB (PKC activator), retinoic acid, Alk5 inhibitor (Alk5i), and YAP inhibitor have been used to control the specific marker expression on the developmental process[44,45,118]. However, these stem cell-derived insulin-producing cells fail to perform GSIS[44,45].

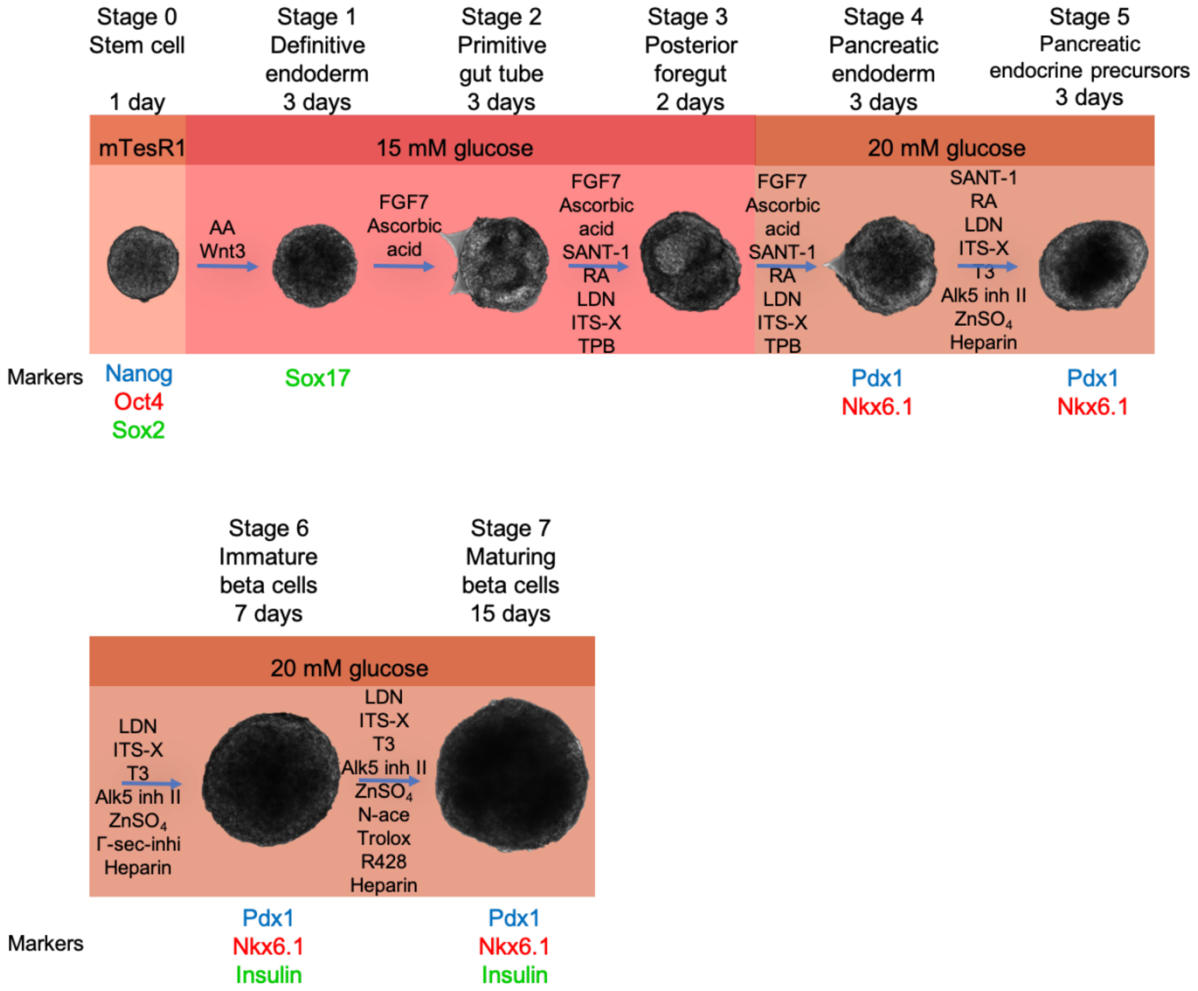

Figure 3. Overview of the seven-stage differentiation protocol and morphology of the individual aggregate. Growth factors and small molecules that are added at each stage of the differentiation protocol, as well as the key markers of differentiating pancreatic cells are illustrated.

Leonardo and his associates have reported that activating TGFβ signaling is necessary for the differentiation of mature β cell comparing with inhibitor of TGFβ signaling (Alk5i) treatment[46]. Their hESCs-derived insulin-producing cells are able to perform GSIS and KCl depolarization[46].

1.7 The KCNQ1/KCNQ1ot1 locus and pancreatic β cells mass

Long noncoding RNAs (lncRNAs) may act as powerful regulators of gene expression in higher organisms[119]. lncRNAs are larger than 200 nucleotides and have some similar features to mRNAs, while unable to translate into proteins[120]. lncRNAs can function as chromosomal scaffolds and recruit epigenetic regulators to specific chromatin loci[119,121]. Previous researches suggest that gene regulation by lncRNAs

and epigenetic modifications may represent a novel layer of modulation in pancreas development and β cell function[122].

From the 1980s, researchers have discovered that dozens of mammalian genes are regulated by imprinting, expressed from either the paternal or the maternal allele of the gene[123]. Imprinted genes play a pivotal regulatory role in mammalian development-disturbed regulation by imprinting results in several developmental disorders and contributes to various diseases[124]. Imprinted genes are rich in CpG islands, and are regulated via their differentially methylated regions (DMRs)[125,126]. One kind of DMRs is methylated in the parental germ cells and maintains its methylation mark forever. The other one is a tissue-specifically imprinted that can be changed or acquired during development[123].

KCNQ1 is regulated by imprinting. The KCNQ1 imprinted locus is controlled by the KCNQ1ot1 lncRNA that is generated as a 91.7 kb antisense transcript from the paternal chromosome[121,126]. The KCNQ1/KCNQ1ot1 imprinted locus contains 8-10 ubiquitously and/or tissue-specifically imprinted genes. This imprinted locus contains diabetes-related gene INS-IGF2, tumor suppressor genes TSPAN32, CDKN1C, and SLC22A18. Polycomb group proteins (PCG), comprising PRC1 and PRC2, are involved in defining cell fate trajectories[126,127]. It has been shown that the Kcnq1ot1 lncRNA directly regulates pancreatic β cell mass in mice by recruiting the Polycomb protein complex to its protein-coding neighbors[125]. Zhang and his associates have shown that KCNQ1ot1 recruits PRC2, and plays an important role in maintaining the monoallelic expression of KCNQ1 and its neighboring imprinted genes[121].

1.8 Permanent neonatal diabetes patient with a *KCNQ1* mutation

In our current project, I analyze a diabetes patient with the *KCNQ1* mutation (1189 C>T) from a consanguineous family (Figure 4A). The patient had intrauterine growth retardation with low birth weight and was diagnosed with a permanent neonatal diabetes (PND). The patient was hyperglycemic. No insulin was detectable in his blood after birth. Fortunately, his condition is stable under regular insulin treatment. My clinical collaborators, Prof. Dr. Klemens Raile and Dr. Maolian Gong found four candidate gene variants after whole-exome sequencing, including *MIA3*, *KCNQ1*, *CARKD*, and *MYO1F*. Even though both *MIA3* (80 RPKM) and CARKD (25 RPKM) are expressed in human islets (from Prof. Dr. Maike Sander's unpublished RNA-seq data),

neither of them has a strong association with diabetes, suggested by T1D/T2D GWAS data (*MIA3*, p value< 1e-4; *CARKD*, p value=2.4e-5)[128]. Notably, *KCNQ1* has been previously reported to be related to diabetes in the T2D portal (www.type2diabetesgenetics.org). Thus, I followed up *KCNQ1* as a candidate gene to explain his diabetic phenotype. Sanger sequencing was used to verify the *KCNQ1* mutation in the patient's family (Figure 4B). The point mutation was mapped to the exon 9 of KCNQ1. Other members of this consanguineous family are heterozygous mutation in the KCNQ1 gene and healthy.

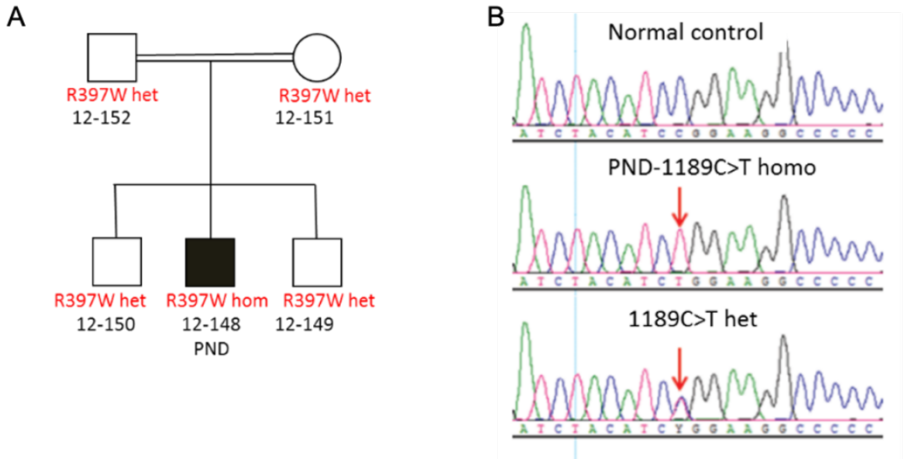

Figure 4. Permanent neonatal diabetes patient with the KCNQ1 mutation from a consanguineous family. (A) Pedigree of the patient's family. Squares and circles represent males and females, respectively. The patient (marked in black) has a homozygous mutation and permanent neonatal diabetes. Other members of his family are heterozygous and healthy. (B) Sander DNA sequences of the KCNQ1 from normal control, patient (homozygous mutation,1189 C>T), and patient's family (heterozygous mutation, 1189 C>T).

Previous research has reported that the mutation at the *KCNQ1* locus can regulate the expression of *KCNQ1ot1*, and *KCNQ1ot1* possesses a direct regulatory role in mice pancreatic β cell mass development by recruiting the Polycomb protein complex to its protein-coding neighbors, such as *CDKN1C* and *SLC22A18*[125]. Additionally, unbalanced expression of *CDKN1C* and *Phlda2* in the placenta could have contributed to intrauterine growth retardation[129], which observed in our patient. Because the proper level of CDKN1C is required for the maintenance of the non-proliferative state of β cell cells[130], I thought that the hyperexpression of *CDKN1C* might terminate β cell development. However, it is still unclear how the mutation at the *KCNQ1* locus can regulate the expression of *KCNQ1ot1*. Bryant and his colleagues have reported a variety of enhancers in intron 10 and 11 of *KCNQ1*[131]. Afterward, I have found that

intron 11 of *KCNQ1* has a dynamic enhancer signal in different stages of β-cells differentiation (Figure 5A)[132]. However, the mutation locus of our patient (1189 C>T) does not overlap with any enhancer signal (Figure 5A).

Notably, the 1189 C>T mutation affects a putative CTCF binding motif, occupied in GM12892 (human B-lymphocyte, lymphoblastoid) and K562 (human myelogenous leukemia) cells in the UCSC Genome Browser. I analyse Escalada and her colleagues' human islets Hi-C data and identify that the putative CTCF motif is not utilized in the human islets (Figure 5B)[133]. Therefore, the permanent neonatal diabetes phenotype, resulting from the 1189 C>T mutation is unlikely associated with regulatory genomics.

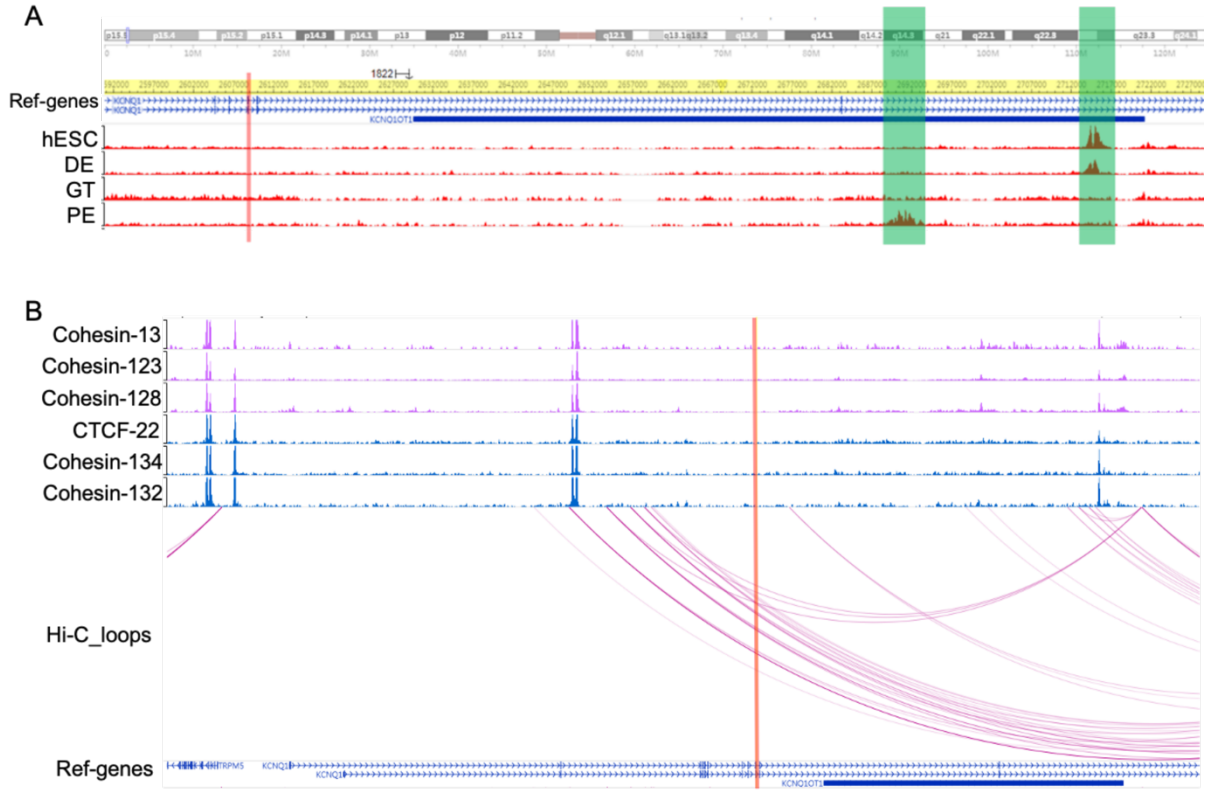

Figure 5. Epigenetic signals are neighboring patient's mutation locus. (A) The dynamic enhancer signal during β-cell differentiation is revealed by CHIP assay[132]. Tracks show signals of H3K27ac (potential enhancer, is highlighted with light green) in the stages of hESCs, definitive endoderm (DE), primitive gut tube (GT), and pancreatic endoderm (PE). (B) The CTCF binding signal and loops are neighboring KCNQ1 locus shown by Escalada's Hi-C data[133]. Tracks show signals of Cohesin and CTCF binding, and CTCF-loops in human islet samples. The exon9, including our patient's mutation locus, is highlighted with red.

1.9 Functional KCNQ1 in cardiomyocyte and other cells

The tetramer KCNQ1 (α subunit) co-assembles with KCNE accessory subunits (β subunit) to generate the $K_V7.1$ channel. Each KCNQ1 subunit consists of six

transmembrane segments, named S1 through S6 (Figure 6A)[134]. It is documented that the KCNQ1 subunit forms the voltage sensor and pore domain, whereas the KCNE subunit regulates the trafficking and functional attributes of K_V7.1 channel[135]. K_V7.1 channels play a crucial role as borders between the internal and external cell environment in epithelia[136].

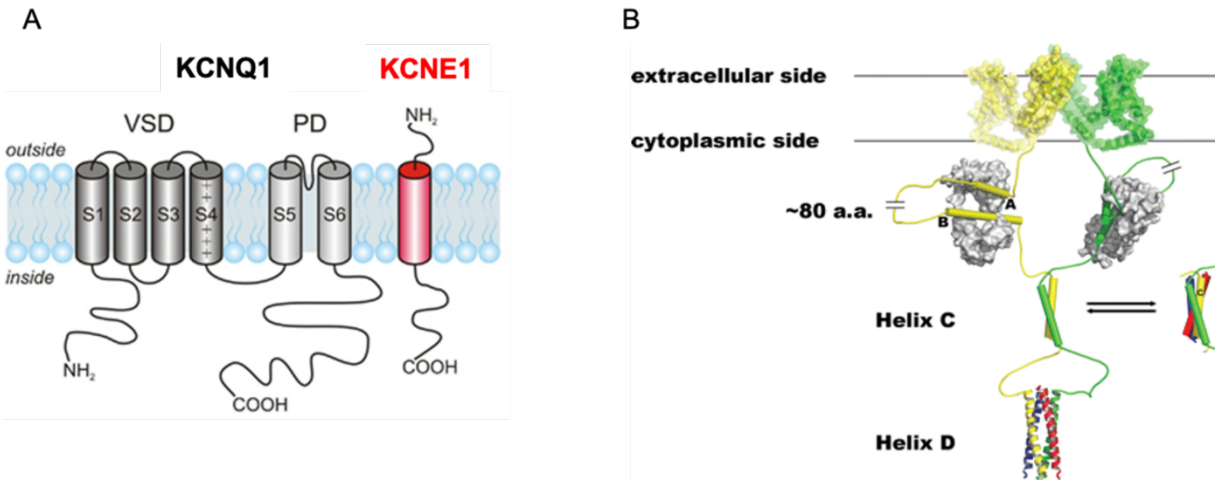

Figure 6. Topological model of Kv7.1 channel. (A) The structure of KCNQ1 and KCNE1. Figure was taken from published figure 3A[134]. The voltage sensor domain (VSD) of KCNQ1 is drawn as dark gray. The pore domain (PD) is drawn as light gray. KCNE1 is colored red. (B) Quaternary structure model of the KCNQ1-CaM complex. Figure was taken from published figure 6[137]. Two KCNQ1 subunits are drawn as yellow and green. CaM (drew as gray) binds to helices A and B of KCNQ1 C-terminus.

The C-terminus of KCNQ1 is suggested to be essential for channel gating, assembly, and trafficking. Secondary structure analysis of the C-terminus of KCNQ1 predicts four helical regions (helices A-D), conserved in all family members (Figure 6B)[137-145]. It has been documented that the extensive versatility of the KCNQ1 channel function depends on the ability of the C-terminus of KCNQ1 to interact with various auxiliary proteins and accessory factors[136]. It is documented that KCNQ1 subunit co-assembles with various KCNE subunits to generate an efficient channel complex in the cytosol of different epithelial tissue[146]. Co-expression of KCNE subunits with KCNQ1 shows that up to four KCNE subunits can associate with and modulate the channel kinetic properties[136,146,147]. In human cardiac cells, KCNQ1 is associated with KCNE subunits (KCNE1-5) except for KCNE2[148]. Inherited variants of KCNE4 or KCNE5 subunits affect KCNQ1-channel function resulting in cardiac arrhythmias in humans[149,150]. KCNE1 and KCNE3 have opposing effects of regulating K_V7.1 channel asserting from various cardiac arrhythmias reports[151]. Even though the association of KCNQ1 and KCNE2 has yet to be elucidated in human cardiomyocytes, it is shown that KCNE2 deletion can delay ventricular repolarization in KCNE2 null mice[152].

Specifically, helix A is vital for binding auxiliary proteins (e.g., KCNE subunits) and accessory factors (e.g., CaM and phosphatidylinositol 4,5-bisphosphate (PIP2))[153,154]. CaM is an obligate factor of KCNQ1 and contributes to functional channel forming and localization. The standard structure of helix A and helix B are necessary and sandwiched between the N- and C-lobes of CaM[154]. Significantly, the development and functionating of mature β cells also relate to the activation of CaM kinase II and calcineurin[155,156]. Previous research has shown that CaM kinase II localizes to the insulin secretory granules and processes granules to the plasma membrane by phosphorylation of transporting, docking, and priming related proteins[155]. Zhao and his associates have found that inhibition of calcineurin significantly reduced the function of β cells. Additionally, activation of calcineurin could rescue the malfunction of β cells[156].

The KCNQ1 channel activity is also modulated by PIP2, which couples with the voltage sensor and pore[157]. The KCNQ1 channels fail to open the pore after PIP2 depletion[157]. PIP2 binding seems to strengthen the coupling between VSD and PD of KCNQ1, enabling VSD to control PD[154]. PIP2 hydrolysis forms second messengers InsP3 and diacylglycerol by phospholipase (PLC)[158]. InsP3 binds and activates InsP3R allowing cytosolic Ca^{2+} mobilization[159].

1.10 *KCNQ1* and diabetes

K_V channel has been reported to work as a link between depolarization and polarization[87,160]. K_V channels and K_{ATP} channels interact with voltage-dependent Ca^{2+} channels to trigger and maintain glucose-stimulated insulin secretion in pancreatic β cells[88]. Several single nucleotide polymorphisms (SNPs) of KCNQ1 are associated with T2D via reduced insulin secretion in pancreatic β cells[161,162]. However, little is known about the molecular mechanisms responsible for this association[161,162].

Our patient's homozygous point mutation has been mapped to the exon 9 of *KCNQ1*, resulting in an amino acid change in the helix A of *KCNQ1*-encoded protein (R 397 W). Notably, the amino acid sequence around the mutation is highly conserved in the KCNQ1 gene across species (Figure 7A), suggesting that the mutated amino acid might be functionally essential. Indeed, the PolyPhen2 algorithm predicts that the mutation might damage the function of K_V channels (Figure 7B), The amino acid mutation of KCNQ1 is expected to change the structure of the helix A (Figure 7C),

which may affect the binding between KCNQ1 to its interacting protein partners. Helix A and helix B form a clamshell-like structure together with the N- and C-lobes of CaM[154]. Thus, the amino acid change in the of KCNQ1 is expected to affect CaM binding. The fact that CaM interacts with other binding partners, also associated with insulin secretion, such as CaM kinase II and calcineurin[155,156]. I speculate that our patient's mutation might influence the function of K_V channels.

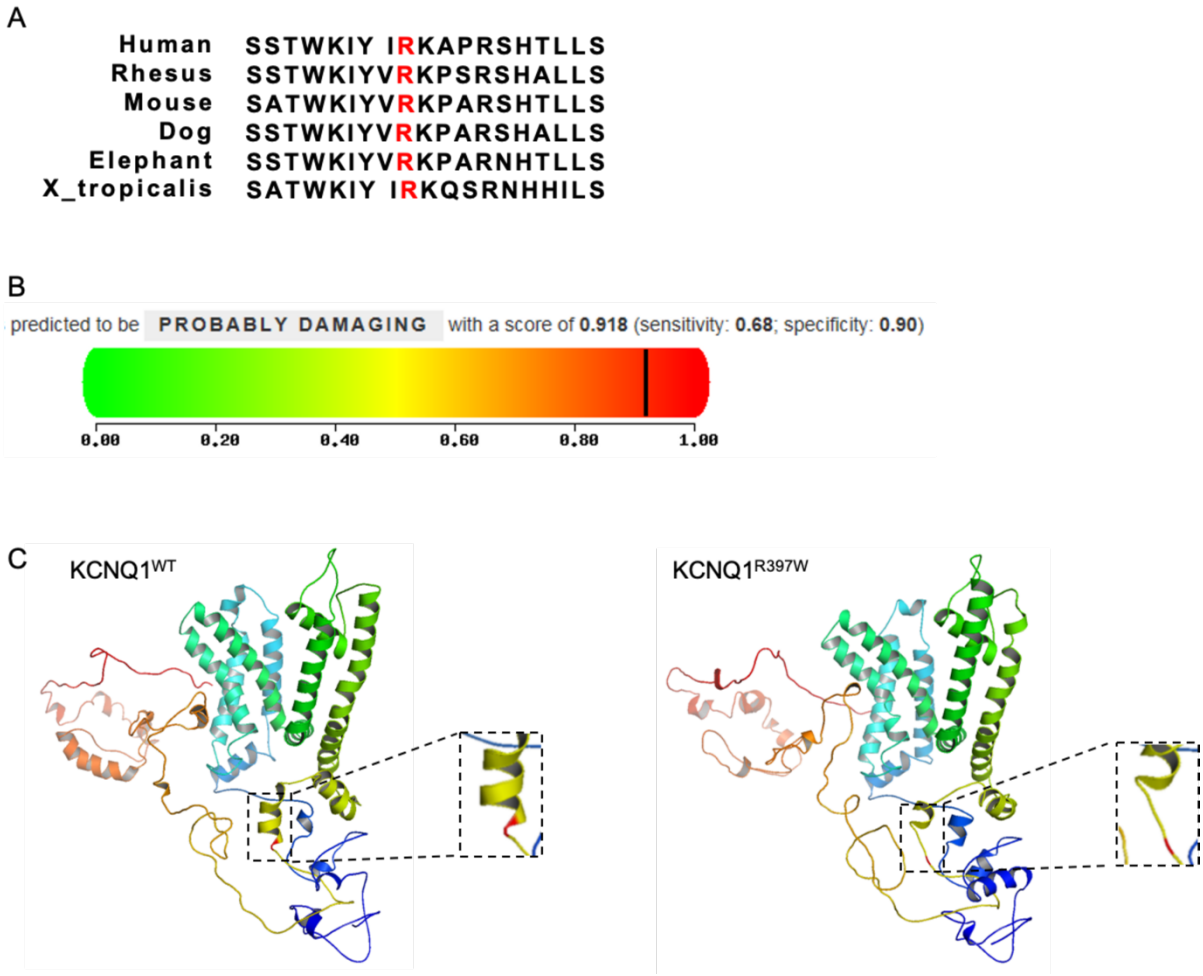

Figure 7. The association between the mutated amino acid and function of KCNQ1. (A) Amino acid sequence around the mutation (red) is conserved in KCNQ1. (B) Polyphen2 prediction for the destructive potential of the mutation in KCNQ1. (C) 3D structure prediction of wild type ($KCNQ1^{WT}$) and mutation ($KCNQ1^{R397W}$). The figures are generated with PyMOL viewer. Left panel, $KCNQ1^{WT}$ with the mutation locus (highlighted in red) locates in helix A, an α helix. Right panel, $KCNQ1^{R397W}$, the mutation locus becomes a random coil (The mutation locus is highlighted in red).

First, to confirm our hypothesis, our collaborators (Prof. Dr. K. Raile and Dr. M Gong) have performed patch-clamp studies in Chinese hamster ovary (CHO) cells. Prof. Dr. Raile's lab has constructed plasmids encoding $KCNQ1^{WT}$ (*KCNQ1*), $KCNQ1^{R397W}$ (*KCNQ1-R397W*), and a mutation from another hyperinsulinemic patient *(KCNQ1-*

G292D). These constructs are transfected into KCNQ1-null CHO cells. KCNQ1 current traces for KCNQ1^{WT}, KCNQ1^{R397W}, and KCNQ1^{G292W} are recorded by patch-clamp in the transfected cells (Figure 8A). The KCNQ1^{WT}, KCNQ1^{R397W} proteins are readily detectable in the plasma membrane of the transfected CHO cells, suggesting that the mutation does not affect membrane targeting of the mutated proteins (Figure 8B). Notably, compared to WT cells, both KCNQ1^{R397W}, and KCNQ1^{G292W} cells have lower current densities. The current density of KCNQ1^{R397W} is especially affected, which suggests that the mutation has a significantly reduced outward current and voltage-gated activation. Nevertheless, as the K_V channels limit Ca^{2+} influx and subsequently regulate insulin secretion in β cells[88,163], the patch-clamp results can not directly explain the opposite phenotypes of the hypo- and the hyperinsulinemic patients harboring the *KCNQ1-R397W* and *KCNQ1-G292D* mutations, respectively.

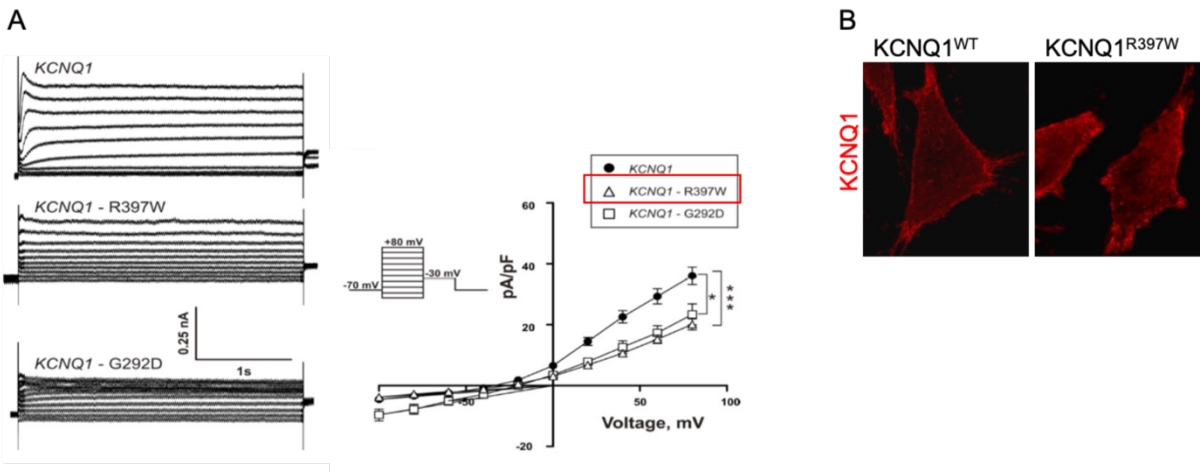

Figure 8. KCNQ1-null CHO cells are transfected with expression constructs of *KCNQ1^{wt}* (*KCNQ1*), *KCNQ1^{R397W}* (*KCNQ1-R397W*), and *KCNQ1^{G292D}* (*KCNQ1-G292D)* respectively. (A) Current traces for KCNQ1^{WT}, KCNQ1^{R397W}, and KCNQ1^{G292W} in transfected KCNQ1-null CHO cells (patch clamp). (B) Immunostaining for KCNQ1^{WT} and KCNQ1^{R397W} expressed in KCNQ1-null CHO cells. KCNQ1 expression is shown in red. The figures are generated by Prof. Dr. K. Raile's lab.

To uncover the association between the mutation (1189 C>T) with insulin secretion, our collaborators have performed overexpression studies in mouse β cells. The above constructs are transfected into mouse β cells. qRT-PCR and Western blot are shown that KCNQ1^{R397W} transfection increases the expression of mMafB, which is a marker of mouse β cells (Figures 9A and 9B). Seventy-two hours post-transfection, ELISA is used to measure the insulin secretion of KCNQ1^{R397W} and KCNQ1^{G292W}-transfected β cells. β cells have shown the same phenotype of two patients: hypo- (KCNQ1^{R397W}) and the hyperinsulinemic (KCNQ1^{G292W}) (Figure 9C). However, the total insulin level

of both KCNQ1^{R397W} and KCNQ1^{G292W} mouse β cells was significantly less than the KNCQ1^{WT} transfected and non-transfected mouse β cells (Figure 9D).

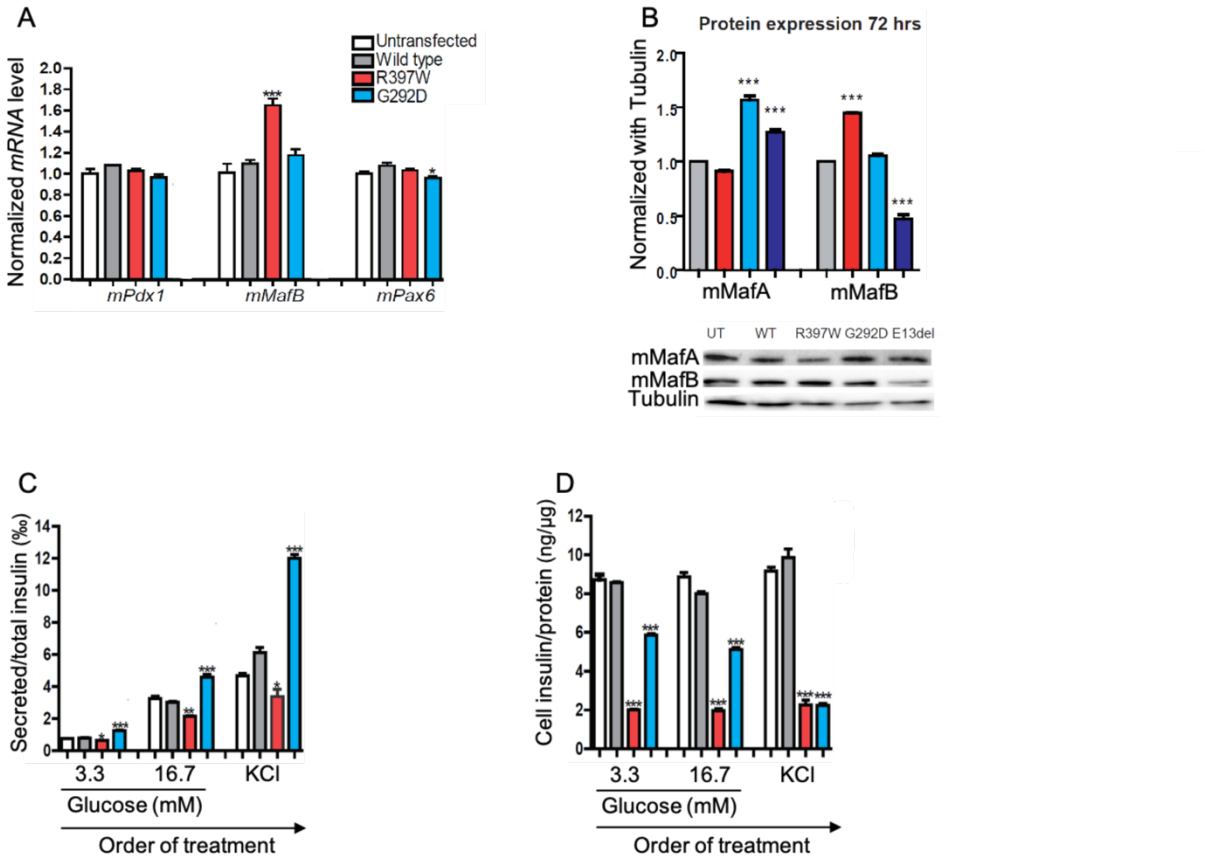

Figure 9. Insulin secretion in mouse β cells untransfected or transfected with expression constructs of KCNQ1^{WT} (Wild type), KCNQ1^{R397W} (R397W), and KCNQ1^{G292D} (G292D). (A) Real-time PCR analyzes the transcripts of mouse β cells marker: *mPDX1*, *mMafB*, and *mPax6*. (B) Western blot analyzes of the expression of mouse β cells marker: mMafA and mMafB. Insulin secretion assay (C), and total insulin assay (D) using ELISA. Western blot data are normalized to tubulin; insulin secretion is normalized to total insulin; insulin content is normalized to total protein in β cells. The figures are generated by Prof. Dr. K. Raile's lab.

To understand more about the pathogenesis of neonatal diabetes, our collaborators measure the pancreatic β cell mass of *KCNQ1* knock out (KCNQ1$^{-/-}$) and WT mice, donated by Prof. Völkl[164]. They determine the numbers of both α and β cells, identified by immunostaining using insulin and glucagon antibodies. KCNQ1$^{-/-}$ mice have a 4.1% reduction of β cells (insulin^{+} cells) compared to WT (Figure 10). Similar, Krishna *et al.* have reported that knocking out KCNQ1 resulted in significantly lower fasted and nonfasted plasma insulin levels[165]. In contrast, Zeng *et al.* report that knocking out of KCNQ1 had no effect on mature β-cell generation in humans[166]. This suggests that that the conflicting observations might be explained by the complexity of the phenomenon and the differences between mouse models and human generated cells *in vitro*.

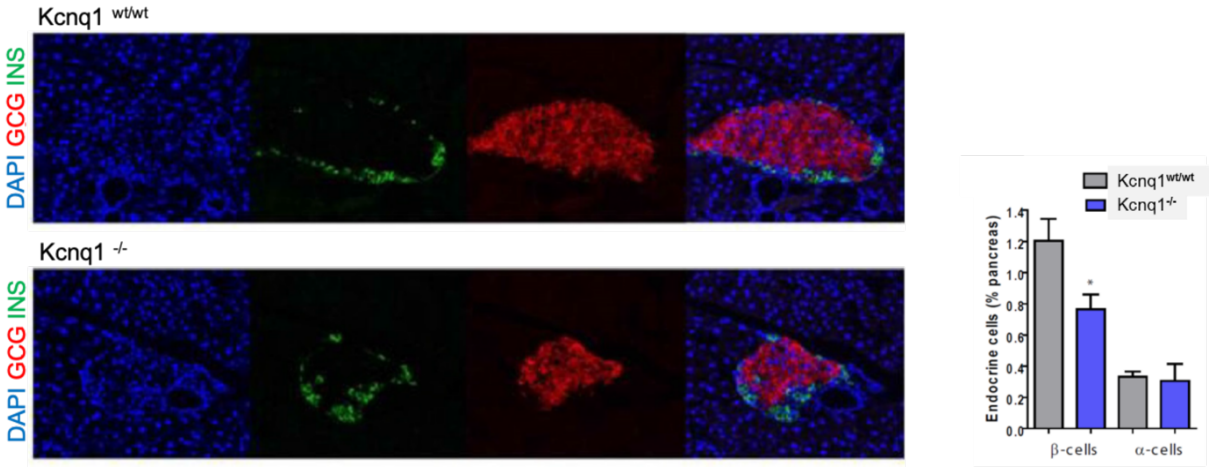

Figure 10. Analysis of pancreatic islets of KCNQ1$^{wt/wt}$ and KCNQ1$^{-/-}$ mice. (A) Immunostaining of pancreatic islets of KCNQ1$^{wt/wt}$ and KCNQ1$^{-/-}$ mice. (insulin^{+}, green; glucagon^{+}, red; DAPI, blue). (B) Quantification of β cells and α cells in KCNQ1$^{wt/wt}$ and KCNQ1$^{-/-}$ pancreas. Normalized to total number of pancreatic cells. The figures are generated by Prof. Dr. K. Raile's lab.

1.11 Genome editing with CRISPR

Gene engineering for mimicking disease-causing mutations represents an excellent strategy to increase our understanding of disease-causing and eventually eradicate related diseases[167]. CRISPR (clustered regularly interspaced short palindromic repeats)-Cas (CRISPR-associated) proteins is an adaptive immune system against invading genetic elements in prokaryotes[168]. CRISPR-Cas9 offers a useful technology for genome engineering by forming a Cas9 and guide RNA entity capable of binding and cutting double-stranded DNA[169]. Cas9 has an HNH and RuvC nuclease domains, which respectively cut the target and non-target DNA strands after binding the DNA duplex[170]. Guide RNA entity contains a 20 nt single-guide RNA (sgRNA), that directs Cas9 to target DNA through Watson-Crick base pairing[171]. Notably, the upstream of the recognition site must have a requisite adjacent motif (5'-NGG PAM), for Cas9 to recognize the DNA locus and make a double-stranded DNA break around 3 bp upstream of the PAM[169,171]. Previous research on CRISPR-Cas9 and other related enzymes have engineered the genomes of cultured cells, plants, and animals in a site-specific manner via error-prone non-homologous end joining (NHEJ) or homology-directed repair (HDR)[171-173]. To increase the efficiency of precise editing by HDR, Christopher *et al.* have found that sgRNA non-target strand released from Cas9-DNA complex firstly, and investigated a 128bp single-stranded DNA (ssDNA) donor complementary to the non-target strand could increase the rate of HDR to 50-60% in human cells[170].

Interestingly, previous researchers have presented that the presence of Cas9 activates or exacerbates p53 pathway[174,175]. The double-strand breaks (DSBs) induced by Cas9 are toxic and can be defeated by transient p53 inhibition and p53-inactivating mutations[174,175]. Although Cas9-mediated genome editing is possible in almost all cell types, the accuracy, precision, and safety of genome editing remain an active topic of investigation in the field[176].

1.12 Objectives of this work

Yang and his associates have recently reported that the dysfunction of the KCNH6 K_V channel protein resulted in a high level of intracellular Ca^{2+} in mice that triggered the hyperinsulinemia term. In the long term, by contrast, the intracellular elevation of Ca^{2+} caused β-cell apoptosis and loss of β-cell mass, which subsequently lead to a hypoinsulinemic phenotype in mice[87]. Curiously, the different mutations of KCNQ1 activation might cause either hypoinsulinemia or hyperinsulinemia (e.g., KCNQ1-R397W and KCNQ1-G292W-phenotypes). Therefore, this work aimed to elucidate the association between Kv7.1 channel and insulin secretion in human β cells.

Disease-relevant hPSC-based models can provide a vital tool for diabetes research and precision therapies[166]. The establishment of diseased and WT models *in vitro* using the hPSCs can faithfully mimic early events of human pancreas differentiation and possibly contribute to our understanding of why PND occurs. Homozygous point mutation of our neonatal diabetes patient cause PND, but his condition is stable under regular insulin treatment, suggesting that the homozygous point mutation affects the insulin production and/or secretion function of β cells. This work aimed to understand when diseased models had an aberrant insulin secretion. Using these disease-relevant hPSC-based models, we want to understand the interaction between β cells and other pancreatic cells as well.

2. Materials and methods

2.1 Materials

2.1.1 Instruments and cell culture supplies

7900HT Fast Real-Time PCR System	Applied Biosystems
CFX96 Touch Real-Time PCR Detection System	BIO-RAD
Bioanalyzer 2100	Agilent
DS-11 FX	DeNovix
CO_2 Incubator	Binder
CO_2 hypoxic Incubator	Binder
Rotating Shaker	Binder
SHAKER DOS-10L	NeoLab
Themomixer compact	Eppendorf
Centrifuge 5415 D	Eppendorf
Centrifuge 5417 R	Eppendorf
Centrifuge 5810R	Eppendorf
Multifuge X3R Centrifuge	Thermo Scientific
FACSCalibur	BD Biosciences
FACSAria II	BD Biosciences
FACSAria III	BD Biosciences
Gene Pulser II Electroporation System	BIO-RAD
LSM 700	Zeiss
MAESTRO Pro	AXION BIOSYSTEMS
Shaker Celltron	INFORS HT
Neon™ Transfection System	Invitrogen
GFL Shaking 3033	GFL
CRYOSTAT MICROTOM	Thermo Scientific
37°C microbiological incubator	Heraeus
Shaking incubator	GFL
Cell R Real Time Imaging System	Olympus
Bioruptor Pico Sonicaion	diagenode
Morgagni electron microscope	Thermo Fisher
CCD camera	Morada
Variomag MONOTHERM hotplate stirrer	Merck

EVOS FL imaging system	EVOS
SAFE 2020 hood	Thermo Scientific
Axiovert 25 microscope	Zeiss
DMi8 microscope	Leica
Wasserbad GFL 1003	GFL
4°C fridge	Bosch
-20°C fridge	Bosch
TSX -80°C fridge	Thermo Scientific
Thermal cycler	MJ RESEARCH
Thermal cycler	BioRad
Trans-Blot Turbo transfer system	BioRad
PowerPac Basic	BioRad
ChemiDoc™ MP imaging system	BioRad
BioVortex V1	labortechnik
Microwave	Siemens
Delimiting pen	Agilent technologies
TPP 6-well plate	Merck
TPP 75cm^2 flask	Merck
TPP 96-well plate, round bottom	Merck
Sterile ultra-low attachment 6-well plates	Corning
Falcon® 5 mL Round Bottom Polystyrene Test Tube, with Cell Strainer Snap Cap	Corning
Peel-A-Way® Disposable Embedding Molds	VWR
Stericup®-GP, 0.22 µm, polyethersulfone, 500 mL	Millipore
Steriflip-GP, 0,22 µm, Polyethersulfon, 50 mL	Millipore
LS Columns	MACS Miltenyi Biotec
Pre-Separation Filters (30 µm)	MACS Miltenyi Biotec
MidiMACS™ Separator	MACS Miltenyi Biotec
MACS MultiStand	MACS Miltenyi Biotec
Anti-PE Microbeads	MACS Miltenyi Biotec
CytoView MEA 48	AXION BIOSYSTEMS
Superfrost™ Plus microscope slides	Fisher Scientific
PVDF membrane	BioRad
10 cm cell culture dishes	Cellstar
96 Well Black/Clear Bottom Plate	ThermoFisher

2.1.2 Chemicals and Cytokines

Sodium chloride, NaCl	Sigma
Agarose	Serva
LB Medium (Lennox), powder	Serva
LB-Agar (Lennox)	Roth
Non-fat milk powder	Sigma
Sodium dodecyl sulfate (SDS)	Serva
Sodium bicarbonate (NaHCO3)	Sigma
Trizma® hydrochloride	Sigma
Tris base	Sigma
KCl	Fluka
Na_2HPO_4	Fluka
KH_2PO_4	Sigma
HEPES BioPerformance Certified	Sigma
$CaCl_2$	Merck
$MgCl_2$	Merck
Sodium acetate	Sigma
Bromophenol blue	Sigma
96% PFA extra pure	Acros Organics
Ethylenediaminetetraacetic acid	Sigma
cOmplete™ Protease Inhibitor Cocktail	Roche
Sucrose	Sigma
Fatty acid-free BSA	Proliant Biologicals
ROCK Inhibitor (Y-27632)	Millipore
Recombinant Activin A	R&D Systems
Recombinant Wnt-3a	R&D Systems
Recombinant KGF/FGF-7	R&D Systems
SANT-1	Sigma
Retinoic Acid (RA)	Sigma
LDN193189	Stemgent
TPB	EMD Millipore
3,3′,5-Triiodo-L-thyronine sodium salt (T3)	Sigma

ALK5 inhibitor II	Enzo Life Sciences
Heparin	Sigma
γ-secretase inhibitor XX	Calbiochem
SCR7 pyrazine	Sigma
L-Ascorbic Acid (Vitamin C, VIT-C)	Sigma
ZnSO4 zinc sulfate	Sigma
N-Acetyl-L-cysteine	Sigma
R428	SelleckChem
Trolox	EMD Millipore
Chromanol293B	Sigma
isradipine	Tocris

2.1.3 Media and reagents

Essential 8 medium	Thermofisher
MCDB131	Life Technologies
DMEM/F12	Gibco
mTeSR1 Complete Kit for hES maintenance	Stem Cell Technologies
OPTIMEM, Reduced Serum Medium	Gibco
CMRL Medium, no glutamine	Gicbo
Essential 6 medium	Thermofisher
GlutaMAX supplement	Life Technologies
Matrigel (Corning) hESC qualified	Corning
Accutase	StemPro
Antibiotic-Antimycotic, 100x, liquid	Gibco
β-mercaptoethanol	Life Technologies
MEM non-essential amino acids	Life Technologies,
Dulbecco's PBS	PAN Biotech
BSA Fraction V (7.5%)	Gibco
ReleasR	Stem Cell Technologies
Trace Elements A	Corning
Trace Elements B	Corning

Proeinase K	invitrogen
XtremeGene 9 DNA Transfection Reagent	Roche
QuickExtract DNA Extraction Solution	Epicentre Technologies
Nuclear free H_2O	Sigma
Dimethyl sulfoxide (DMSO)	Sigma-Aldrich
CloneR	Stem Cell Technologies
ReLeSR	Stem Cell technologies
primocin	InvivoGen
Donkey Serum	VWR
Insulin-Transferrin-Selenium-Ethanolamine (ITS-X)	ThermoFisher
TrypLE™ select Enzyme (10x)	ThermoFisher
CryoStor® CS10	Stem Cell technologies
glutaraldehyde	Sigma
Poly/Bed^R 812	Polysciences Inc.
VECTASHIELD® Antifade Mounting Medium	Vector Laboratories
Ca^{2+}-sensitive fluorescent probe Fluo4-AM	Life Technologies
GlutaMAX	Life Technologies
D-Glucose solution	Sigma
Roti®-Phenol/Chloroform/Isoamylalkohol	Rothe
Enthanol	Rothe
Isopropanol	Rothe
Tween 20	Merck
Triton X-100	Sigma
CoverGripTM Coverslip Sealant	Biotium
Tissue-Tek OCT Sakura Finetek compound 4583	VWR
Ammonium hydroxide	Merck
Midori Green Advance DNA Stain	Genetics
Glycine	Roche
2-mercaptoethanol	Life Technologies
Hoechst 33342	Fisher scientific

2.1.4 Enzymes

Restriction Enzymes	New England Biolab
T4 DNA ligase	New England Biolab
T4 ligase buffer	New England Biolab
SsoAdvanced Universal SYBR Green Supermix	Bio-Rad
Power SYBR Green PCR Master Mix	Applied Biosystems
GoTaq Green Mastermix	Promega
BpiI (BbsI)	ThermoFisher

2.1.5 Kits

High Capacity RNA-to-cDNA kit	Applied Biosystems
CloneJET PCR Cloning Kit	Thermo Scientific
BCA Protein Assay Kit	Pierce
QIAGEN plasmid midi kit	Qiagen
Direct-zol RNA MiniPrep Plus	Zymo research
RNA 6000 Nano kit	Agilent
QIAquick Gel Extraction Kit	Qiagen
dsDNA Broad Range Kit	DeNovix
SuperSignal™ West Femto Maximum Sensitivity Substrate Kit	Thermo Scientific
Amersham ECL™ Prime Western Blotting Detection Reagent	Cytiva
TGX Stain-Free FastCast Acrylamide Kit	BioRad
Trans-Blot Turbo transfer system RTA Transfer Kit	BioRad
EpiTect Bisulfite Kits	Qiagen
Human Insulin ELISA	ALPCO
Fixation/Permeabilization Solution Kit	BD Biosciences
Human ES/iPS Cell Characterization Kit	Applied StemCell Inc.
Mix and Go *E. coli* transformation Kit	Zymo Research
PE Annexin V apoptosis detection kit	BD Biosciences

2.1.6 Antibodies

PE Mouse anti-Human Sox17	BD Biosciences
Alexa Fluor® 488 Mouse anti-PDX-1	BD Biosciences
PE Mouse Anti-Nkx6.1	BD Biosciences
Alexa Fluor® 647 Mouse Anti-Nkx6.1	BD Biosciences
Insulin (C27C9) Rabbit mAb (Alexa Fluor® 488 Conjugate)	Cell Signaling Technology
APC anti-Human CD26	Biolegend
PE Mouse Anti-Human CD49a	BD Biosciences
Anti-Tra-1-60-PE, human	MACS Miltenyi Biotec
Alexa Fluor® 647 Mouse IgG1 κ Isotype Control	BD Biosciences
FITC Mouse IgG2a, κ Isotype Control	BD Biosciences
PE Mouse IgG1, κ Isotype Control	BD Biosciences
APC Mouse IgG2a, κ Isotype Control	Biolegend
Rabbit IgG Isotype Control (Alexa Fluor® 488 Conjugate)	Cell Signaling Technology
FITC Annexin V	BD Biosciences
PDX1 Mouse Monoclonal Antibody	Origene
Homeobox protein Nkx-6.1	Developmental Studies
Purified Mouse Anti-Ki-67	BD Biosciences
Anti-KCNQ1 antibody	ATLAS ANTIBODIES
FLEX Polyclonal Guinea Pig Anti-Insulin Ready-to-use	Agilent
Insulin (C27C9) Rabbit mAb	Cell signaling Technology
Monoclonal Anti-Glucagon antibody	Sigma
C-Peptide Antibody	Cell signaling Technology
Sox2 (L1D6A2) Mouse mAb	Cell signaling Technology
Oct-4 Antibody	Cell signaling Technology
Actin, pan Ab-5	Dianova
Alexa Fluor™ 488 Goat Anti-Mouse	Invitroge

Goat anti-Rabbit IgG (H+L) Highly Cross-Adsorbed Secondary Antibody, Alexa Fluor 555	ThermoFisher
Goat anti-Guinea Pig IgG (H+L) Highly Cross-Adsorbed Secondary antibody, Alexa Fluor 647	ThermoFisher
HPR-Anti Rabbit IgG (H+L)	Thermo Scientific
HPR-Anti Mouse IgG (H+L)	Thermo Scientific

2.1.7 Primers and Oligos

Name	Usage	Sequence (5'-3')
KCNQ1	PCR	Forward: CTGGCTCAGGGCTGGTAAAG Reverse: GGAACCTAGCATCGGGTGTA
SeV	PCR	Forward: GGATCACTAGGTGATATCGAGC Reverse: ACCAGACAAGAGTTTAAGAGATATGTATC
SeV-Klf4	PCR	Forward: TTCCTGCATGCCAGAGGAGCCC Reverse: AATGTATCGAAGGTGCTCAA
SeV-cMyc	PCR	Forward: TAACTGACTAGCAGGCTTGTCG Reverse: TCCACATACAGTCCTGGATGATGATG
SeV-KOS	PCR	Forward: ATGCACCGCTACGACGTGAGCGC Reverse: ACCTTGACAATCCTGATGTGG
Hu18sRNA	PCR	Forward: GTAACCCGTTGAACCCCATT Reverse: CCATCCAATCGGTAGTAGCG
STX1A	PCR	Forward: TTCCTACCCCGTCTTTCCTT Reverse: AAGATCAACCTGGGCAACAC
ODF4	PCR	Forward: GGAAAATTCCGTGGCAGTTA Reverse: TCCCCACTCTTCCTTTCCTT
AC093843.1	PCR	Forward: TCCACCCTCCCTCTTTCTCT Reverse: TCTGCCAATCCCAAGTAAGG
GTDC1	PCR	Forward: CACTTGGTCTTTGGGGATGT Reverse: CGCCACATCTGGCTAATTTT

ILDR1	PCR	Forward: GCTTAGGCTGTCCCTGTCTG Reverse: AAAGAACTGCGGAACCTCAA
Bis-KCNQ1	Bisufite sequencing PCR	Forward: GGAGTTGGGATTATGTTAAGTTTGT Reverse: AAAACCCTCTAAAAAACCTTCTTTC
KCNQ1	Real-Time PCR	Forward: CATCACCCACATCTCACAGC Reverse: GTCCCGCACATCGTAAGG
KCNQ1ot1	Real-Time PCR	Forward: CTTTGCAGCAACCTCCTTGT Reverse: TGGGGTGAGGGATCTGAA
SLC22A18	Real-Time PCR	Forward: CATCTTGCTTACCTACGTGCTG Reverse: CCCAGTTTCCGAGACAGGTA
PHLDA2	Real-Time PCR	Forward: TCCAGCTATGGAAGAAGAAGC Reverse: GTGGTGACGATGGTGAAGTACA
CDKN1C	Real-Time PCR	Forward: AGATCAGCGCCTGAGAAGTCGT Reverse: TCGGGGCTCTTTGGGCTCTAAA
FOXA2	Real-Time PCR	Forward: TGGGAGCGGTGAAGATGGAAGG Reverse: CGTACGACGACATGTTCATGGAGC
EOMES	Real-Time PCR	Forward: AGAGGGCTGTGCCTTCCGTTTC Reverse: AGCACACAGCAGAGGCCTAGCAAG
LMO2	Real-Time PCR	Forward: ACTTCCTGAAGGCCATCGACCAG Reverse: CACCCGCATTGTCATCTCATAGGC
NANOG	Real-Time PCR	Forward: CCAAAGGCAAACAACCCACTT Reverse: CGGGACCTTGTCTTCCTTTTT
OCT4	Real-Time PCR	Forward: CGACCATCTGCCGCTTTG Reverse: GCCGCAGCTTACACATGTTCT
Pax6	Real-Time PCR	Forward: GTCCATCTTTGCTTGGGAAA Reverse: TAGCCAGGTTGCGAAGAACT
Sox1	Real-Time PCR	Forward: ACCAGGCCATGGATGAAG Reverse: CTTAATTGCTGGGGAATTGG
Sox2	Real-Time PCR	Forward: ACAGCAAATGACAGCTGCAAA Reverse: TCGGCATCGCGGTTTTT
Insulin	Real-Time PCR	Forward: AGCCTTTGTGAACCACACC Reverse: GCTGGTAGAGGGAGCAGATG

FGFRL1	Real-Time PCR	Forward: CCTGAGCGTCAACTACACC Reverse: CTCATCTTGGAGGGCTGTG
FGFR1	Real-Time PCR	Forward: AACCTGACCACAGAATTGGAGGCT Reverse: ATGCTGCCGTACTCATTCTCCACA
FGFR3	Real-Time PCR	Forward: AGGTGAATGGCAGCAAGGT Reverse: CTAGCTCCTTGTCGGTGGTG
PLD2	Real-Time PCR	Forward: CAGGTTTGCCTTGAGTCTGC Reverse: TTGCCACAACTGGAAGAAGTC
PDX1	Real-Time PCR	Forward: AAGTCTACCAAAGCTCACGCG Reverse: GTAGGCGCCGCCTGC
GLUT1	Real-Time PCR	Forward: TCCCTGCAGTTTGGCTACA Reverse: GTGGACCCATGTCTGGTTGT
GLUT2	Real-Time PCR	Forward: CACCAATTCCAGCTACCGAC Reverse: CCGTCTGAAAAATGCTGGTT
Glucagon	Real-Time PCR	Forward: GAGGAAGGCGAGATTTCCCAG Reverse: GAACCATCAGCATGTCTGCG
HNF4α	Real-Time PCR	Forward: CAAACACTACGGTGCCTCG Reverse: GTCTTTGTCCACCACGCACT
NEUROD1	Real-Time PCR	Forward: TCACTGCTCAGGACCTACTAA Reverse: GAGACCAGGTCTGGGCTTTTG
CACNA1A	Real-Time PCR	Forward: AAATCATTGCCCTTGGGTTT Reverse: CAAACTCCGTCCCAACTGTC
CACNA1C	Real-Time PCR	Forward: CTCTGCCTGACCCTGAAGAA Reverse: AGATCGCTAAGGCCACACAA
CACNA1D	Real-Time PCR	Forward: GTGTTGCGACCACTTCGACT Reverse: AAGGGCTATGTGAAGGAGGG
CACNA1H	Real-Time PCR	Forward: TTCTTCATTTTCGGCATCGT Reverse: GCAGGAAGGTCAGGTTGTTG
KCNQ1g-1	sgRNA+BpiI sticky end	Forward: CACCGCCCGACCTCAGACCGCATGG Reverse: AAACCCATGCGGTCTGAGGTCGGGC
KCNQ1g-2	sgRNA+BpiI sticky end	Forward: CACCGCCACCTGGAAGATCTACATC Reverse: AAACGATGTAGATCTTCCAGGTGGC
KCNQ1t-1	ssDNA	CTGGGTGACAGCAGAGTGTGGCTCCGGGGG

		GCCTTCCGGATGTAGATCTTCCAGGTGGAGG AGTCGGGGTTCTCGGCAGCATAGCATCTCCA TGCGGTCTGAGGTCGGGCAGGGGGACAGGC TGTCAC
KCNQ1t-2	ssDNA	GCCCTGGTGGCAGGTGGGCTACTCACCACCA CAGACTTCTTGGGTTTGGGGCTGGGTGACAG CAGAGTGTGGCTCCGGGGGGCCTTTCGGAT GTAGATCTTCCAGGTGGAGGAGTCGGGGTTC TCGGC

2.1.8 Plasmids

pSBbi-RP	Addgene
pX330-U6-Chimeric_BB-CBh-hSpCas9	Addgene
Px458-GFP	Addgene

2.1.9 Bacteria strains and Cell lines

Esherichia coli DH10β	Invitrogen
Esherichia coli DH5α	New England Biolab
PBMC	Blood collection from patient's family
hESCs_H1	WiCell
Human islets	Prodolabs

2.1.10 Buffers and Solutions

LB media (liquid)	20 g/L LB Medium (power) in ddH_2O
LB media (solid)	20 g/L LB Medium (power), 35 g/L LB-Agar in ddH_2O
1% Matrigel solution	250 µL Matrigel in 25 mL DMEM/F12 medium
10x PBS	80 g/L NaCl, 2 g/L KCl, 14.4 g/L Na_2HPO_4, 2.4 g/L KH_2PO_4

RIPA buffer	150mM NaCl, 1.0% Triton X-100, 0.5% Na-deoxycholate, 0.1% SDS, 50mM Tris (pH 8.0), protease inhibitor cocktail
6x denaturing protein loading buffer (pH 6.8)	10% SDS, 15% 2-mercaptoethanol, 30% glycerol, 0.004% bromophenol blue, 1 M Tris-HCl
10x SDS running buffer	250 mM Tris base, 1.9 M glycine, 1% SDS
1x PBST buffer	1x PBS, 0.1% Tween 20
1x TBST buffer	2.4 g/L Tris-HCl, 0.56 g/L Tris, 8.8 g/L NaCl, 0.1% Tween 20
WB blocking buffer	5% milk in 1x TBST buffer
Stripping buffer (Mild)	15 g Glycine, 1 g SDS, 10 mL Tween 20, add ddH_2O to 1 L, pH 2.2
Lysis buffer	100 mM Tirs-HCl, 0.5 M EDTA, 10%SDS, 5 M NaCl, 0.05% Protein K
Sonication buffer	10 mM Tirs, 1 mM EDTA, 0.2% Triton-X 100, 0.05% Protein K
10x TBE electrophoresis buffer	121.1 g/L Tris, 61.8 g/L Boric acid, 7.4 g/L EDTA
KRB buffer	130 mM NaCl, 5 mM KCl, 1.2 mM CaCl2, 1.2 mM MgCl2,1.2 mM KH2PO4, 20 mM Hepes (pH 7.4), 25 mM NaHCO3, 0.1% BSA
Low glucose KRB buffer	2.75 mM glucose in KRB buffer
High glucose KRB buffer	16.75 mM glucose in KRB buffer
Acid ethanol	1.5% HCl, 80% ethanol
0.1 M phosphate buffer	18.2% 0.1 M KH_2PO_4, 81.8% 0.1 M Na_2HPO_4 in ddH_2O

2.2 Bacterial and biochemical methods

2.2.1 Preparation of CRISPR-Cas9 constructs

Two sgRNA were designed and selected from an online CRISPR Design Tool (http://tools.genome-engineering.org). ssDNA donors were designed as per

Christopher' protocol[170]. The oligos of phosphorylated sgRNA with BpiI sticky end and ssDNA were ordered from LGC. The phosphorylated sgRNA was inserted into Px458-GFP cloning backbones for co-expression with Cas9 by combining the following:

Components	Amount
Px458-GFP	100 ng
oligo duplex of sgRNA (50 nM)	2 µL
DTT (10 mM)	1 µL
ATP (10 mM)	1 µL
T4 ligase	0.5 µL
T4 ligase buffer	2 µL
BpiI	1 µL
ddH_2O	to 20 µL

The ligation reaction was cycling 12 times in a thermocycler by following parameters: 37°C for 5 min, 21°C for 5 min. The heat-denatured ligation reaction was incubated in a thermocycler by following parameters: 70°C for 15 min.

2.2.2 Transformation of chemically competent *E. coli*

Mix and Go chemically competent *E. coli* cells were prepared according to the manufacturer's protocol. CRISPR-Cas9 constructs were transformed according to the manufacturer's protocol. The candidate colonies were amplified for plasmid isolation.

2.2.3 Transformation of electrocompetent *E. coli*

Desalination of CRISPR-Cas9 constructs was carried out for 1 hr at RT. The constructs were transformed according to the Invitrogen's protocol. The candidate colonies were amplified for plasmid purification. The plasmid was purified according to the Qiagen's protocol and confirmed by Sanger sequencing with LGC.

2.3 Cell biological and biochemical methods

2.3.1 Preparation of hPSCs culture plates

6-well plates, 48-well plates, or T75 flasks were coated by adding 1mL/well, 0.3 mL/well, or 5 mL/flask of 1% Matrigel solution and incubated for at least 1 hr at 37°C.

2.3.2 Characterization of hiPSCs pluripotency

hiPSCs were seeded on coverslips. The cells were stained by using Human ES/iPS Cell Characterization Kit following the manufacturer's instructions.

2.3.3 Embryoid body (EB) formation

hiPSCs were cultured in E8 media until 80% confluence. Cell-clusters of one well of 6-well plate were dissociated with cell-clusters using DPBS supplemented with 50 μM EDTA. The cell-clusters were gently resuspended in pre-warmed E6 medium and were transferred onto a 10 cm plate. EBs were formed after 2 weeks according to E6 medium protocol.

2.3.4 Generation gene mutation mimicking patient's homozygous mutation by the CRISPR-Cas9 system

2.3.4.1 Cell transfection and sorting

$8x10^5$ cells/well were seeded to a 6-well plate. The plasmids and ssDNA were transfected into hESC_H1 or hiPSCs when cells had 70-85% confluency using the XtremeGENE 9 transfection reagent. The transfected cells were incubated for 24 hr before sorting. The cells were incubated for 12 hr in mTeSR1 media supplemented with CloneR before dissociation. The cells were dissociated to single-cell suspension using Accutase for sorting GFP positive cells. Untransfected cells were used as a negative control for correct gating GFP positive cells. 5,000 cells/well of a 6-well plate were sorted into 2 mL mTeSR1 supplemented with primocin and CloneR. The plate was incubated 48 hr before changing to fresh mTeSR1 media without CloneR. Single colonies were separately picked up to Matrigel-coated 48-well plates after 1 week of cells recovery.

2.3.4.2 Candidate colony generation

1.5 mL tubes containing the old cell culture media were centrifuged for 5min at the speed higher than 13,000 rpm to pellet dead cells/debris. The pellet was resuspended in 20 µL QuickExtract Buffer after aspirating supernatant. The suspension was transferred to a PCR tube to prepare genomic DNA. KCNQ1 primers were used to amplify the locus of KCNQ1 mutation in a thermocycler. The PCR product was purified according to the Gel Extraction Kit. Depending on the PCR product's quality, the purified PCR product was used for sequencing or cloned into pJET before sequencing. Positive colonies and some unmodified colonies were continually cultured. Cell colonies were separately dissociated and were transferred into 6-well plates using ReLeSR. Differentiated cells were removed by using a pipette tip to minimize spontaneous differentiation. The stable colonies and isolated RNA were frozen down at -80°C.

2.3.4.3 The pluripotent status of candidate colony examination

Total RNA was extracted from cells using the Direct-zol RNA MiniPrep Plus kit following the manufacturer’s instructions. 1 µg RNA was used for cDNA reverse transcription following the High Capacity RNA-to-cDNA manual. Gene expression of hESC pluripotency maker, *Oct4*, *Sox2*, and *Nanog*, were assessed on BioRad CFX96 Real-Time PCR detector using the SsoAdvanced Universal SYBR Green Supermix. Data were normalized to *GAPDH* expression using the △△Ct method.

Coverslips were added into a 12-well plate and coated with 1% Matrigel. Cells were seeded into plates and cultured for 3 days. Cells were washed twice with DPBS. Cells were fixed in 300 µL 4% PFA for 30min at RT. The coverslips were incubated with 300 µL blocking buffer (0.15% Triton X-100, 1% normal donkey serum in DPBS) at RT for 1 hr. Respective primary antibody solutions (Sox2 and Oct4) were prepared by mixing appropriate volumes of every antibody in blocking buffer. Every coverslip was incubated with 300 µL/slide pre-mixed primary antibody solution at 2-8°C overnight. The next day, the coverslips were 3 times washed with DPBS. Respective secondary antibody solutions were prepared by mixing appropriate volumes of in the blocking buffer. The coverslips were incubated with 300 µL/slide pre-mixed secondary antibody solution at RT for 1.5 hr in dark. The coverslips were incubated with 300 µL pre-mixed

nuclear staining solution at RT for 8 min in dark. The slides were washed with DPBS 5 times. The coverslips were mounted with VECTASHIELD® Antifade Mounting Medium and were covered with microscope slides. The mounted and covered slides were sealed with CoverGripTM Coverslip Sealant and were allowed to thoroughly dry before analyzing on an inverted fluorescent microscope. The slides were stored long-term at -80°C.

2.3.4.4 Stable hESCs selection

The high pluripotent stem cells were isolated by Anti-Tra-1-60-PE and Anti-PE MicroBeads. The colonies cells were incubated for 12 hr in media supplemented with CloneR before dissociating into single cells. Wash buffer was prepared by mixing DPBS and mTeSR1 media supplemented with CloneR. The cell pellet was resuspended to 98 µL/10^6 cells of buffer. The suspension was mixed with 2 µL/10^6 cells of Anti-Tra-1-60-PE and incubated for 10 min at 4°C. The cells were washed by adding 2 mL buffer. The pellet was resuspended in 40 µL/10^6 cells of buffer after aspirating supernatant. The suspension was mixed with 10 µL/10^6 cells of Anti-PE MicroBeads and incubated for 15 min at 4°C. The cells were washed by adding 2 mL buffer and were resuspended in 500 µL of wash buffer. The cell suspension was loaded onto a prepared LS Column. The labeled cells were flushed out from the column into 5 mL mTeSR1 media supplemented with CloneR after washing 3 times with 3 mL of buffer. The selected cells were cultured until 70-85% confluency. The cells were dissociated into single cells and froze for pancreatic differentiation.

2.3.5 Mechanism examination of our PND patient

2.3.5.1 Generation of human pancreatic β-like cells

hPSCs were developed toward insulin-producing cells in a suspension-based format on a shaker with some modification to the published protocol[44,46]. Undifferentiated hPSCs were dissociated to single cells by treating them with Accutase. The single cells were seeded in mTeSR1 media supplemented with CloneR in 6-well ultra-low attachment plates at 5.5 × 10^6 cells/well. The plates were cultured on the shaker at 100 rpm in a CO_2 incubator for 24 hr. Undifferentiated aggregates were cultured in daily differentiation media.

S1/S2 basal media: 500 mL MCDB131 supplemented with 0.75 g $NaHCO_3$, 1% GlutaMAX, 15 mM glucose and 2.5 g fatty acid-free BSA.

S3/S4 basal media: 500 mL MCDB131 supplemented with 1.25 g $NaHCO_3$, 1% GlutaMAX, 15 mM glucose and 10 g fatty acid-free BSA.

S5/S6 basal media: 500 mL MCDB131 supplemented with 0.75 g $NaHCO_3$, 1% GlutaMAX, 20 mM glucose and 10 g fatty acid-free BSA.

Day 0 media: S1/S2 basal media, 100 ng/mL Activin A, 25 ng/mL mouse Wnt3a.

Day 1 - Day 2 media: S1/S2 basal media, 100 ng/mL Activin A.

Day 3 - Day 5 media: S1/S2 basal media, 50 ng/mL KGF, 0.25 mM ascorbic acid.

Day 6 - Day 7 media: S3/S4 basal media, 50ng/mL KGF, 0.25 μM SANT-1, 1 μM RA, 100 nM LDN-193189, 200 nM TPB, 0.25 mM ascorbic acid, 0.5% ITS-X.

The plates were cultured on the shaker at 120 rpm in CO_2 incubator from day 8 to day 20.

Day 8 - Day 10 media: S3/S4 basal media, 2ng/mL KGF, 0.25 μM SANT-1, 0.1 μM RA, 200 nM LDN-193189, 100 nM TPB, 0.25 mM ascorbic acid, 0.5% ITS-X.

Day 11 - Day 13 media: S5/S6 basal media, 0.25 μM SANT-1, 0.05 μM RA, 100 nM LDN-193189, 1 μM T3, 10 μM ALK5i II, 10 μM ZnSO4, 10 μg/mL heparin, 0.25 mM ascorbic acid, 0.5% ITS-X.

Day 14 - Day 20 media: S5/S6 basal media, 100 nM LDN-193189, 1 μM T3, 10 μM ALK5i II, 10 μM ZnSO4, 10 μg/mL heparin, 100nM ɣ-secretase inhibitor XX, 0.5% ITS-X.

Option 1: S7 media (day 21-day 40): 500 mL MCDB131 supplemented with 1% GlutaMAX, 10 g fatty acid-free BSA, 5mg heparin, 5mL MEM nonessential amino acids, 84 μg ZnSO4, 500 μL Trace Elements A and 500 μL Trace Elements B. Day 21 aggregates were dissociated to single cells and were seeded in S7 media supplemented with CloneR in 6-well ultra-low attachment plates at 5.5×10^6 cells/well. The plates were cultured on the shaker at 100 rpm in a CO_2 incubator for 24 hr. Day22 aggregates were cultured in standard S7 media at 120 rpm.

Option 2: S7 standard protocol: (day 21-day 28): 500 mL MCDB131 supplemented with 0.75 g $NaHCO_3$, 1% GlutaMAX, 20 mM glucose, 10 g fatty acid-free BSA, 100 nM LDN-193189, 1 μM T3, 10 μM ALK5i II, 10 μM ZnSO4, 10 μg/mL heparin, 1 mM N-acetylcysteine (Sigma), 10 μM Trolox (EMD Millipore), 2 μM R428 (SelleckChem), 0.5% ITS-X.

2.3.5.2 Flow cytometry analysis

1.5 mL microcentrifuge tubes and pipette tips were pre-coated with 0.2% BSA in PBS. 15 µL of cell aggregates were loaded into 0.2% BSA coated microcentrifuge tubes. Cell aggregates were washed with 1 mL DPBS and were settled down by gravity before carefully removing the supernatant. The cell aggregates were treated with 300 µL TrypLE (10X) to dissociate to single cells, they were washed with 1.5 mL of 0.2% BSA and centrifuged at 4°C 400 rcf for 5min. The cell pellet was re-suspended with a 200 µL cold BD fixation/permeabilization solution and fixed for 20 min at 2-8°C after aspirating supernatant. Fixed cells were washed twice with 1.1 mL cold 1 × BD Perm/Wash Buffer and centrifuged at 4°C 400 rcf for 5min. Cells were suspended into 150 µL 1 × BD Perm/Wash Buffer after aspirating supernatant. One sample had three replicates. To analyze of SOX17 expression at day 3, 5 µl Sox17-PE antibodies were loaded into 50 µL cells suspension aliquot, 0.5 µL PE isotypes were loaded into 50 µL isotope control. 5 µl PDX1-FITC antibodies were loaded into 50 µL cells suspension aliquot, 0.5 µL FITC isotypes were loaded into 50 µL isotope control to analyze PDX1 expression after 11 days. 5 µl Nkx6.1-AlexaFluor® 647 antibodies were loaded into 50 µL cells suspension aliquot, 0.5 µL AlexaFluor® 647 isotypes were loaded into 50 µL isotope control to analyze of Nkx6.1 expression after 11 days. 1 µl Insulin-AlexaFluor® 488 antibodies were loaded into 50 µL cells suspension aliquot, 0.5 µL AlexaFluor® 488 isotypes were loaded into 50 µL isotope control to analyze of Insulin expression after 20 days. The mix of cells and antibodies was incubated in the dark for 1 hr at 2 - 8°C. Cells were washed with 1.5 mL cold 1 X BD Perm/Wash Buffer and centrifuged at 4°C 400 rcf for 5min. Cells were suspended into 200 µL 0.2% BSA after aspirating supernatant. The entire suspension was allowed to flow through the cell strainer of an appropriately labeled polystyrene tube. The samples were analyzed on a flow cytometer after the compensation setting. The exported FACS data were analyzed using FlowJo.

2.3.5.3 Immunofluorescence analysis

1.5 mL microcentrifuge tubes and pipette tips were pre-coated with 0.2% BSA in PBS. 10 µL of organoids were loaded into 0.2% BSA coated microcentrifuge tubes. Organoids were washed with 1mL DPBS. The supernatant was carefully removed after

organoids settling down by gravity. Organoids were suspended with 300 µL 4% PFA and fixed for 30min at RT. 4% PFA was carefully removed after organoids settling down by gravity. Organoids were washed with 1mL DPBS and were settled down by gravity before carefully removing the supernatant. 1 mL 30% sucrose (w/v) in DPBS was added the tube to dehydrate organoids. Tubes were placed at 2-8°C overnight. Organoids were transferred to the center of flat bottom cryosectioning molds after carefully removing the supernatant. The left sucrose solution was removed from the mold as much as possible. The mold was filled with OCT and then were placed in a dry ice ethanol bath to freeze OCT. Organoids were embedded in frozen OCT and should be stored at -80°C. The embedded organoids were sectioned by using a cryostat micro-sectioning machine. Sectioned slides were placed into a DPBS filled glass slide holder with stirring for 5 min, which was repeated 3 times to get rid of OCT. The regions of the sample were delimited by the Delimiting pen. The slide was incubated with 300 µL blocking buffer at RT for 1 hr. Respective primary antibody solutions were prepared by mixing appropriate volumes of every antibody in blocking buffer. The slides were loaded 300 µL/slide pre-mixed primary antibody solution and incubated at 2-8°C overnight. The next day, the slides were washed with DPBS 3 times. Respective secondary antibody solutions were prepared by mixing appropriate volumes of antibodies in the blocking buffer. The slides were loaded 300 µL/slide pre-mixed secondary antibody solution and incubated at room temperature for 1.5 hr avoiding light. The slides were loaded 300 µL/slide pre-mixed nuclear staining solution and incubated at room temperature for 8 min avoiding light. The slides were washed with DPBS 5 times. The slides were mounted with VECTASHIELD® Antifade Mounting Medium and covered with coverslips. The mounted and covered slide was sealed with CoverGripTM Coverslip Sealant and allowed to dry fully before analyzed on an inverted fluorescent microscope. The slides were stored long-term at -80°C.

2.3.5.4 KCNQ1 mutation locus methylation analysis

15 µL of every stage of aggregates were collected and washed with 1 mL DPBS. The cell aggregates were lysed by adding 500 µL lysis buffer and incubated at 55°C overnight. The lysate was mixed with an equal volume of phenol: chloroform: isoamyl alcohol solution. The aqueous phase (upper) was transferred to a new tube after centrifugation. The aqueous phase was mixed with a 10% volume of 3 M sodium

acetate (pH 5.2) and a 2-fold volume of -20°C cold 100% ethanol. The tube was flicked several times with a finger for completion of blending. The mixture was placed at -80°C overnight. The supernatant was carefully removed after DNA was settled down by gravity. The DNA pellet was washed with 70% ethanol. The DNA pellet was allowed to air dry for 15 min and was resuspended in 100 µL ultra-pure water.
Sodium bisulfite conversion of unmethylated cytosines in DNA was based on EpiTect Bisulfite Handbook. I designed primers from MethPrimer to sequence the KCNQ1 mutation locus.

2.3.5.5 Gene expression analysis (qRT-PCR)

Total RNA was extracted from cells using the Direct-zol RNA MiniPrep Plus kit following the manufacturer's instructions and used for cDNA reverse transcription. Gene expression was assessed on the 7900HT Fast Real-Time PCR System using the Power SYBR Green PCR Master Mix. Data were normalized to *TBP* expression using the △△Ct method.

2.3.5.6 Cytosolic Ca^{2+} level measurement

A 96-well black plate was treated with a 50 µl/well of hESC-qualified Matrigel that had been diluted 1:75 in DMEM: F12. The plate was incubated for 2 hr in the incubator. The Matrigel solution was moved out to leave a thin layer of matrix. Human islet and hPSC-derived differentiated organoids (approximately 20 organoids or human islets per well) were respectively resuspended in 100 µl of S7 media and were added to these coated wells for incubation and attachment.
After 24 hr, the wells were washed with prewarmed (37 ℃) KRB buffer containing 2.5 mM glucose. The organoids were incubated with 50 µM Ca2+-sensitive fluorescent probe Fluo4-AM in 2.5 mM glucose KRB buffer for 45 min in a 37℃ incubator. The cell aggregates were washed with 2.5 mM glucose KRB buffer twice. The plate was incubated further in a 37℃ incubator for 15 min. The plate was immediately staged on a Cell R Real-Time Imaging System to acquire time-series imaging.
Fluo-4 AM was illuminated at 488 nm, and its emission was between 490-560 nm. Time-series images were recorded at a resolution of 80x magnification with a 20-sec interval. The progression of glucose challenges and time of the stimulation during imaging was as follows. Imaging started after 5 min incubation in low glucose KRB

buffer containing 2 mM glucose and ran 16 cycles. The next step was followed by a 5 min incubation in high glucose KRB buffer containing 20 mM glucose and ran 16 cycles. Sequential low and high glucose challenges were repeated one more time after washing with low glucose KRB buffer. The aggregates' imaging was resumed after adding low or high glucose solution. Fluorescence intensity was measured by using Fiji. StackReg was applied to anchor the aggregates throughout the imaging. The positions of aggregate were added to the ROI manager. The fluorescence intensity of the aggregates was measured throughout the imaging. Finally, all of the fluorescence intensity of the same aggregate was normalized to its first image.

2.3.5.7 Electrical activity analysis

1.5 mL microcentrifuge tubes and pipette tips were pre-coated with 0.2% BSA in PBS. 10 µL of organoids were treated with 300 µL TrypLE (10X) to dissociate to single cells, and then washed with 1 mL 0.2% BSA and centrifuged at 4°C 400 rcf for 5 min. The 5% Matrigel solution was prepared by diluting 250 µL Matrigel in 2.4 mL S7 media supplemented with CloneR. The cell pellet was re-suspended with 10 µL cold 5% Matrigel after aspirating supernatant.

8 µL cell suspension was dotted to recording electrodes avoiding ground electrodes, and incubated 0.5 hr in a CO_2 incubator until cell attachment. 300 µL S7 media supplemented with CloneR was added against the wall of the well. The electrical activity (Spike Detector) was recorded in Neural Spikes mode on MAESTRO Pro. The threshold-baseline of Spike Detector was set by using 3 mM glucose.

2.3.5.8 ELISA measurements

Pipette tips were pre-coated with 0.2% BSA in PBS. The organoids were transferred to 6-well ultra-low attachment plates with 5 mL low glucose buffer. Organoids were incubated in low glucose for 1 hr in a 37℃ incubator. 5 organoids/well were transferred to 96-well plates with 10 replicates.

Insulin secretion stimulated by glucose or KCl was firstly measured by adding low glucose KRB buffer until 200 µL/well. The organoids were incubated 30 min in a 37℃ incubator. 190 µL solution per well was transferred into a new 96-well plate, respectively. The new 96-well plate was frozen at -80°C for ELISA measurement. New 190 µL high glucose KRB buffer solution or 30 mM KCl KRB buffer per well was added

back to the previous well following by incubation for 30 min in a 37℃ incubator. 190 µL solution per well was transferred into a new well of 96-well plate, respectively. The new 96-well plate was frozen at -80°C for ELISA measurement.

Total insulin was measured by adding the acid ethanol solution until 200 µL/well. The organoids were incubated at 4℃ overnight. 190 µL solution per well was transferred into a new well of 96-well plate, respectively. The new 96-well plate was frozen at -80°C for ELISA measurement.

The released and total insulin was measure by the Human insulin ELISA Kit following the manufacturer's instructions. The organoids were collected into 50 µL/well sonication buffer. The organoids were sonicated 5 cycles (30 s ON and 30 s OFF) in Bioruptor Pico Sonication device. The DNA of organoids was detected by using DeNovix® dsDNA Broad Range Assay. The DNA concentration was calculated by using DeNovix DS-11 FX Fluorometer. Insulin secretion was normalized to low glucose stimulation, and insulin content was normalized to DNA mass.

2.3.5.9 Western blot

1.5 mL microcentrifuge tubes and pipette tips were pre-coated with 0.2% BSA in PBS. 45-60 µL/sample of organoids were loaded into 0.2% BSA coated microcentrifuge tubes. Organoids were washed with 1mL DPBS and were settled down by gravity before carefully removing the supernatant. Organoids were lysed in RIPA buffer. The procedure of protein concentration determination was based on the manual of the Pierce BCA Protein Assay Kit.

Protein samples were boiled at 95°C for 5 min and were run on a TGX Stain-Free acrylamide gel. The gel was prepared by following the manual of the TGX Stain-Free FastCast Acrylamide Kit. The proteins were transferred onto a PVDF membrane following the guide of the Trans-Blot Turbo transfer system RTA Transfer Kit. The PVDF membrane was blocked in WB blocking buffer 2 hr and then incubated with KCNQ1 antibodies (1:5000 diluted in WB blocking buffer) overnight at 4°C. The PVDF membrane was washed with TBST buffer and incubated with anti-rabbit antibodies for 1hr at room temperature. For detection of KCNQ1, the PVDF membrane was developed with SuperSignal West Femto Maximum Sensitivity Substrate. The PVDF membrane was imaged on the ChemiDocTM MP imaging system.

The antibodies were removed by the mild stripping buffer. The PVDF membrane was blocked and incubated with Actin antibodies (1:5000 diluted in WB blocking buffer) overnight at 4°C. The PVDF membrane was incubated with anti-mouse antibodies for 1h at room temperature. For detection of Actin, the membrane was developed with ECL. The PVDF membrane was imaged on the ChemiDocTM MP imaging system. The intensity of protein was analyzed with GelAnalyzer.

2.3.5.10 Electron Microscopy

1.5 mL microcentrifuge tubes and pipette tips were pre-coated with 0.2% BSA in PBS. 15 organoids/sample were loaded into 0.2% BSA coated microcentrifuge tubes. The organoids were washed with 1mL DPBS and were settled down by gravity before carefully removing the supernatant. Fix buffer was prepared by a mix of 2 % formaldehyde and 2 % glutaraldehyde in 0.1 M phosphate buffer. The organoids were fixed for 1 hr at room temperature following by fixing at 4°C overnight. The organoids were sequentially stained with 1% OsO4 for 2 hr after washing with a 0.1 M phosphate buffer. Samples were dehydrated in a graded ethanol series and propylene oxide and were embedded in Poly/BedR 812. Ultrathin sections were contrasted with uranyl acetate and lead citrate. Finally, sections were examined with a Thermo Fisher Morgagni electron microscope. Digital images were taken with a Morada CCD camera and the iTEM software.

2.3.5.11 RNAseq and data analysis

mRNA of samples was extracted from cells using the Direct-zol RNA MiniPrep Plus kit. mRNA quality was checked by using Agilent 2100 Bioanalyzer following the protocol of RNA 6000 Nano Kit. BGI Hongkong prepared the DNA libraries and sequenced the libraries on a DNBseq Eukaryotic-T resequencing.

A 30 million 100 bp paired-end reads were obtained per sample. Discarding low-quality reads, trimming adaptor sequences, and eliminating poor-quality bases were done using FASTX-Toolkit and Trimmomatic. Building index and alignment, the reads were performed using Salmon after discarding outliers with over 30 % disagreement. GC content and gene length biases were checked using R package NOISeq to quality control of count data. Mean-variance and PCA were calculated between biological replicates using the tximport package in R. The parameters of lengthscaledTPM were

CPM cutoff >2 and sample cutoff 2 between the replicates for the analyzed groups (WT-Mutation clone 1, WT-Mutation clone 2, Unmodified clone-Mutation clone 1, Unmodified clone -Mutation clone 2). The RUv package from Bioconductor was used to eliminate batch effects. Therefore, all of the samples were normalized to TMM (weighted trimmed mean of M-values). Gene counts were used for differential expression analysis using the EdgeR package.

The gene ontology enrichment was performed using ShinyGo v0.61(KEGG, FDR 0.1). The common genes from categories were selected and made heatmaps using the complexheatmap package from Bioconductor[177].

2.3.5.12 Pro-apoptosis analysis

The 1% Matrigel solution was prepared in S7 media to coat the wells of the 6-well plate. 1.5 mL microcentrifuge tubes and pipette tips were pre-coated with 0.2% BSA in PBS. 20 µL of organoids were treated with 300 µL TrypLE (10X) to dissociate to single cells and then washed with 1 mL 0.2% BSA. The cell pellet was re-suspended with 2 mL S7 media supplemented with CloneR after aspirating supernatant. The cells were incubated for two days in a CO_2 incubator.

The flat culture cells were treated with 300 µL TrypLE (10X) to dissociate to single cells and then washed with 1 mL 0.2% BSA. FITC Annexin V antibodies and 7-AAD were loaded into 100 µL cells suspension aliquot to analyze pro-apoptosis following the manufacturer's instructions. 0.5 µL FITC isotypes were loaded into 50 µL isotope control. Cells were suspended into 200 µL 1X binding buffer after aspirating supernatant. One well of cells were treated with 200 µM H_2O_2 6 hr as a positive apoptosis sample for compensation setting. The samples were analyzed on a flow cytometer after the compensation setting. The exported FACS data were analyzed using FlowJo.

2.4 Statistical analysis

All qRT-PCR data were analyzed by the △△Ct method. Data were analysed for normal distribution where applicable. Data were analyzed using unpaired/paired t-tests. Dynamic Ca^{2+} flux was analyzed using two-way ANOVA and was generated with Prism8. Figures with boxes, violins, or plots were generated with Prism8. The DNA sequence was visualized on Benchling. FlowJo was used to analyze Flow cytometry

data. Immunofluorescence analysis was performed with Fiji. The intensity of protein on the PVDF membrane was analyzed with GelAnalyzer.

3. Results

3.1 The differentiation of patient-derived hiPSCs to functional β cells is problematic.

To decipher the patient's phenotype, Dr. Sebastian Diecke generated hiPSCs from our neonatal diabetes patient (KCNQ1^{R397W}) and his brother (heathy control) blood material. These hiPSCs expressed pluripotency markers, including *Nanog*, *Oct4*, and *Sox2* (Figure 11B). Both of hiPSCs stained positive for Oct4, Sox2, and Tra-1-81 (Figure 11A). The two hiPSC lines were subjected to the embryoid body (EB) formation[178]. Unfortunately, the EB random differentiation results were consistent with the observation of Thruner *et al*.[42], indicating that our hiPSCs generated from PBMC (originates from mesoderm) had a bias to differentiate to ectoderm and mesoderm (Figure 11C). Generated patient's hiPSCs and healthy hiPSCs had variable differentiation efficiencies consistent with the observation of Grabundzija *et al*.[43], indicating that our hiPSCs had a different expression of the gene markers of germ layers (Figure 11C).

CRISPR/Cas9 engineering was used to correct the mutation and generated CRISPR-corrected hiPSCs. I initially tried to differentiate hiPSCs to functional β cells, using the optimized Resania's protocol[44]. Unfortunately, the results were only (semi)reproducible, and the hiPSC lines could not be fully differentiated further from the pancreatic endoderm stage, expressing low *PDX1* level (Figure 12). Following consultation with experts of the field (e.g., to differentiate hiPSCs to functional β cells), I learned that the differentiation of hiPSCs is indeed a common problematic. Fortunately, the laboratory of our collaborator Prof. Dr. M. Sander (UC San Diego), has established a further-optimized differentiation protocol of β cells[44] using human embryonic stem cells (hESC_H1) that is reproducible and suitable for obtaining functional β cells.

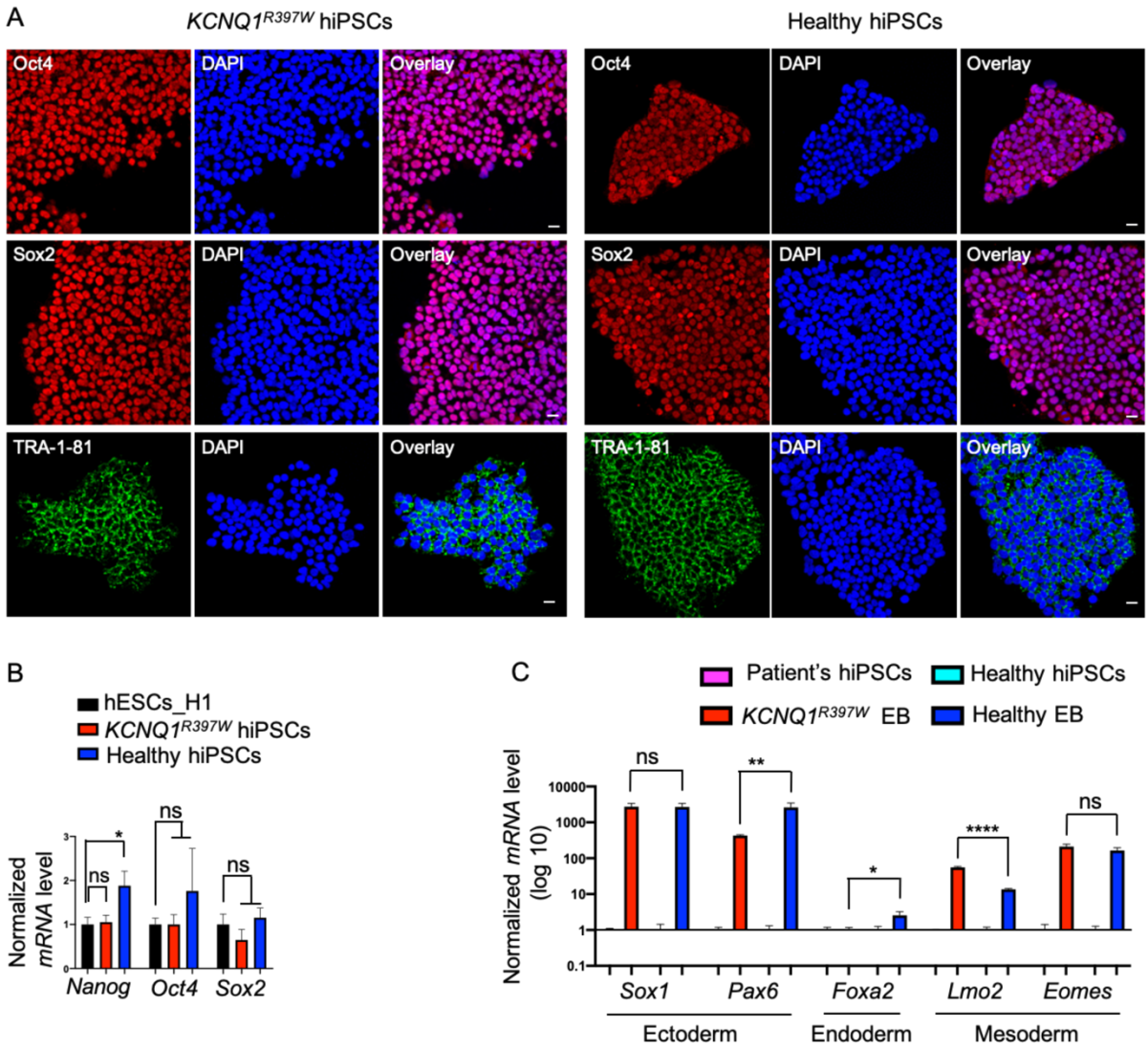

Figure 11. Pluripotency characterization of hiPSCs. (A) Immunostaining of pluripotency markers Oct4, Sox2, and Tra-1-81. (B) hiPSCs, including patient-derived mutant KCNQ1^{R397W} and healthy, were characterized by qRT-PCR using markers of pluripotency *Nanog*, *Oct4*, and *Sox2*. (C) EBs derived from hiPSCs, including patient-derived KCNQ1^{R397W} and healthy, were characterized by qRT-PCR using markers of the three germ layers. Data was relative to respective undifferentiated hiPSCs. qRT-PCR data were normalized to *Gapdh*. Scale bar=20 µm. The data presented as mean ± SD. p values calculated by unpaired two-tailed t-test. n.s indicates a non-significant difference, $p < 0.05$ (*), $p < 0.01$ (**), $p < 0.001$ (***), and $p < 0.0001$ (****). hiPSCs were generated by Dr. Sebastian Diecke; the analysis was performed by me.

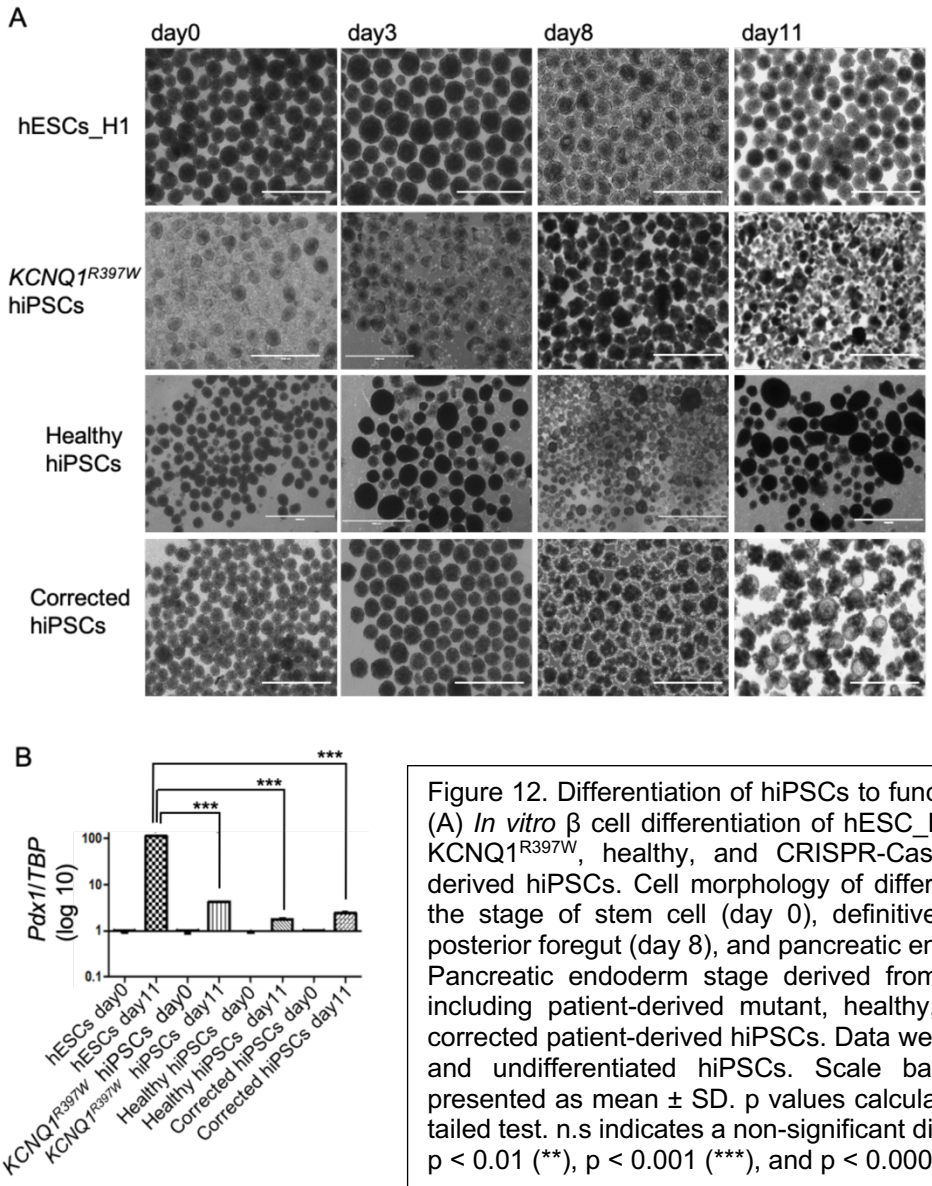

Figure 12. Differentiation of hiPSCs to functional β cells *in vitro*. (A) *In vitro* β cell differentiation of hESC_H1, hiPSCs including KCNQ1^{R397W}, healthy, and CRISPR-Cas9 corrected patient-derived hiPSCs. Cell morphology of different stages, including the stage of stem cell (day 0), definitive endoderm (day 3), posterior foregut (day 8), and pancreatic endoderm (day 11). (B) Pancreatic endoderm stage derived from hESC_H1, hiPSCs including patient-derived mutant, healthy, and CRISPR-Cas9 corrected patient-derived hiPSCs. Data were normalized to *TBP* and undifferentiated hiPSCs. Scale bar=1 mm. The data presented as mean ± SD. p values calculated by unpaired two-tailed test. n.s indicates a non-significant difference, $p < 0.05$ (*), $p < 0.01$ (**), $p < 0.001$ (***), and $p < 0.0001$ (****).

3.2 KCNQ1 homozygous mutant hESC_H1 was generated by the CRISPR-Cas9 system.

To further decipher the mechanism of patient's phenotype, I used CRISPR/Cas9 engineering to generate homozygous point mutation (1189 C>T) in hESCs_H1 mimicking our neonatal diabetes patient. The web tool of Tide (http://shinyapps.datacurators.nl/tide/) showed that pre-genome editing occurred in 97.5% and 68.6% of two hESCs with transfected sgRNAs expressed CRISPR plasmids, respectively (Figures. 13A and 13B).

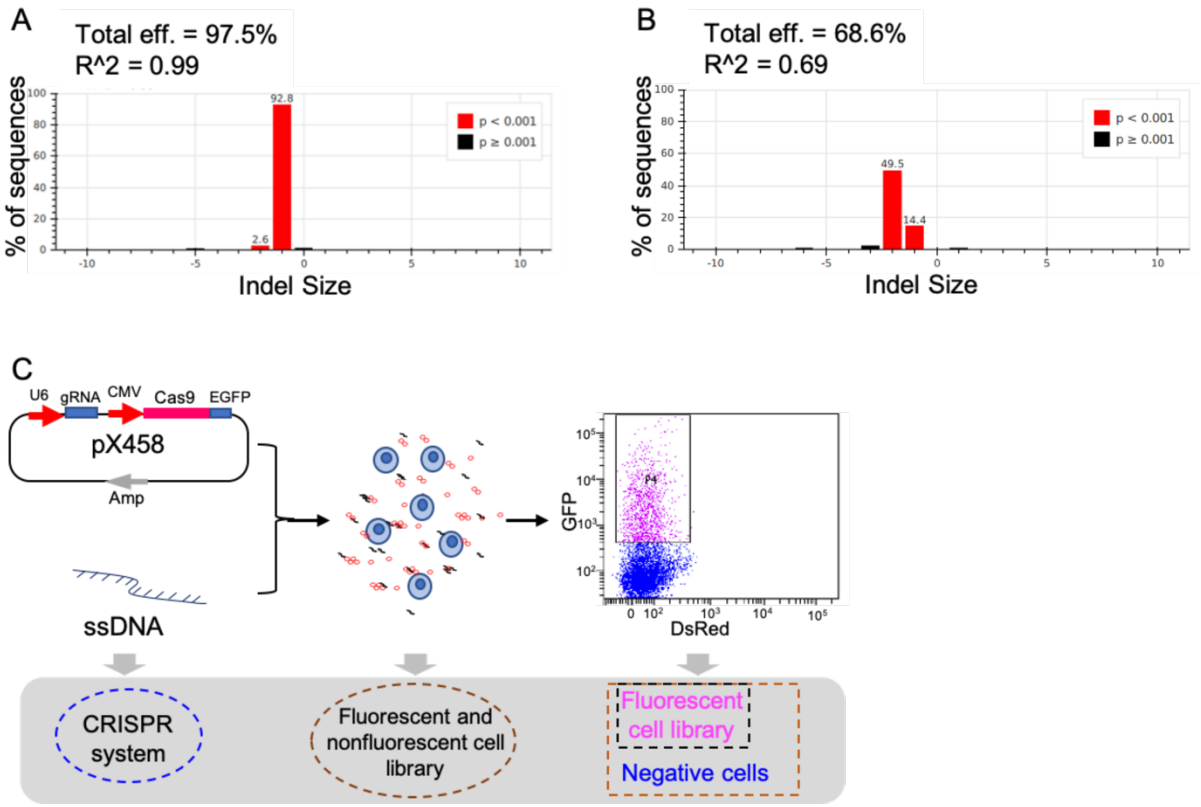

Figure 13. Validation of candidate sgRNA and colonies. (A and B) sgRNAs frequency of targeted mutation locus. (C) Schematic diagrams illustrated homology-directed genome editing by CRISPR-Cas9 using asymmetric donor DNA. Firstly, hESC_H1 was co-transfected with CRISPR plasmids and ssDNA. The EGFP fluorescence gene in the plasmid was used as a positive marker to sort co-transfected hESCs. The gene-edited hESCs were included in the positive sorted hESCs library.

To select stable hESCs colonies from the fluorescent cell library (Figure 13C), qRT-PCR was used to analyse the expression of pluripotency markers, including *Nanog*, *Oct4*, and *Sox2* (Figures 14A, 14B, and 14C). To eliminate the potential off-target events generated by the CRISPR system, we selected one unmodified clone and two *KCNQ1*^{R397W} clones from the fluorescent cell library. The colonies were confirmed by Sanger sequencing (Figure 14D).

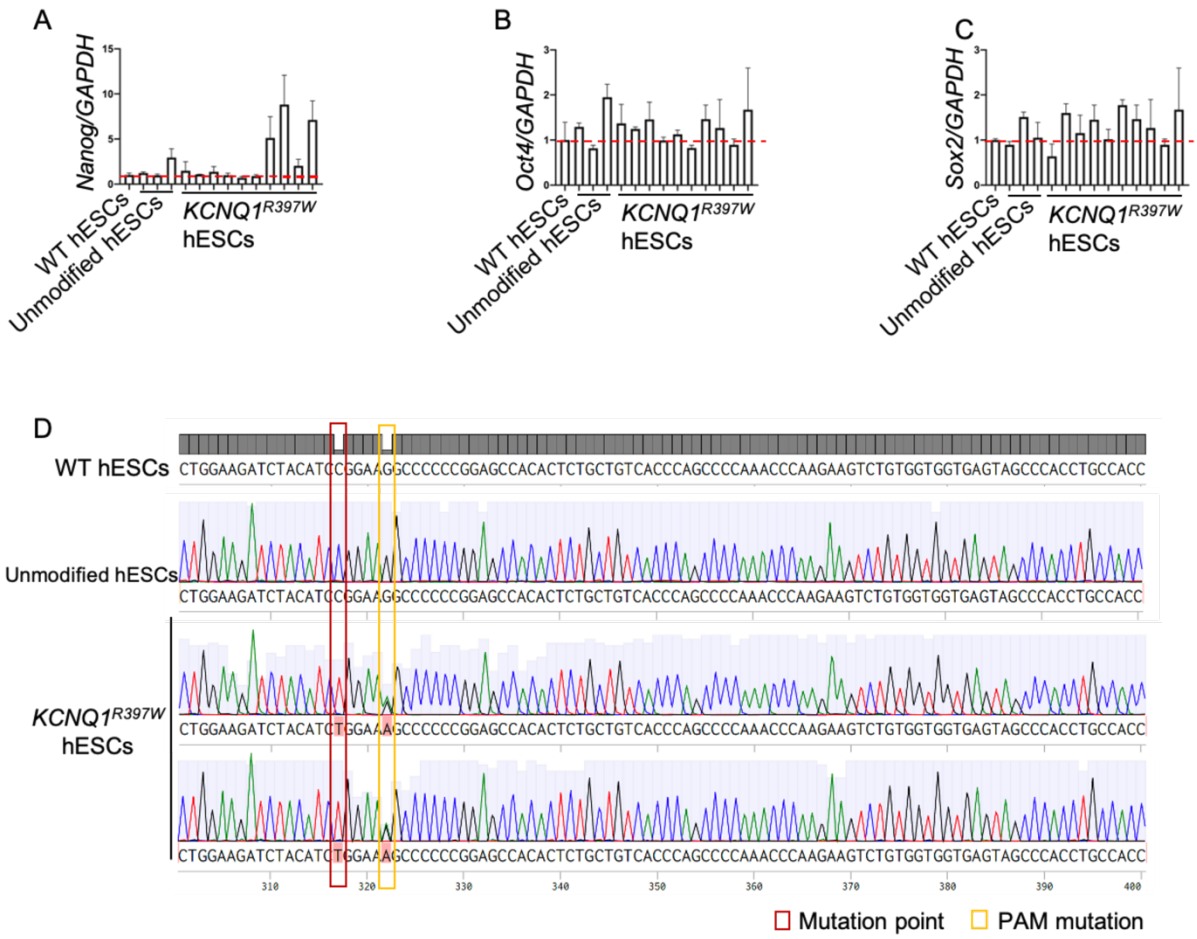

Figure 14. Generation KCNQ1 homozygous mutant hESCs_H1 by CRISPR-Cas9 system. Candidate hESC colonies were characterized by qRT-PCR using markers of pluripotency, including *Nanog* (A), *Oct4* (B), and *Sox2* (C). Data were normalized to *Gapdh*. The data presented as mean ± SD. (D) Sanger DNA sequencing results of WT, unmodified, and KCNQ1^{R397W} hESCs. The patient's mutation is shown in the red box. Cas9 related PAM mutation is shown in the yellow box.

To remove the differentiated cells from all colonies, we used Anti-Tra-1-60-PE antibody and anti-PE microbeads selection, and sorted out the pluripotent stem cells. At the end of the procedure, all generated colonies had expressed similar levels of *Oct4*, *Sox2*, and *Nanog* to hESCs_H1(Figure 15A). In addition, all generated colonies had identical hESCs morphology and stained positive of Sox2 and Oct4 (Figure 15B).

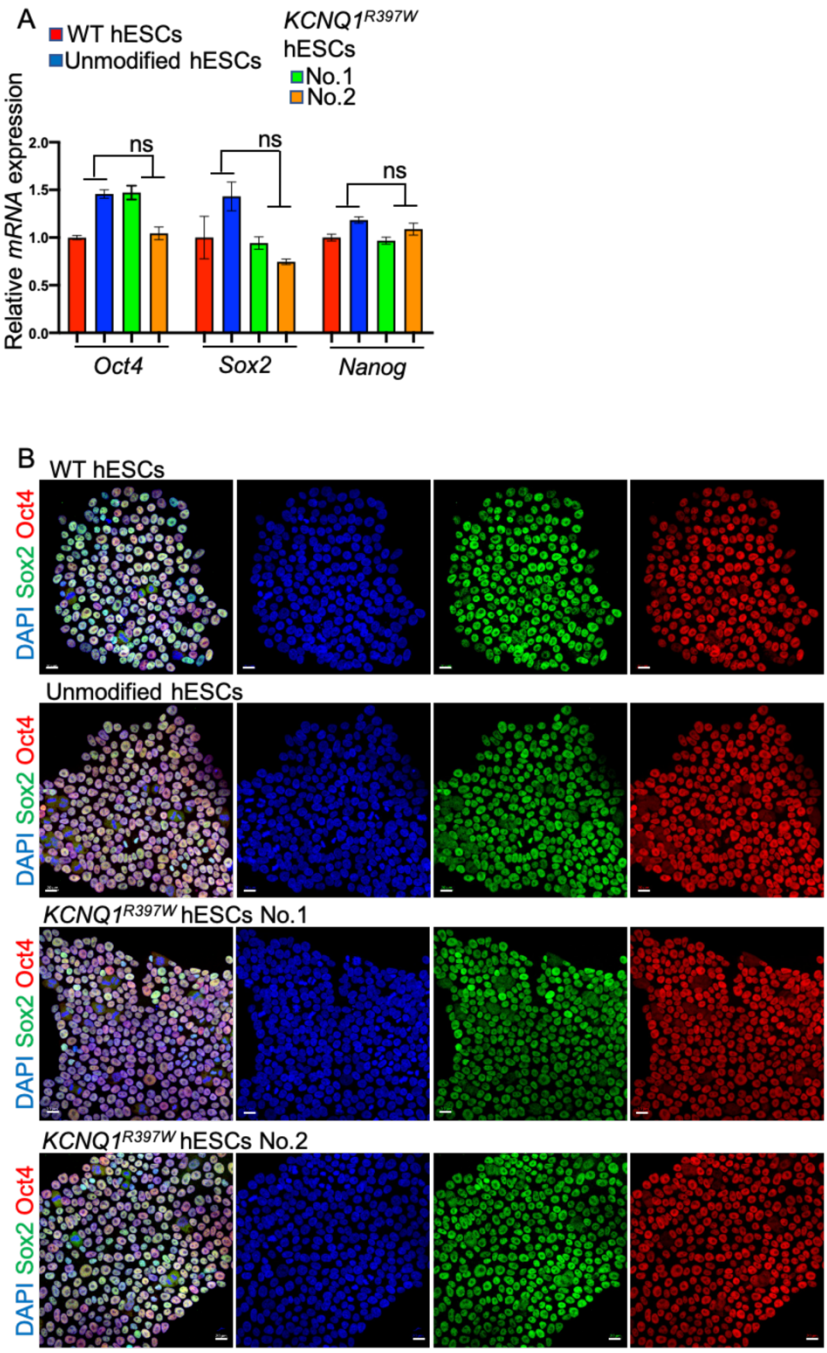

Figure 15. Generation highly pluripotent KCNQ1 homozygous mutant hESCs_H1. (A) WT, unmodified, and KCNQ1^{R397W} hESCs were characterized by qRT-PCR using markers of pluripotency (*Oct4*, *Sox2*, and *Nanog*). Data were normalized to *Gapdh* and presented as mean ± SD. (B) Immunostaining of pluripotency markers Sox2 and Oct4. Scale bar=20 μm. All of the data are presented as mean ± SD. p values calculated by unpaired two-tailed t-test. n.s indicates a non-significant difference, $p < 0.05$ (*), $p < 0.01$ (**), $p < 0.001$ (***), and $p < 0.0001$ (****).

3.3 KCNQ1^{R397W} hESCs_H1 could differentiate to human pancreatic islet-like organoids.

To decipher the islet development of the KCNQ1^{R397W} hESCs_H1, two KCNQ1^{R397W} hESC lines together with one unmodified hESC from the fluorescent cell library and

one WT hESC_H1 line were differentiated toward insulin^{+} cells using a protocol modified and combined from Rezania's and Leonardo's protocol[44,46]. The morphology of organoids was recorded daily between KCNQ1^{R397W} hESC lines (KCNQ1^{R397W} #1/2), unmodified hESCs (UC), and WT hESCs (WT). No significantly different morphology was detected between organoids (Figure 16).

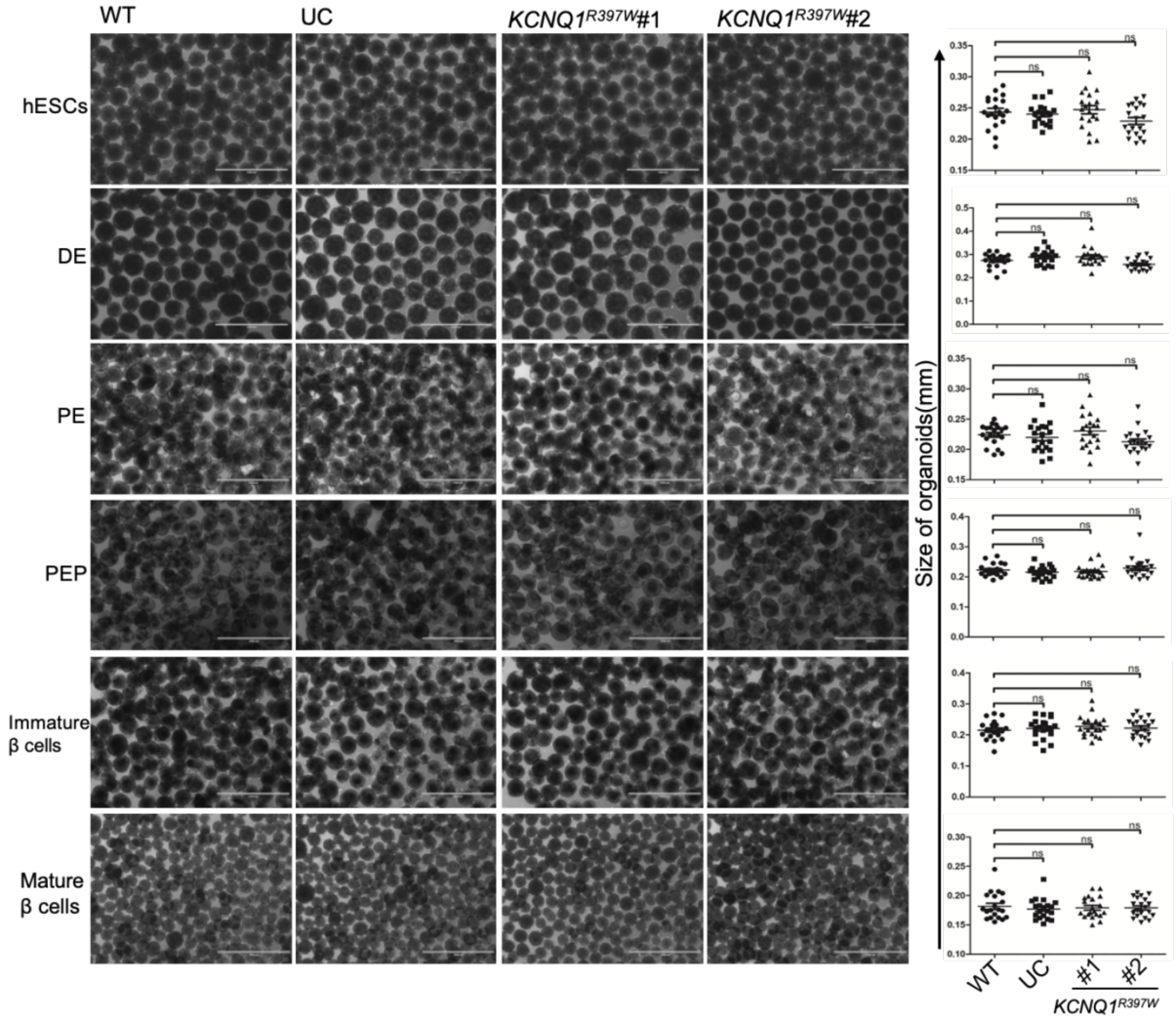

Figure 16. The morphology and size quantification of six-stage differentiated organoids. Cell morphology of different stages, including the stage of hESCs (day 0), DE (day 3), PE (day 11), pancreatic endocrine precursors (PEP, day 14), immature β cells (day 21), and mature β cells (day 32). The stage-specific organoids were derived from KCNQ1^{R397W} hESC lines (KCNQ1^{R397W} #1/2), unmodified hESCs (UC), and WT hESCs (WT). Scale bar=1 mm. Data are presented as mean ± SD. p values calculated by unpaired two-tailed t-test. n.s indicates a non-significant difference, $p < 0.05$ (*), $p < 0.01$ (**), $p < 0.001$ (***), and $p < 0.0001$ (****).

To monitor the differentiation process, I used flow cytometry and quantified cells against the stage-specific markers at each stage (Figure 17). The percentage of PDX1^{+} cells (PE; Figures 17A and 17B), double-positive of PDX1^{+} and NKX6.1^{+} cells (PEP;

Figures 17C and 17D), double-positive of insulin^{+} and NKX6.1^{+} cells (immature β cells; Figures 17E and 17F), and insulin+ cells (mature β cells; Figures 17G and 17H) were determined, but did not differ between samples.

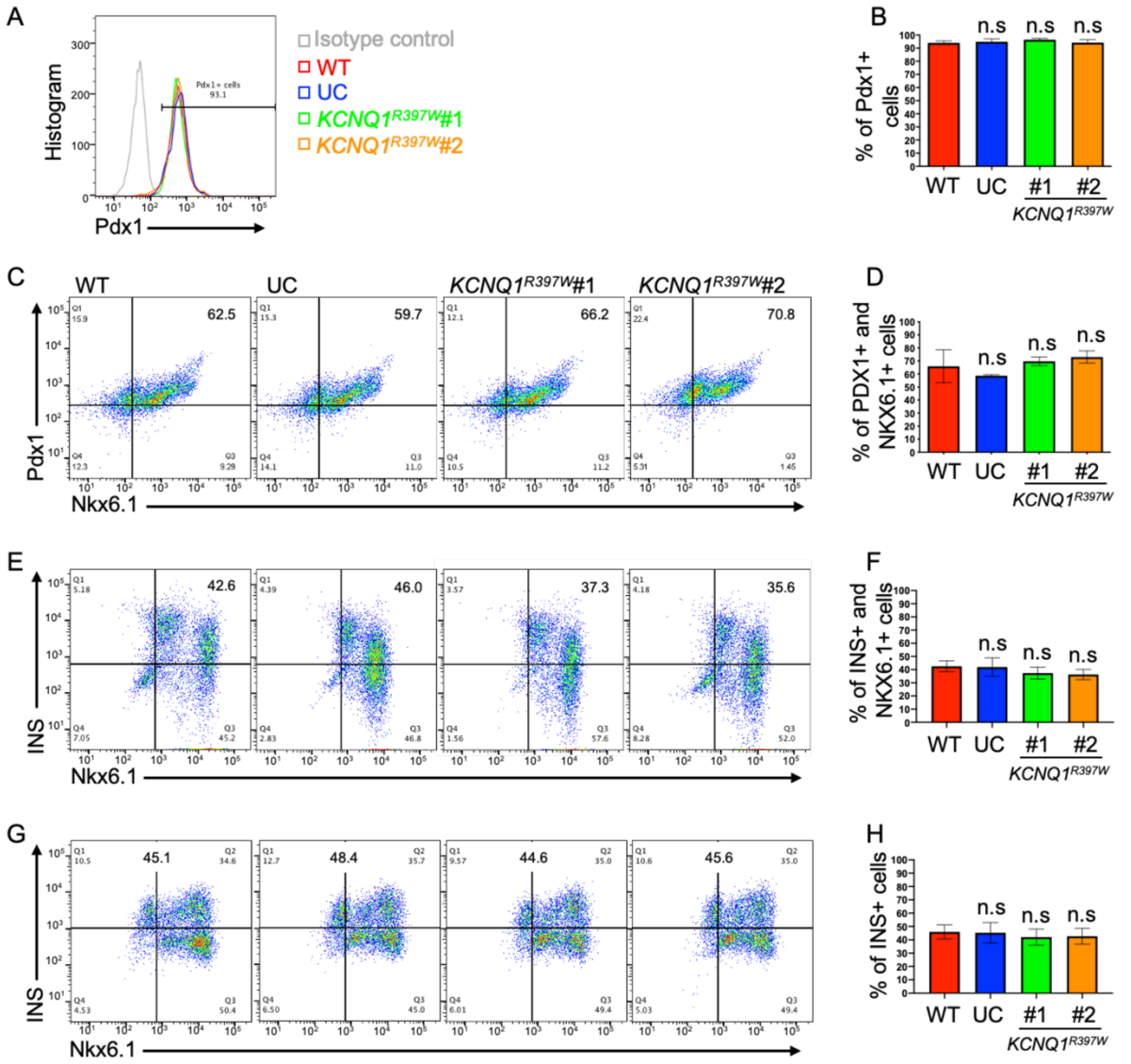

Figure 14. The differentiation efficiency analysis of the last four-stage differentiated organoids by flow cytometry. Flow cytometry analysis (A, C, E, and G) and quantification (B, D, F, and H) of cells with stage-specific makers. (A and B) Pancreatic endoderm cells express PDX1. (C and D) Pancreatic endocrine precursor cells express PDX1 and NKX6.1. (E and F) Immature β cells express Nkx6.1 and insulin. (G and H) Mature β cells express insulin. Data presented as mean ± SD. p values calculated by unpaired two-tailed t-test. n.s indicates a non-significant difference, $p < 0.05$ (*), $p < 0.01$ (**), $p < 0.001$ (***), and $p < 0.0001$ (****).

The reference gene *TBP* expression is stable in the β-cell differentiation. Therefore, I used *TBP* to quantify the other genes expression during the β-cell differentiation. RT-qPCR indicated that the expression of the marker of β cells characterized by *insulin*, α cells characterized by *glucagon*, did not differ between samples (Figure 18A). The

percentage of Insulin$^+$ or glucagon$^+$ cells in pancreatic islet-like organoids were similar between samples in immunoassay as well (Figures 18B-18D).

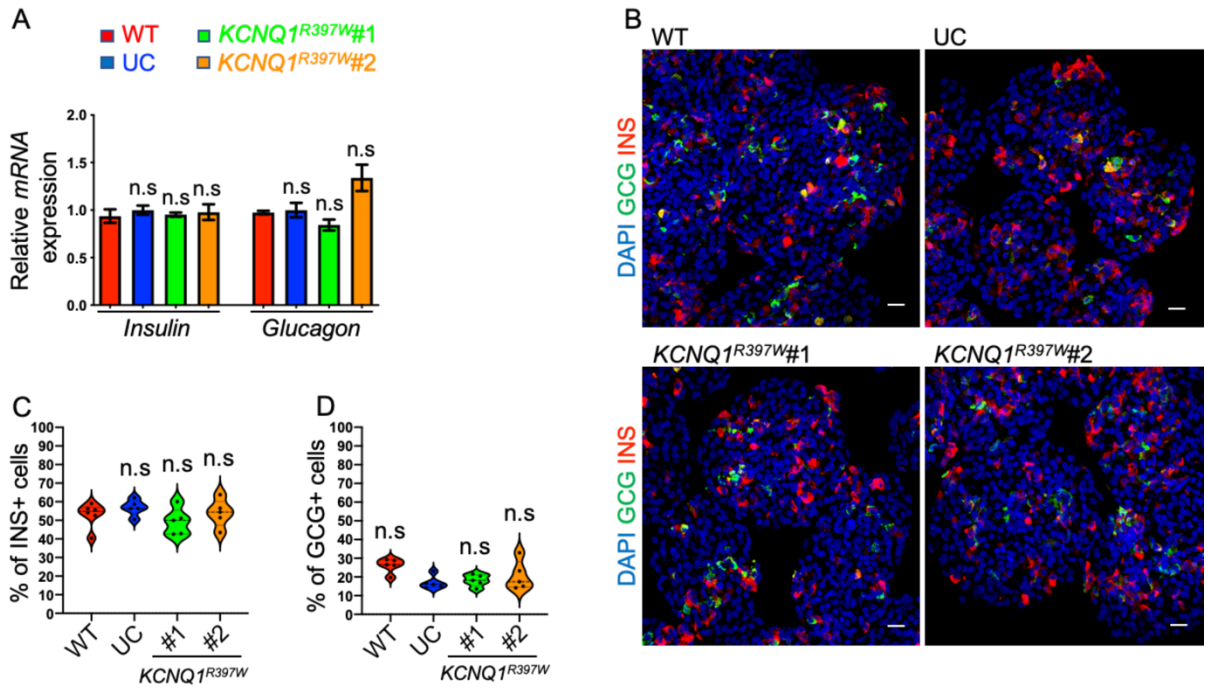

Figure 18. Characterization of human pancreatic islet-like organoids. (A) Pancreatic islet-like organoids from WT, UC, and KCNQ1^{R397W} were characterized by qRT-PCR using makers of β cells (*insulin*) and α cells (*glucagon*). Data were normalized to *TBP* and presented as mean ± SD. Immunostaining (B) and quantification of insulin$^+$ (INS+, C) and glucagon$^+$ (GCG+, D) were characterized in the stage of maturing β cells. Scale bar=20 μm. Data presented as Violin plots. p values calculated by unpaired two-tailed t-test. n.s indicates no significant difference, $p < 0.05$ (*), $p < 0.01$ (**), $p < 0.001$ (***), and $p < 0.0001$ (****).

The proliferation of human β cells is extremely low, with a range from 3.2 ± 0.5% in juvenile to 0.13 ± 0.08% in adult[179]. To analyze the proliferative feature of β-like cells, the proliferation marker (Ki67) was used to mark the cells with propagation. The day 32 of β-like cells had a low proliferation ability (2-5%, Figure 19B), being consistent with the reported human adult β cells[179]. Immunostaining showed that *KCNQ1* mutation did not affect the proliferation of pancreatic islet organoids derived from KCNQ1^{R397W} hESCs (Figure 19). Thus, taken together, the results showed that KCNQ1^{R397W} hESCs could normally differentiate to human pancreatic islet-like organoids behaved similarly to WT and unmodified hESCs.

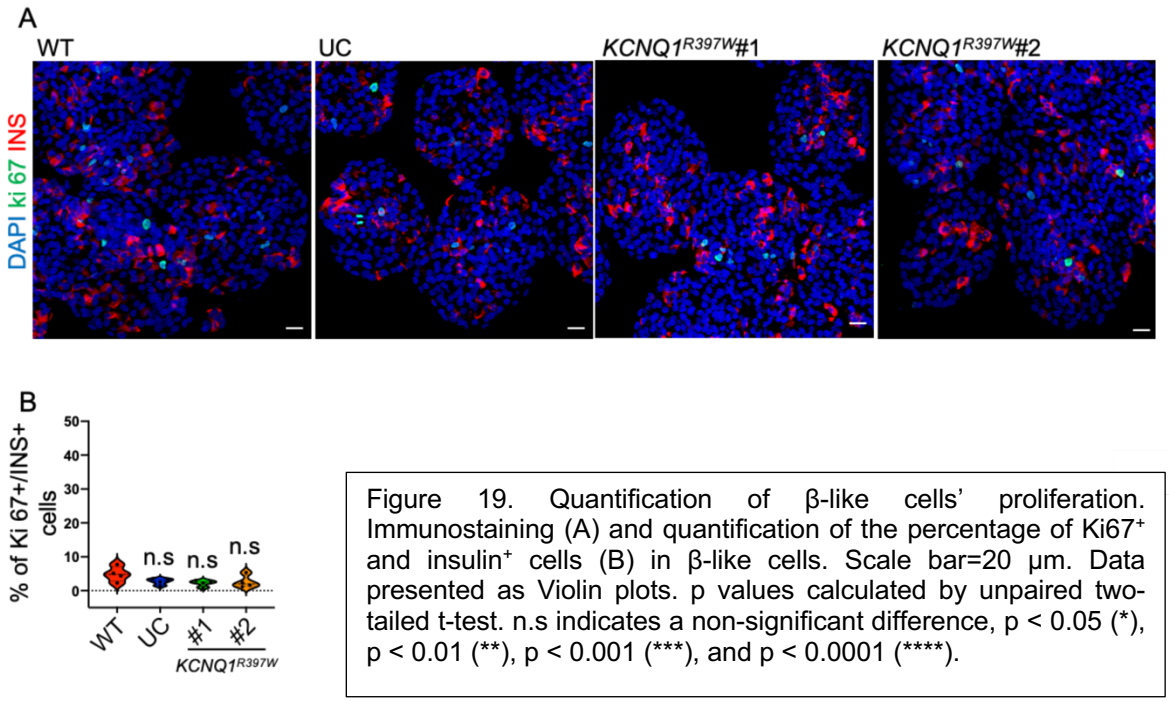

Figure 19. Quantification of β-like cells' proliferation. Immunostaining (A) and quantification of the percentage of Ki67^{+} and insulin^{+} cells (B) in β-like cells. Scale bar=20 μm. Data presented as Violin plots. p values calculated by unpaired two-tailed t-test. n.s indicates a non-significant difference, $p < 0.05$ (*), $p < 0.01$ (**), $p < 0.001$ (***), and $p < 0.0001$ (****).

3.4 The KCNQ1^{R397W} accelerated membrane repolarization of human β-like cells.

3.4.1 KCNQ1^{R397W} and neighboring genes did not aberrant expression.

According to published RNAseq data (E-MTAB-1086)[132], the KCNQ1 transcript level was gradually increasing between human pancreatic endoderm and transplanted islets (figure 20A). I found that the transcript of KCNQ1 could be detected using RT-qPCR from day 28 in the maturing β-like cells (data not shown), suggesting that KCNQ1 is required for the β-cell developing. However, the KCNQ1 transcript level did not differ between β-like cells derived from controls (WT and UC) and KCNQ1^{R397W} (Figure 20B).

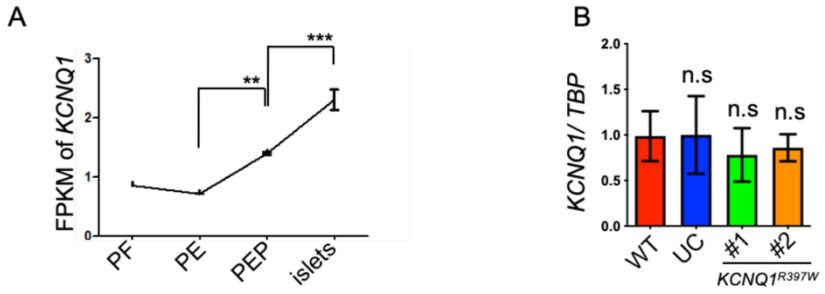

Figure 20. The expression of *KCNQ1* in stepwise differentiation. (A) FPKM (Fragments per kilobase of transcript per million mapped reads) showed the mRNA level of *KCNQ1* during human pancreatic differentiation, including posterior foregut (PF), PE, PEP, and mature islets after transplanted into mouse[132]. p values calculated by one-way ANOVA. (B) The *KCNQ1* mRNA level was analyzed by qRT-

PCR in pancreatic islet-like organoids of WT, UC, and KCNQ1^{R397W}. Data were normalized to *TBP* expression. p values calculated by unpaired two-tailed t-test. Data presented as mean ± SD. n.s indicates a non-significant difference, $p < 0.05$ (*), $p < 0.01$ (**), $p < 0.001$ (***), and $p < 0.0001$ (****).

The *KCNQ1* gene is located in an imprinted genomic array, controlled by the lncRNA *KCNQ1OT1*[125]. The paternal allelic knockout *KCNQ1* has been reported to influence pancreatic β cell mass development by regulating KCNQ1ot1 and other flanking genes in pancreatic β-cells of mice[125]. Besides, a proper level of CDKN1C is required for regulating the proliferation of β cells[130]. To identify the association between the mutation (1189 C>T) and *KCNQ1* flanking genes, we performed qRT-PCR on pancreatic β-like cells. The neighboring genes, including *KCNQ1OT1*, *CDKN1C*, and *Slc22a18*, were transcribed at similar level in all samples (Figure 21). However, the expression *PHLDA2* was undetermined in all samples.

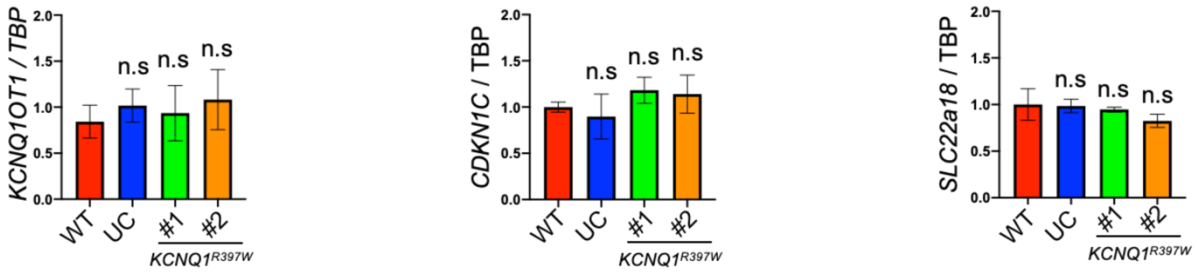

Figure 21. *KCNQ1^{R397W}* neighboring genes did not show aberrant expression. The expressions of neighboring genes were analyzed by q-PCR. Data were normalized to *TBP* and presented as mean ± SD. n.s indicates a non-significant difference.

The homozygous point mutation of our patient was predicted as a methylated cytosine. The previous research has shown that one methylation in exon11 affects KCNE3 expression due to splicing[180]. To analyze the genomic methylation of *KCNQ1*, I performed sodium bisulfite conversion and sequencing. The assay confirmed that the mutation locus was a methylated cytosine, and stayed stable in WT during the differentiation process (Figure 22). Unlike the WT, the mutation (1189 C>T) interfered this methylation in the mutated clone.

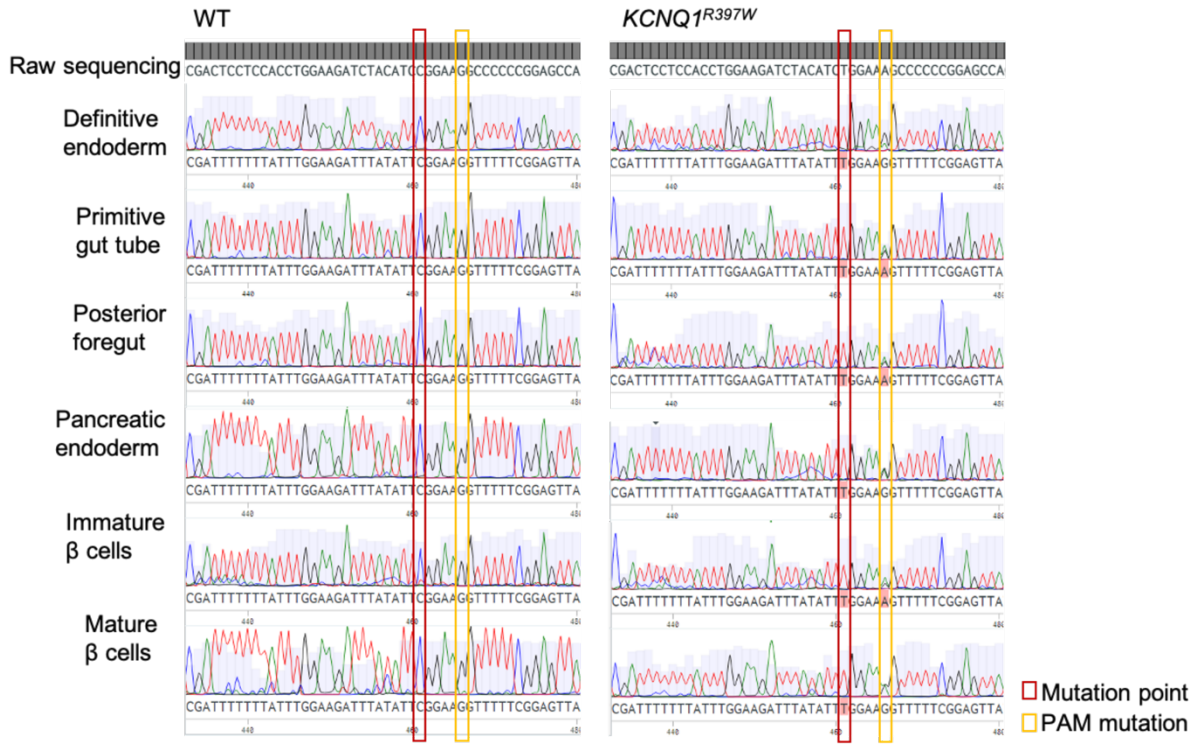

Figure 22. Methylation was interfered in *KCNQ1* mutation locus during pancreatic differentiation, including definitive endoderm, primitive gut tube, posterior foregut, pancreatic endoderm, immature β cells, and mature β cells. The patient's mutation is shown in the red box. Cas9 related PAM mutation is shown in the yellow box.

The human KCNQ1 have kidney isoform (676 amino acids) and pancreas isoform (549 amino acids)[181,182]. In the Western blot analysis, only one isoform was detectable on the PVDF membrane (Figure 23A). Thus, the mutation (1189 C>T) did not influence KCNQ1 expression either at the mRNA level or at the protein level (Figures 20B and 23A). Furthermore, 3D confocal scanning microscopy of immunoassay showed that both the $KCNQ1^{WT}$ and $KCNQ1^{R397W}$ were detectable on the surface of cytosolic insulin, indicating that being consistent with $KCNQ1^{WT}$, $KCNQ1^{R397W}$ could target the membrane of $insulin^{+}$ cells. Immunostaining results suggested that the mutation did not affect KCNQ1 membrane targeting (Figures 8B and 23B).

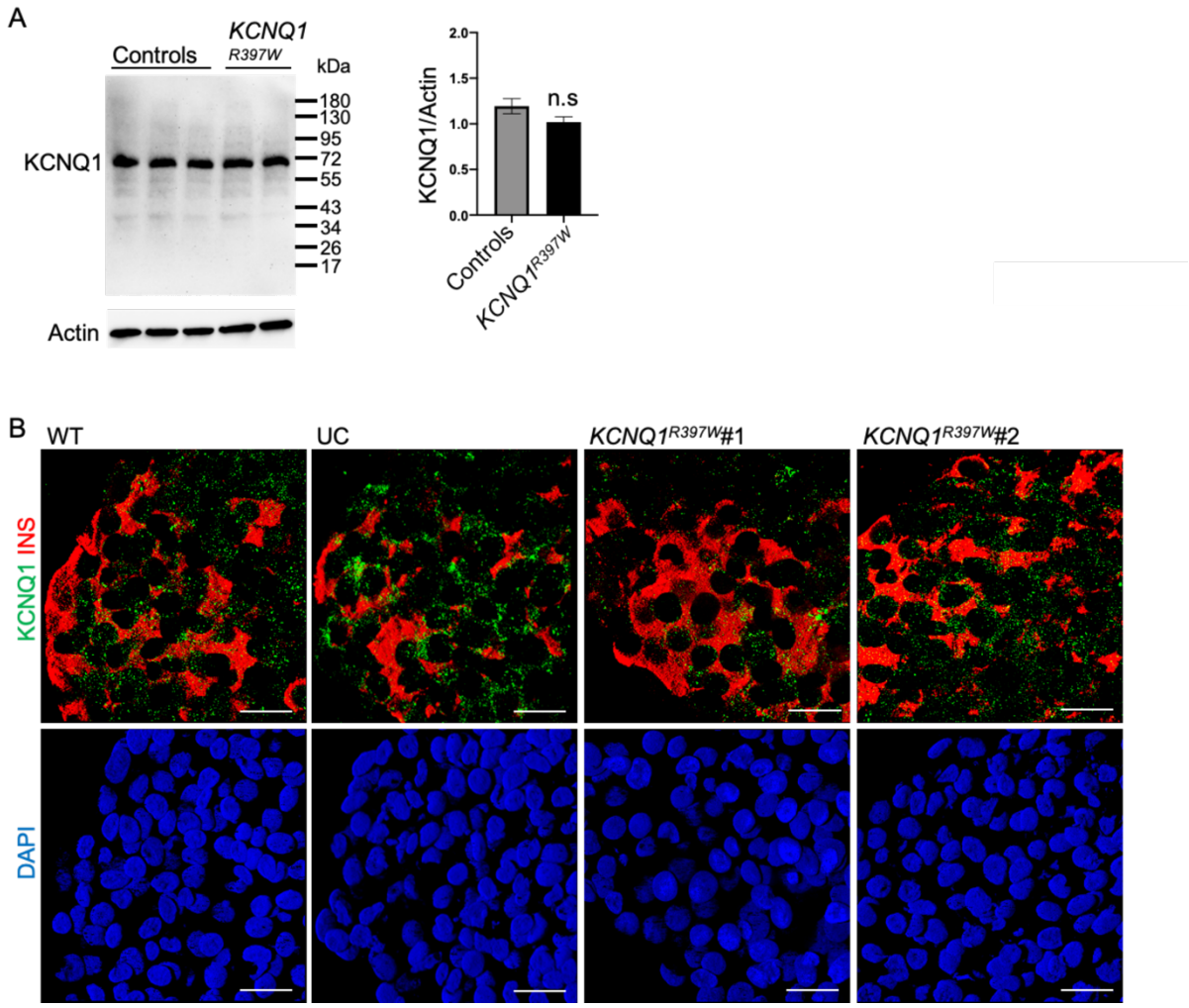

Figure 23. KCNQ1 expression and location analysis. (A) Western blotting analysis and quantification of KCNQ1 expression in pancreatic islet-like organoids of controls (WT and UC) and KCNQ1^{R397W}. Data were normalized to Actin. (B) Immunostaining of insulin and KCNQ1 in the stage of maturing β cells shown by 3D confocal scanning. Scale bar=20 μm. Data presented as mean ± SD. p values calculated by unpaired two-tailed t-test. n.s indicates a non-significant difference, $p < 0.05$ (*), $p < 0.01$ (**), $p < 0.001$ (***), and $p < 0.0001$ (****).

3.4.2 The KCNQ1^{R397W} inhibited K_V7.1 channel function and increased the frequency of action potential firing in human β-like cells.

Glucose uptake stimulated phases of depolarization and repolarization can determine insulin secretion in pancreatic β cells[183]. Depolarization can induce spike activity in pancreatic β cells[64]. High glucose increases the action potential firing of mouse and human β cells[183,184]. Previous research shows that a block of K_V7.1 channels increases glucose-stimulated insulin secretion by increasing action potential firing and cytoplasmic Ca^{2+} concentration in rat islets[91]. To confirm the mutation affecting the function of K_V7.1 channel, I recorded the electrical activity of β-like cells induced by

low glucose (5.5 mM) and high glucose (20mM). For the induction, we also used 10 μM Chromanol 293B, an inhibitor of Kv7.1 channel at low glucose concentration (Figure 24A). The fold of spike frequency was quantified between the spike frequencies induced by high glucose and low glucose with or without Chromanol 293B. The background of electrical activity was minimized with 3.3 mM glucose. Consistent with K_V7.1 blocked by Conkunitzin-S1 in rats[91], the presence of Chromanol 293B also increased the frequency of action potential firing, when compared with the low glucose (5.5 mM) stimulation in UC β-like cells (Figure 24). Unlike pancreatic β-like cells of UC, KCNQ1^{R397W} β-like cells had a higher frequency of action potential firing at 5.5 mM glucose (Figure 24), suggesting that KCNQ1^{R397W} caused K_V7.1 dysfunction, that accelerated the membrane repolarization of β-like cells.

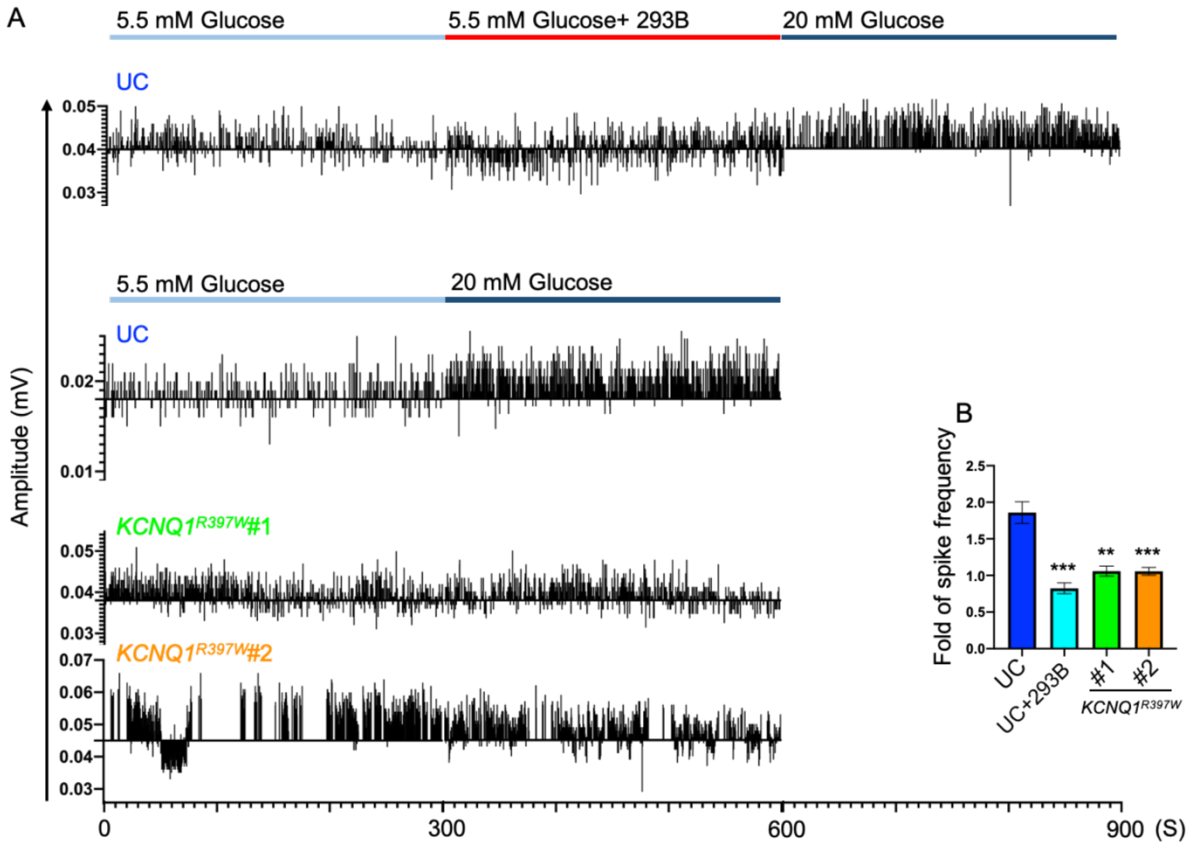

Figure 24. The analysis of β-like cell action potential. Recording of electrical activity (A) and quantification of spike frequency (B) of β-like cells induced by 5.5 mM glucose with/without 10 μM Chromanol 293B (293B) and 20 mM glucose. Data presented as mean ± SD. p values calculated by unpaired two-tailed t-test. n.s indicates a non-significant difference, $p < 0.05$ (*), $p < 0.01$ (**), $p < 0.001$ (***), and $p < 0.0001$ (****).

3.5 KCNQ1^{R397W} results in the accumulation of cytosolic free Ca^{2+} in human β-like cells.

The blockade of K_V7.1 channels increases cytoplasmic Ca^{2+} concentration resulting in hyperinsulinemia in rat[91]. To test the phenotype in human β-like cells and decipher the effects of the mutation in gene expression, Dr. Amit Pande and I performed a RNAseq analysis using β-like cells at day 32. Gene ontology (GO) analysis of differentially expressed genes revealed that the most effect cellular processes were oxidative phosphorylation, cAMP and MAPK pathways, and MODY in KCNQ1^{R397W} β-like cells compared with control (WT and UC) β-like cells (Figures 25A and 25B).

The oxidative phosphorylation process produces ATP and NADPH, malonyl-CoA, and glutamate in the citric acid cycle by mitochondria, crucial for K_{ATP} channel-dependent insulin secretion in β cells[10,185]. The multiple genes involved in oxidative phosphorylation were up-regulated (Figure 25C), which could increase the ATP synthesis and close K_{ATP} channels, opening Ca_V channels in β-like cells.

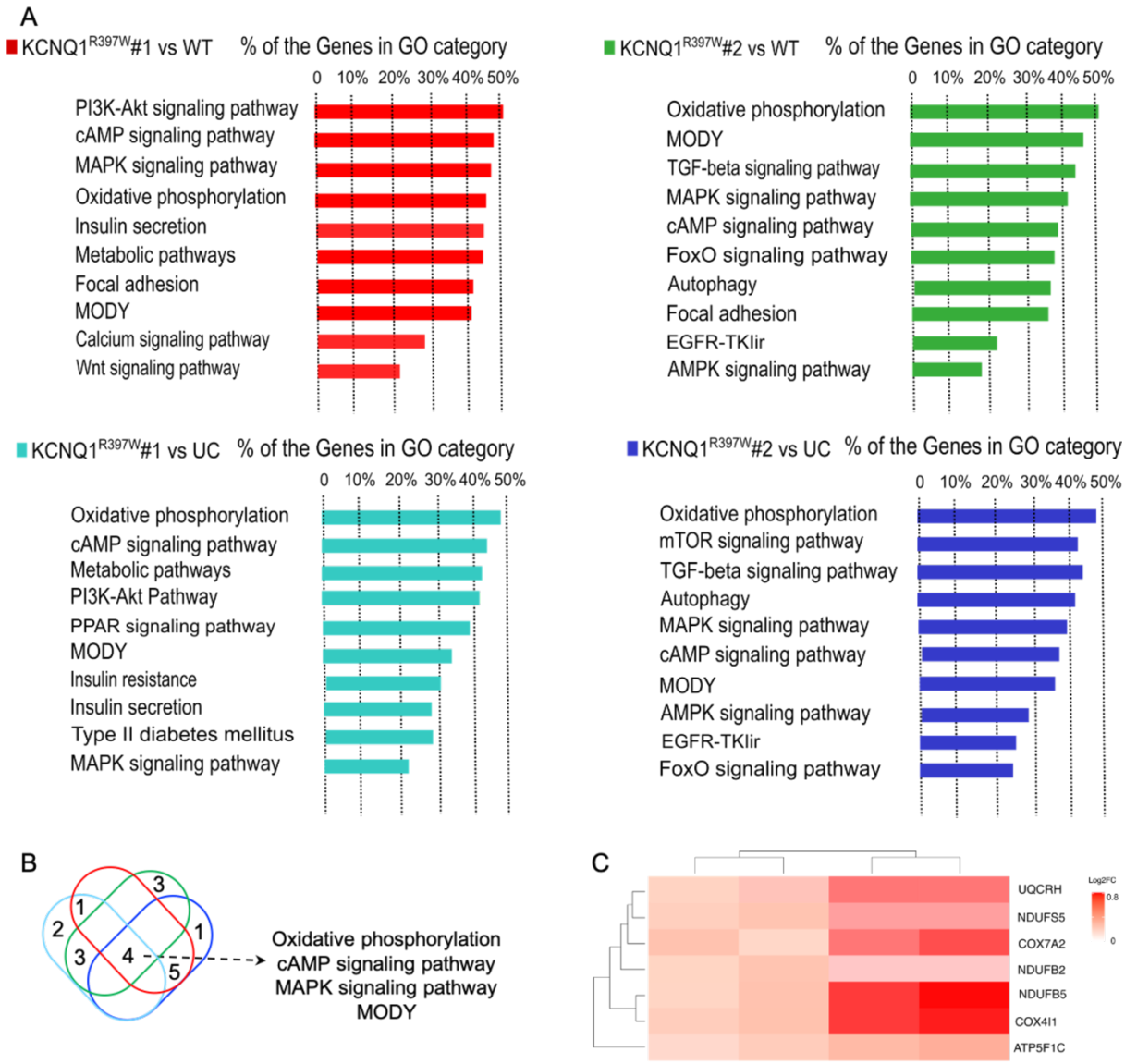

Figure 25. Go category of targeted protein coding genes from KCNQ1^{R397W} β-like cells compared with control (WT and UC) β-like cells at day 32. (A) GO analysis of differentially expressed genes. (B) The intersection calculation of four comparison groups (*KCNQ1^{R397W}*#1/#2 vs. UC/WT). (C) Heatmap represented the genes of differential expression in the oxidative phosphorylation process. The images were generated by Dr. Amit Pande and me.

A periodic change of glucose concentration can synchronize the activity of healthy β cells through calcium signaling[45]. To monitor cytoplasmic Ca^{2+} concentration in human β-like cells, I used Ca^{2+} labelled with Fluo-4AM to analyze Ca^{2+} flux. β-like cells were performed in response to a periodic change of glucose concentration or under Chromanol 293B treatment. The Ca^{2+} flux analysis showed that human β-like cells derived from all cell lines and human pancreatic islets increased cytoplasmic Ca^{2+} concentration in response to stimulation with 20 mM glucose compared with 2 mM glucose condition (Figure 26). Notably, human β-like cells derived from KCNQ1^{R397W} had higher cytoplasmic Ca^{2+} concentration compared with WT and UC β-like cells

(Figure 26A). Periodic exposure to chromanol 293B had a synchronizing effect as well. Human β-like cells derived from WT and UC with chromanol 293B treatment displayed higher cytoplasmic Ca^{2+} concentration elevation when compared with β-like cells derived from WT and UC without chromanol 293B treatment (Figure 26B).

Like human β-like cells, a higher cytoplasmic Ca^{2+} concentration elevation was found in human islets with chromanol 293B treatment compared with islets without chromanol 293B treatment (Figure 26C). The activity of β cells within a rat islet is unsynchronized due to β cells gap junction coupling[79]. I found that the fluorescent signal was transmitted between cells from the surface to the core of human islets. The Ca^{2+} signaling delivery had a Ca^{2+} unsteady plateau phase to respond to 20 mM glucose stimulations (Figure 26C). In contrast, differentiated human β cells had a steady plateau phase of cytoplasmic Ca^{2+} concentration elevation, increasing with 20 mM stimulation (Figures 26A and 26B).

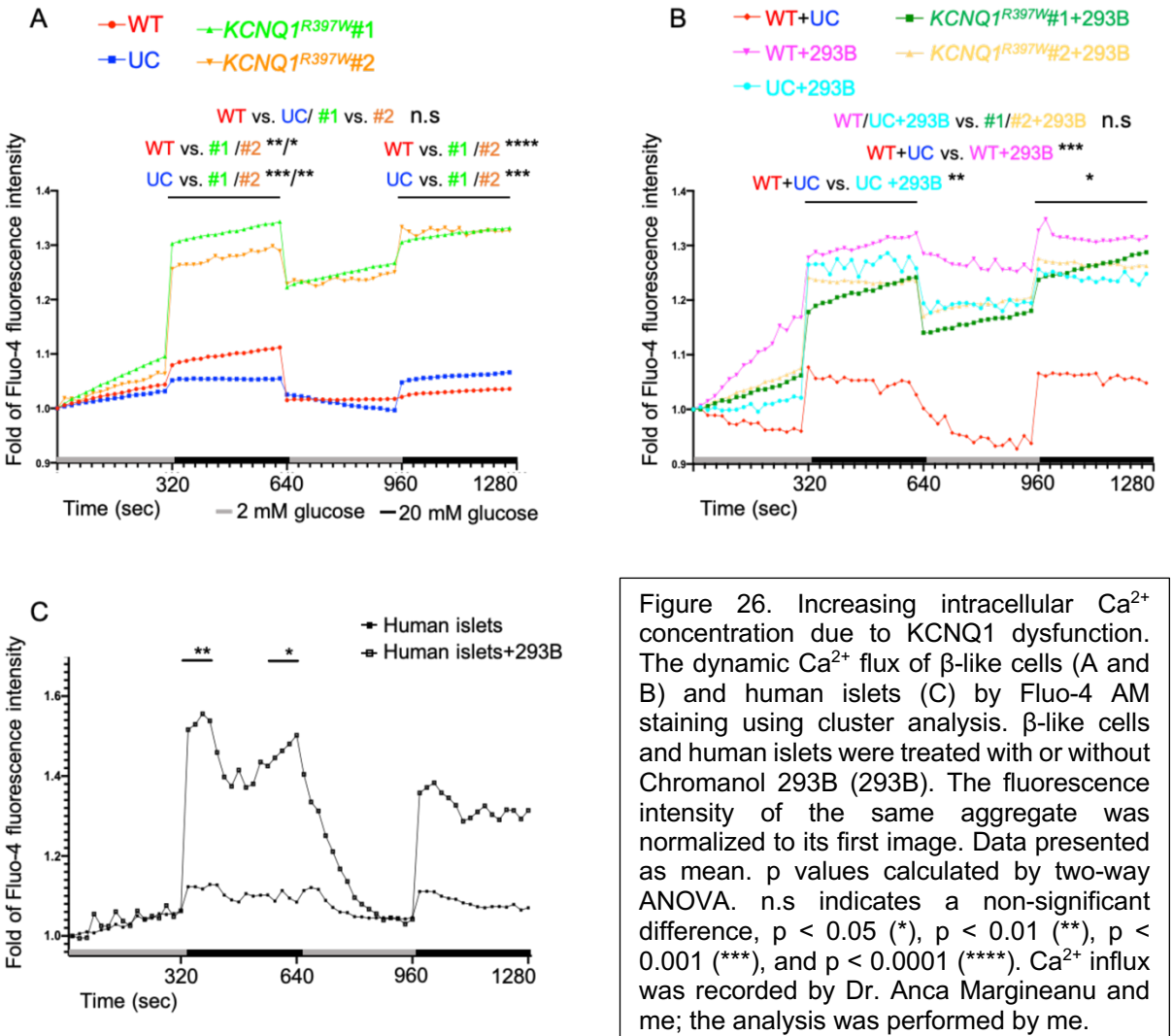

Figure 26. Increasing intracellular Ca^{2+} concentration due to KCNQ1 dysfunction. The dynamic Ca^{2+} flux of β-like cells (A and B) and human islets (C) by Fluo-4 AM staining using cluster analysis. β-like cells and human islets were treated with or without Chromanol 293B (293B). The fluorescence intensity of the same aggregate was normalized to its first image. Data presented as mean. p values calculated by two-way ANOVA. n.s indicates a non-significant difference, $p < 0.05$ (*), $p < 0.01$ (**), $p < 0.001$ (***), and $p < 0.0001$ (****). Ca^{2+} influx was recorded by Dr. Anca Margineanu and me; the analysis was performed by me.

3.6 KCNQ1^{R397W} increased insulin secretion in early β-like cells.

Next, we asked if we find differences in the amount of the crystallized insulin granules between mutated β-like cells and controls. To check the crystallized insulin granules in β-like cells, our collaborator, Dr. Bettina Purfürst, used an electron microscope to take the images from the sections of β-like cells (day 31). The generated insulin granules were structurally similar to human insulin granules[186]. β-like cells derived from KCNQ1^{R397W} had significantly more crystallized insulin granules than WT and UC β-like cells (Figure 27). In addition, we observed that all colonies possessed a similar number of mitochondrial organelles (Figure 27) suggesting potential differences in their ATP synthesis properties.

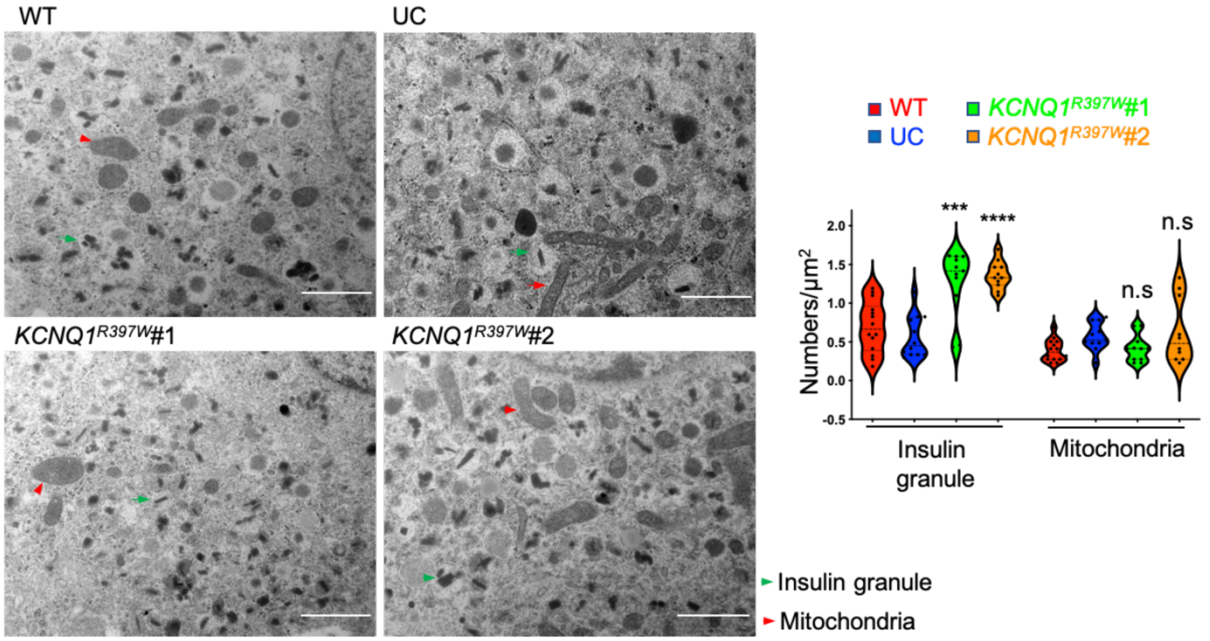

Figure 27 Electron microscopy images and quantification of crystallized insulin granules (green arrow) and mitochondria (red arrow) inside WT, UC, and KCNQ1^{R397W} β-like cells. Scale bar=1 μm. The electron microscopy images were generated by Dr. Bettina Purfürst; the analysis was performed by me.

To analyze insulin secretion of β-like cells, insulin secretion stimulated by KCl depolarization (KSIS) and glucose (GSIS). All colonies were firstly differentiated to maturing β-like cells using the standard protocol. The maturing β-like cells (day 28) generated by standard protocol responded to KCl depolarization. WT responded with an 8.194 ±1.162-fold induction of insulin secretion, whereas the response was significantly increased in the maturing β-like cells of KCNQ1^{R397W}, yielding 17.25 ± 1.635 and 13.11 ± 1.146-fold respectively (Figure 28A). We used the other protocol to mature β-like cells (day31), behaved similarly, mature β-cell can perform GSIS and

KCl depolarization. Both of KCNQ1^{R397W} β-like cells (day 31) were significantly increased their insulin secretion in response to KCl depolarization compared with control β-like cells (WT and UC, Figure 28C). In GSIS analysis, the KCNQ1^{R397W} β-like cells' insulin secretion were significantly increased comparing with control β-like cells (Figure 28B). However, KCNQ1^{R397W} did not influence insulin expression (Figure 28D). Thus, KCNQ1^{R397W} increased the number of crystallized insulin granules and elevated the rate of insulin secretion.

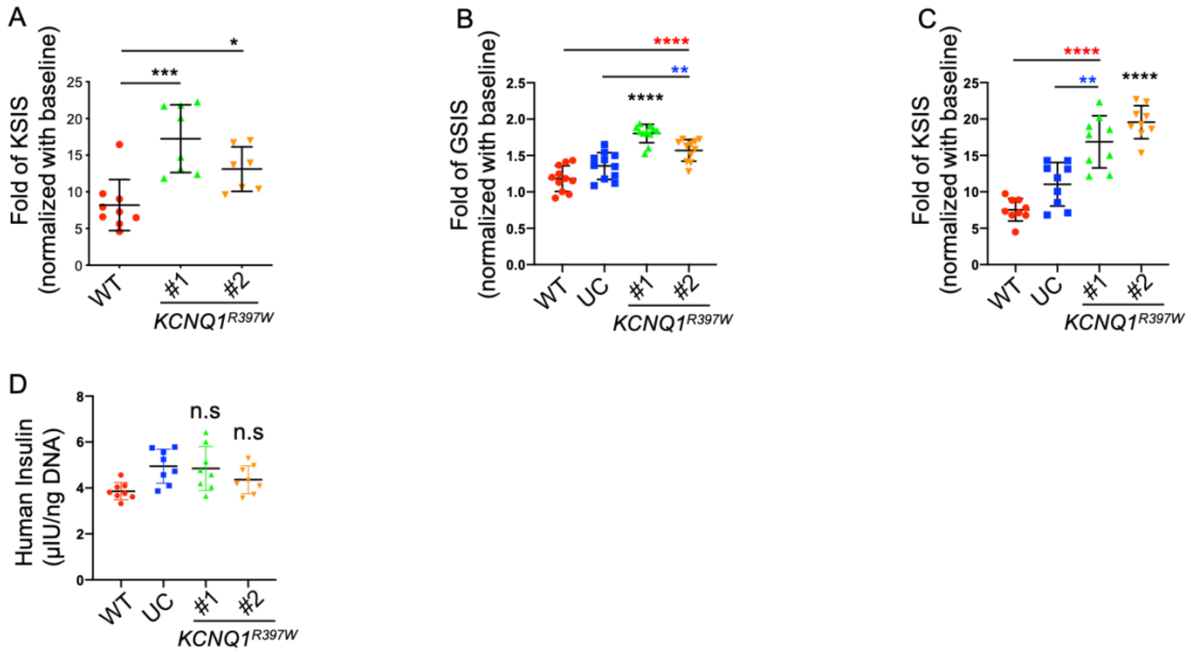

Figure 28. KCNQ1^{R397W} increased insulin secretion. (A) Fold change of insulin secretion in maturing β-like cells (day 28, generated by standard protocol) with 30 mM KCl stimulation between WT and KCNQ1^{R397W} β-like cells. Fold change of insulin secretion in mature β-like cells (day 31) with 16.8 mM glucose (B) and 30 mM KCl (C) stimulation between WT, UC, and KCNQ1^{R397W} β-like cells. (D) Total insulin content per 1ng DNA of insulin^{+} cells between KCNQ1^{R397W} and control (WT and UC) mature β-like cells (day 31). Data presented as mean ± SD. p values calculated by unpaired two-tailed t-test. n.s indicates a non-significant difference, $p < 0.05$ (*), $p < 0.01$ (**), $p < 0.001$ (***), and $p < 0.0001$ (****).

3.7 The mature KCNQ1^{R397W} β-like cells had a low metabolic capability.

The genes of the GPCRs-cAMP-PLD2 pathway were down-regulated in KCNQ1^{R397W} β-like cells compared to control β-like cells (Figure 29A). The other genes involved in the cAMP pathway were unsynchronized expressions, such as PIK3R2 (down-regulated) and PIK3R3 (up-regulated). However, only the upstream genes of the classical MAPK pathway were down-regulated in KCNQ1^{R397W} β-like cells compared to control β-like cells (Figure 29B).

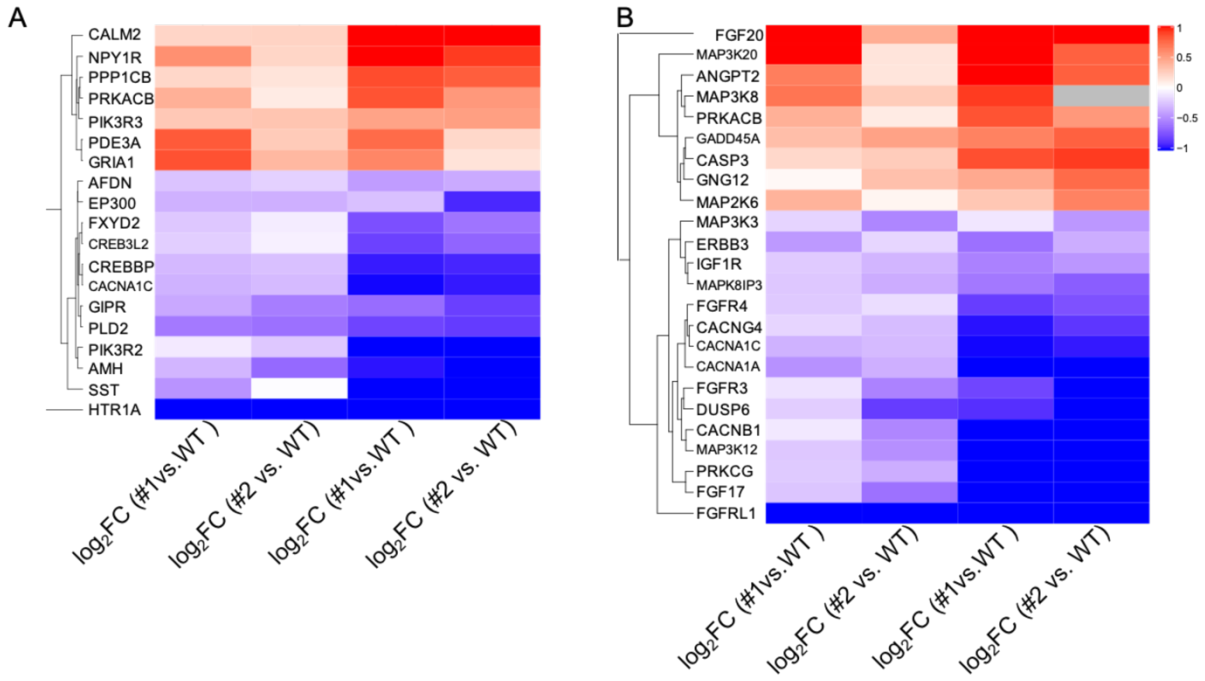

Figure 29. Heatmap represented the genes of differential expression in the pathway of cAMP (A) and MAPK (B) compared between WT, UC, and *KCNQ1*^{R397W} β-like cells. The image was generated by Dr. Amit Pande and me.

Because the upstream genes encode RTK and CACN regulate the metabolic capability of β cells[3,100-102]. Our C1189T patient developed PND and deficient insulin secretion 16 h after birth. To analyse the gene expression in the mature β-like cells, I continually cultured all β-like cells until day 40 *in vitro*. At day 21 the β-like cells are still immature, whereas at day 40 the organoids are considered as late stage. The activation of *PLD2* has been reported to be essential for EGF-dependent insulin secretion in mouse β cells[187,188]. qPCR analysis showed that mature KCNQ1^{R397W} β-like cells (day 40) had a significantly lower expression level compared with control β-like cells (Figure 30A).

FGFRs are class V of RTKs[45]. FGFRs have been implicated as metabolic regulators in murine β cells[100-102]. qPCR analysis showed that *FGFRL1* was down-regulated *FGFRs* genes at both day 31 and day 40, whereas *FGFR1* and *FGFR3* were down-regulated in KCNQ1^{R397W} β-like cells at day 40 (Figures 30B, 30C, and 30D). However, the other terminal genes of cAMP and MAPK pathway did not reach significant difference in KCNQ1^{R397W} β-like cells compared with control β-like cells.

Two common genes in the MODY category, *HNF4α* and *NEUROD1*, were down-regulated in KCNQ1^{R397W} β-like cells compared with control β-like cells. Hepatocyte nuclear factor 4 alpha (*HNF4α*) is a transcription factor expressed in liver, kidneys, and pancreas[189,190]. The pharmacological inhibition of FGFRs dramatically reduces *HNF4α*

expression in hepatic progenitor cells derived from hiPSC[191], suggesting that FGFRs are the upstream genes of *HNF4α*. qPCR analysis showed that mature KCNQ1^{R397W} β-like cells (day 40) had a significantly lower expression level compared with the control β-like cells (Figure 30E). However, the *NEUROD1* level of KCNQ1^{R397W} β-like cells slightly decreased, but this decrease was not significant compared with WT β-like cells (day 40, Figure 30F).

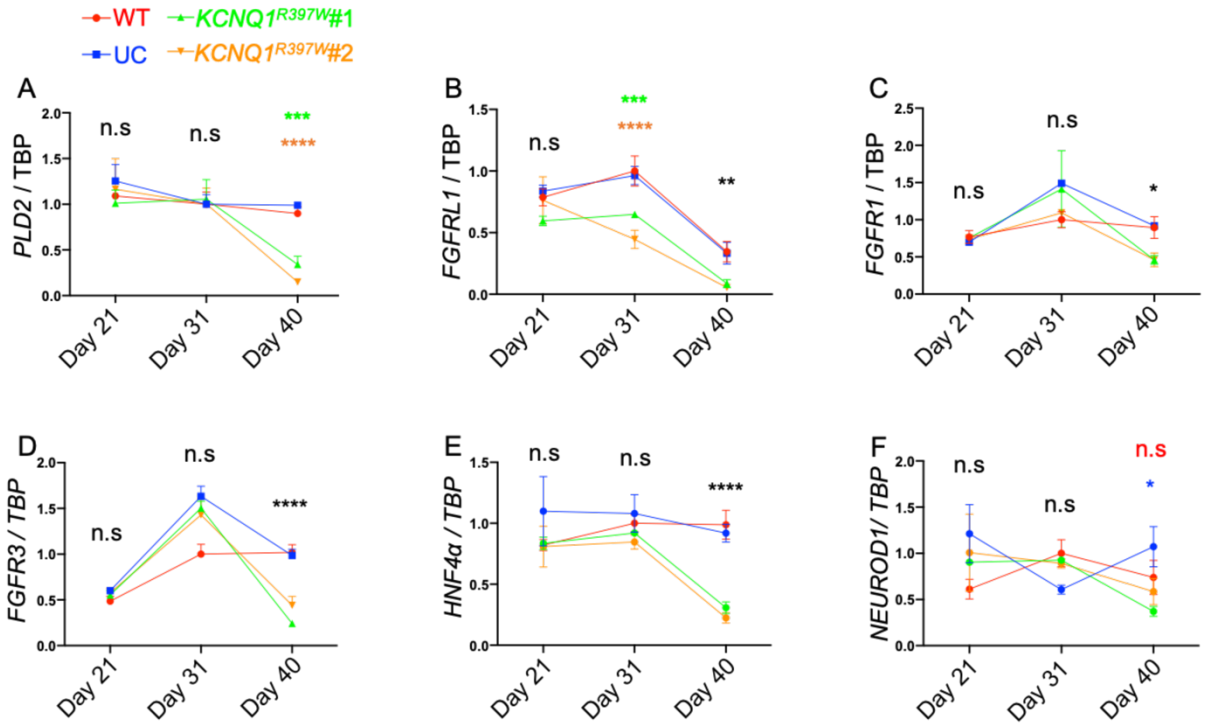

Figure 30. The mature KCNQ1^{R397W} β-like cells inhibited the expression of metabolism-related genes. qRT-PCR analysis of *PLD2* (A), *FGFRL1*(B), *FGFR1* (C), *FGFR3* (D), *HNF4α* (E), and *NEUROD1* (F) expression in pancreatic organoids of WT, UC, and KCNQ1^{R397W}. The differentiation stages include immature β cells (day 21) and mature β cells (day 31 and day 40). Data were normalized to *TBP* transcript expression. Data presented as mean ± SD. p values calculated by unpaired two-tailed t-test. n.s indicates a non-significant difference, $p < 0.05$ (*), $p < 0.01$ (**), $p < 0.001$ (***), and $p < 0.0001$ (****).

To decipher the mechanism behind the altered phenotype caused by the mutation, EdgeR package was used to analyze the genes of significant expression. *FGFRL1* was significantly down-regulated in KCNQ1^{R397W} β-like cells compared with control β-like cells (day 32, figure 32), that was consistent with qPCR analysis.

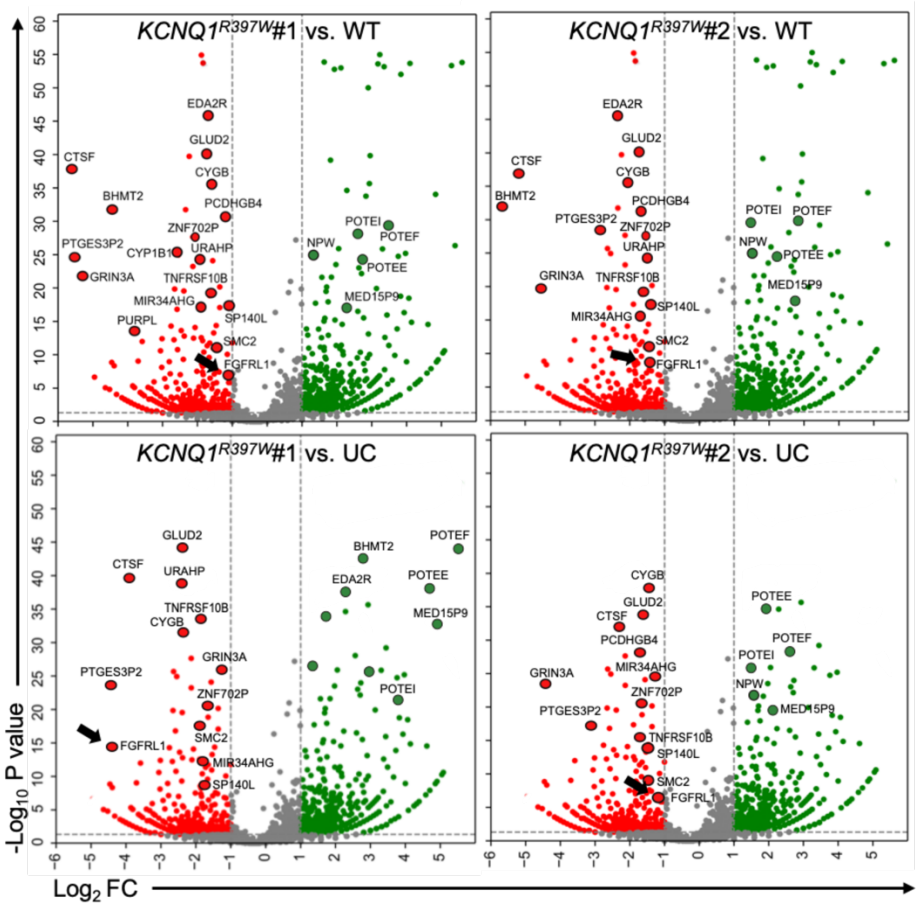

Figure 31. Volcano plots showed significant expression compared with WT, UC, and KCNQ1^{R397W} β-like cells (day32, P-value 0.1). The down or up-regulated genes presented as red or green. A black arrow indicated *FGFRL1*. The image was generated by Dr. Amit Pande and me.

FGFRL1 is co-expressed with FGFR1 to form heterocomplexes in response to FGF2 stimulation[109]. *FGFR1* mutation impairs the expression of *GLUT2* and decreases mouse β-cell function[102]. Interestingly, the expression level of *GLUT2* is also determined by PDX1 in mouse β cells[104-106]. To analysis *PDX1*, *GLUT2* and *GLUT1* expression, I performed qPCR and immunoassays. qPCR analysis revealed that *FGFR1* and *PDX1* were expressed at a lower level in KCNQ1^{R397W} β-like cells compared with control β-like cells (day 40, figures 30C and 32A). Immunoassay investigated KCNQ1^{R397W} β-like cells had less PDX1^{+} and insulin^{+} cells (Figure 32B).

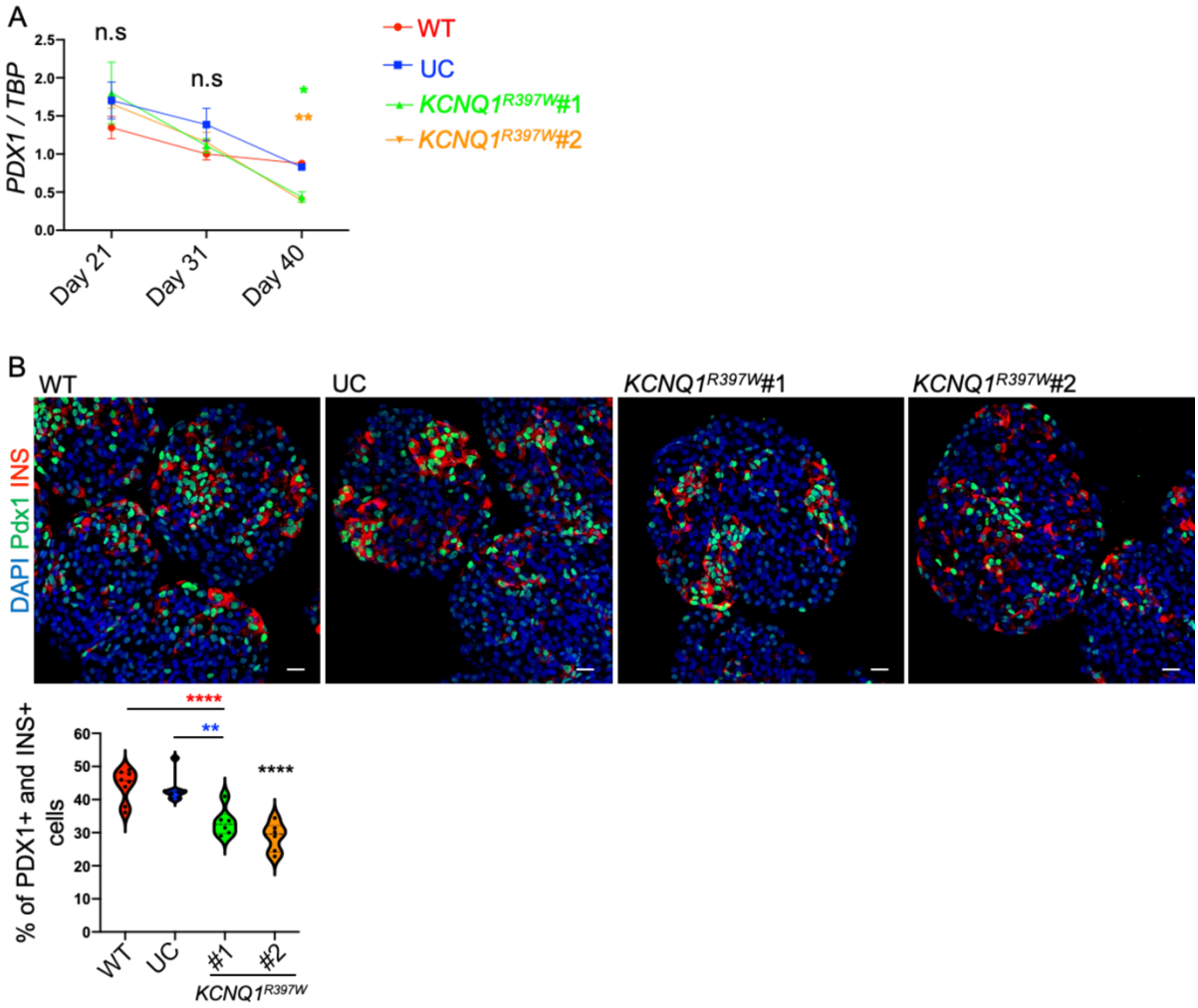

Figure 32. PDX1 was down-regulated in mature KCNQ1^{R397W} β-like cells (day 40). qRT-PCR analysed the expression of *PDX1* (A) in the pancreatic organoid of WT, UC, and KCNQ1^{R397W}. The differentiation stages include immature β cells (day 21) and mature β cells (day 32 and day 40). Data were normalized to *TBP* transcript expression. (B) PDX1 (green) and insulin (red) were immunoassayed and quantified in mature β-like cells cultured in normal S7 media. Scale bar=20 μm. Data presented as mean ± SD. p values calculated by two-way ANOVA. n.s indicates a non-significant difference, $p < 0.05$ (*), $p < 0.01$ (**), $p < 0.001$ (***), and $p < 0.0001$ (****).

Unlike mouse β cells, the *GLUT2* level of KCNQ1^{R397W} β-like cells did not affect by down-regulated FGFR1 or PDX1 (day 40, figure 33A). However, the expression of human primary glucose transporter GLUT1 was inhibited in KCNQ1^{R397W} β-like cells (day 40, figures 33B and 33C). The transcript of KCNQ1 could be detected from maturing β-like cells (day 28), suggesting it contributes the β-cell developing from day 28. To block K_V7.1 function, control β-like cells was cultured in S7 media supplemented with chromanol 293B from day 28. Immunoassay investigated the chromanol 293B treatment decreased GLUT1^{+} cells in control β-like cells (day 40, figure 33C). Taken together, KCNQ1^{R397W} regulated *FGFRs* and *PDX1* expression and further regulated *GLUT1* expression in β-like cells.

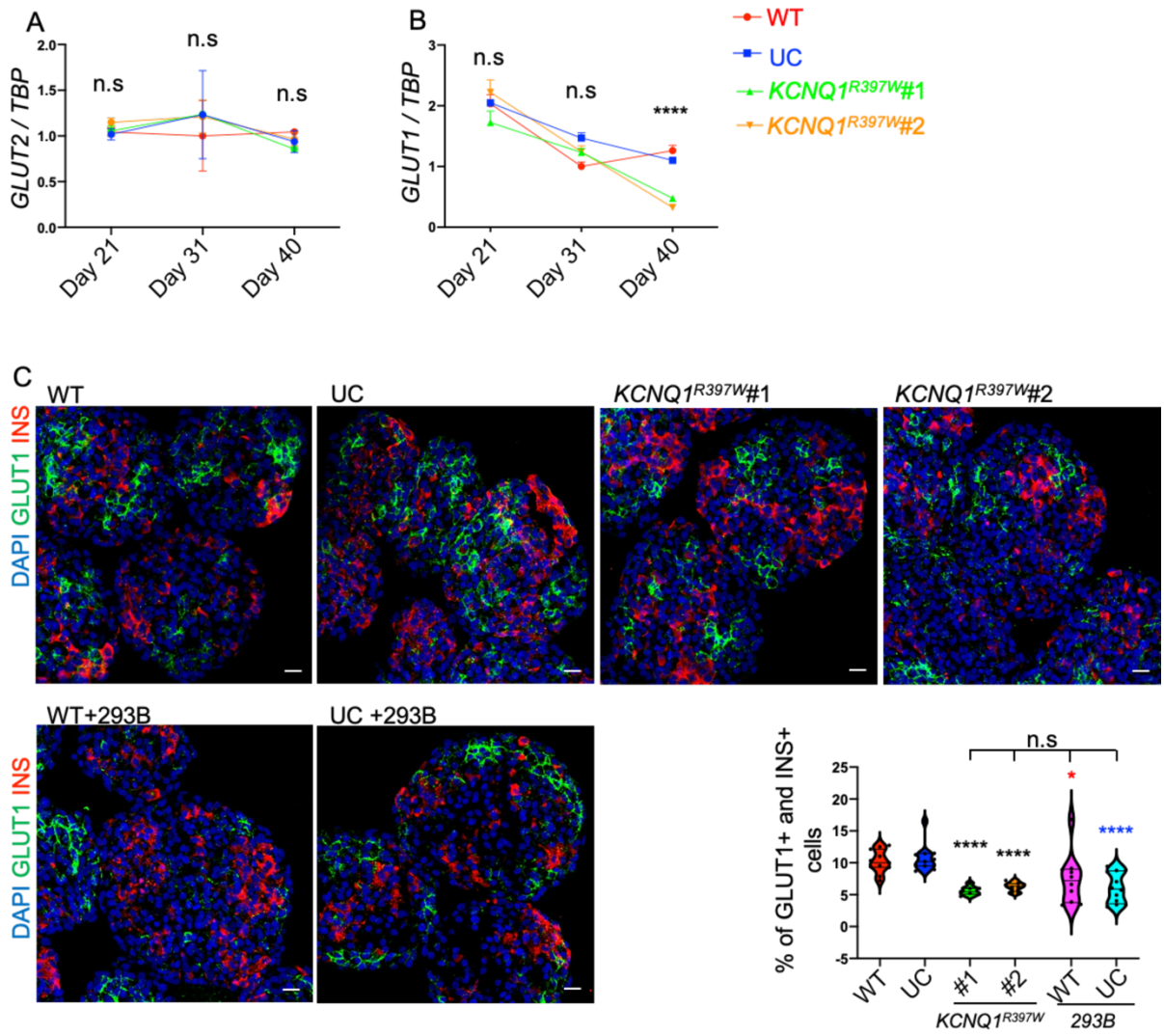

Figure 33. GLUT1 was down-regulated in mature KCNQ1^{R397W} β-like cells (day 40). qRT-PCR analysed the expression of *GLUT2* (A) and *GLUT1* (B) in the pancreatic organoid of WT, UC, and KCNQ1^{R397W}. The differentiation stages include immature β cells (day 21) and mature β cells (day 32 and day 40). Data were normalized to *TBP* transcript expression. (C) GLUT1 (green) and insulin (red) were immunoassayed and quantified in mature β-like cells (day 40) cultured in normal S7 media or S7 media supplemented with chromanol 293B (+293B) from day 28. Scale bar=20 μm. Data presented as mean ± SD. p values calculated by two-way ANOVA. n.s indicates a non-significant difference, $p < 0.05$ (*), $p < 0.01$ (**), $p < 0.001$ (***), and $p < 0.0001$ (****).

To confirm GLUT1 and PLD2 influence mature β-like cells' ability, I measured insulin secretion stimulated by glucose or KCl depolarization using ELISA. Intriguingly, KCNQ1^{R397W} β-like cells decreased insulin secretion in response to glucose stimulation and KCl depolarization at day 32 (Figures 34A and 34B). The decrease resulted in a similar insulin secretion ability in KCNQ1^{R397W} β-like cells to the control β-like cells. One week later, KCNQ1^{R397W} β-like cells (day 40) continually decreased insulin secretion in response to glucose stimulation (Figure 34C) but not in response to KCl depolarization (Figure 34D). However, the insulin content of KCNQ1^{R397W} and control β-like cells (day 40) did not reach a statistically significant difference (Figures 34E).

Taken together, KCNQ1^{R397W} controlled *FGFRs* expression and further regulated *PDX1* and *GLUT1* expression, resulted in a low metabolic capability in β-like cells.

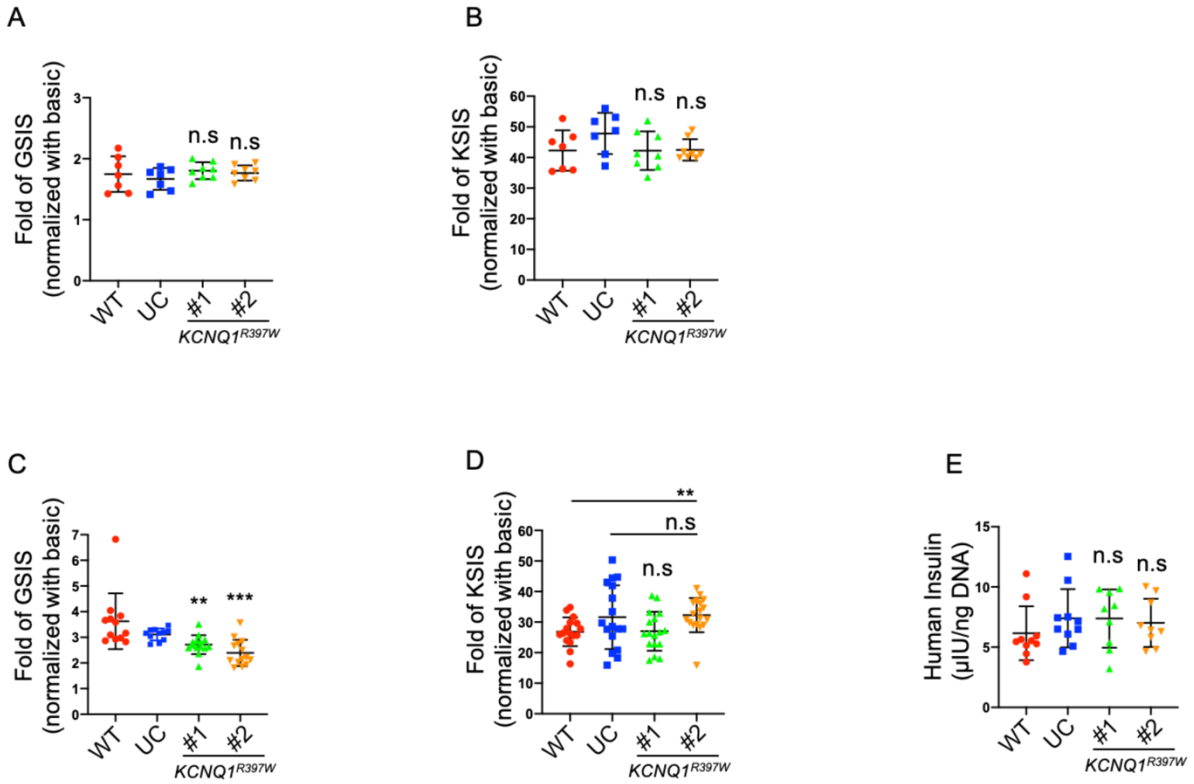

Figure 34. KCNQ1^{R397W} β-like cells with decreasing insulin secretion. (A) Fold change of insulin secretion in mature (day 32, A and B) and mature (day 40, C and D) β-like cells with 16.8 mM glucose (GSIS; A and C) and 30 mM KCl (KSIS; B and D) stimulation between WT, UC, and KCNQ1^{R397W} β-like cells. (E) Total insulin content per 1ng DNA of insulin^{+} cells between KCNQ1^{R397W} and control mature β-like cells (day 40). Data presented as mean ± SD. p values calculated by unpaired two-tailed t-test. n.s indicates a non-significant difference, $p < 0.05$ (*), $p < 0.01$ (**), $p < 0.001$ (***), and $p < 0.0001$ (****).

3.8 Chronic exposure to high glucose resulted in the loss of KCNQ1^{R397W} β-like cells.

Diabetes patients' blood glucose becomes abnormal after a meal that leads to irreversible β-cell deterioration[192]. To identify the glucose toxicity in KCNQ1^{R397W} β-like cells, I continuously incubated control and KCNQ1^{R397W} β-like cells for one week, starting in regular S7 media (Control) and S7 media supplemented with high (20 mM) concentration of glucose (HG) from day 32 of differentiation. Insulin^{+} cells had a trend towards decrease in KCNQ1^{R397W} β-like cells which was not statistically significant when compared with the control β-like cells cultured in regular S7 media (Figure 35). In addition, the immunoassay detected that KCNQ1^{R397W} β-like cells had a higher variance in the percentage of insulin+ cells, when compared to the control, but the

difference was not statistically significant (Figure 36). In contrast, Flow cytometry analysis and immunostaining showed that insulin^{+} cells had a significant decrease in KCNQ1^{R397W} β-like cells compared with the control β-like cells in 20 mM glucose S7 media culturing (Figures 35 and 36). Thus, chronic exposure to high glucose accelerated the decrease of insulin+ cells in KCNQ1^{R397W} β-like cells.

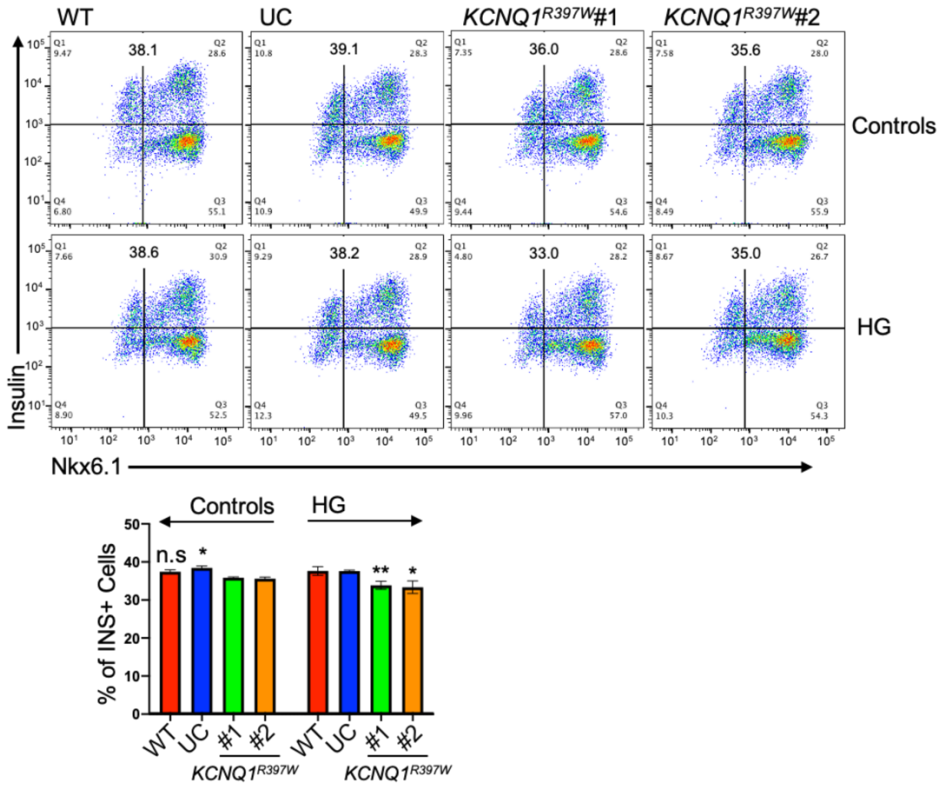

Figure 35. Flow cytometry analysis and quantification of normal β-like cells and high glucose chronic exposure of β-like cells. β-like cells (day40) with insulin expression were cultured in regular S7 media (Control) or S7 media supplemented with 20 mM glucose media (HG). Data presented as mean ± SD. p values calculated by unpaired two-tailed t-test. n.s indicates a non-significant difference, $p < 0.05$ (*), $p < 0.01$ (**), $p < 0.001$ (***), and $p < 0.0001$ (****).

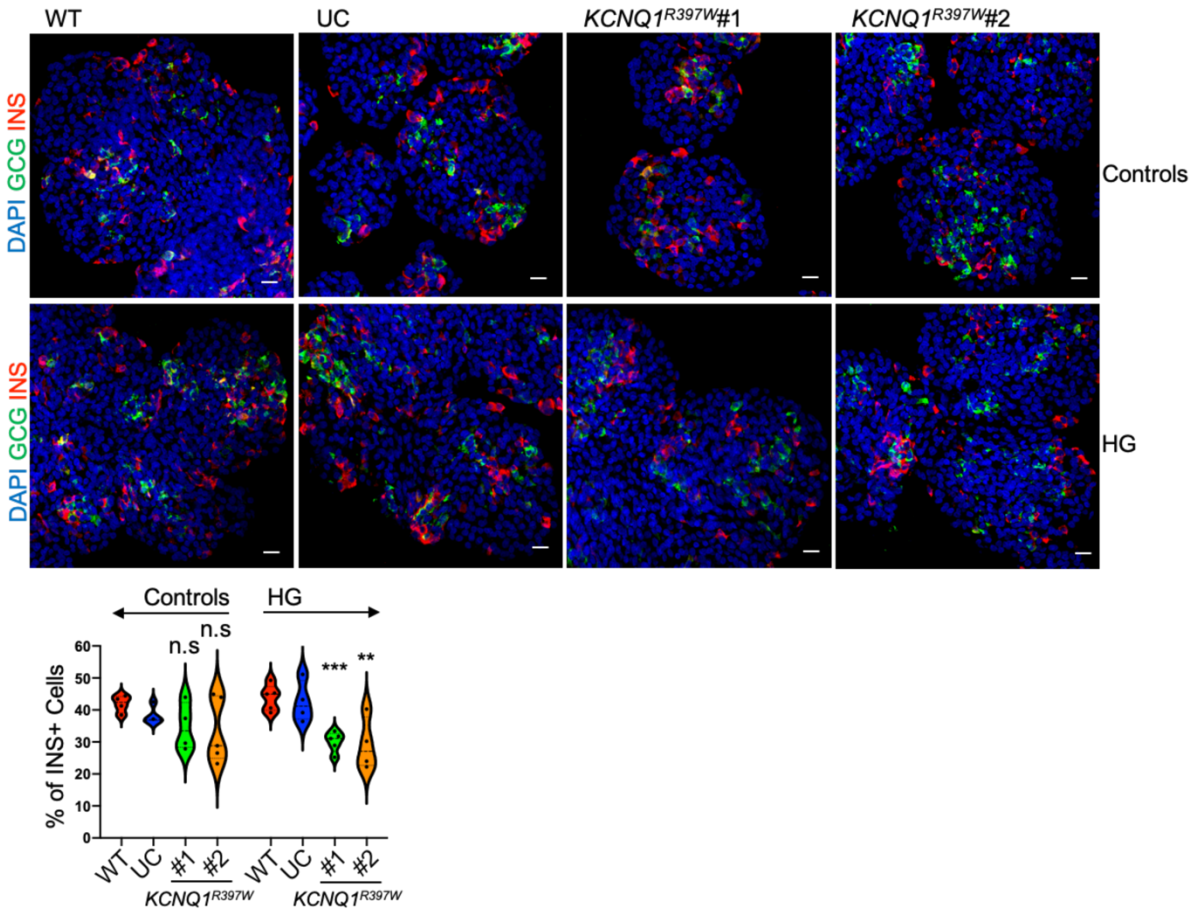

Figure 36. Immunoassay and quantification of normal β-like cells and high glucose chronic exposure of β-like cells. Glucagon (green) and insulin (red) were immunoassayed and quantified in mature β-like (day 40) cells cultured in regular S7 media (Control) or HG media. Scale bar=20 μm. Data presented as mean ± SD. p values calculated by unpaired two-tailed t-test. n.s indicates a non-significant difference, $p < 0.05$ (*), $p < 0.01$ (**), $p < 0.001$ (***), and $p < 0.0001$ (****).

Yang and his associates report that dysfunction of the KCNH6, a K_V channel protein, results in a high level of intracellular Ca^{2+} in mice that triggers hyperinsulinemia in the short term. In long term, by contrast, the intracellular elevation of Ca^{2+} caused β-cell apoptosis and loss of β-cell mass, leading to a hypoinsulinemic phenotype in mice[87]. GO analysis revealed that the mutation affected the cAMP and MAPK pathway, which are reported to regulate cell proliferation and apoptosis[193,194]. To measure apoptosis in β-like cells, the apoptosis markers, Annexin V and 7-AAD, were used to distinguish dead cells and pro-apoptotic cells. The KCNQ1^{R397W} β-like cells (day 40) with Annexin V+/ 7-AAD- were significantly higher than controls except for unmodified clone vs. first mutated clone (Figure 37). Thus, the subtle decrease of insulin$^+$ cells could be caused by apoptosis in *KCNQ1^{R397W}* β-like cells.

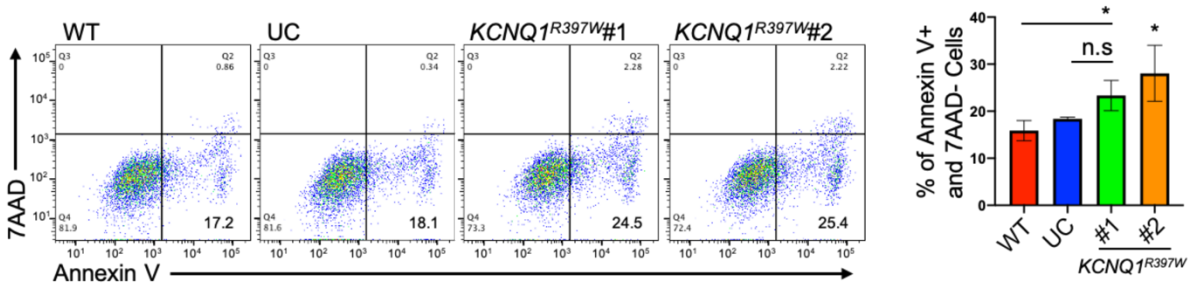

Figure 37. Flow cytometry analysis and quantification of the percentage of pro-apoptotic cells among β-like cells. Data presented as mean ± SD. p values calculated by unpaired two-tailed t-test. n.s indicates a non-significant difference, $p < 0.05$ (*), $p < 0.01$ (**), $p < 0.001$ (***), and $p < 0.0001$ (****).

3.9 Disruption of Tp53-apoptosis pathway

Recently human cancer cell lines harboring Cas9-expression have been found to an upregulation of the Tp53 pathway, but with Tp53-inactivating mutations[174]. *CDKN1A* is a TP53 negative regulator[195]. Notably, *CDKN1A* was downregulated when CRISPR-Cas9 transfected clones (UC and KCNQ1^{R397W}) were differentiated to the last 2 stages (Figure 38A). No difference, however, was found on the qPCR analysis of *Tp53* expression (Figure 38B). *PHLDA3*, a Tp53 targeted gene, contributes to Tp53-dependent apoptosis by repressing AkT1 activation[196]. In contrast, *PHLDA3* of CRISPR-Cas9 transfected clones was remarkably downregulated during differentiation (Figure 38C). Thus, the expression of *PHLDA3* was inconsistent with the *CDKN1A* and *p53* in CRISPR-Cas9 transfected clones.

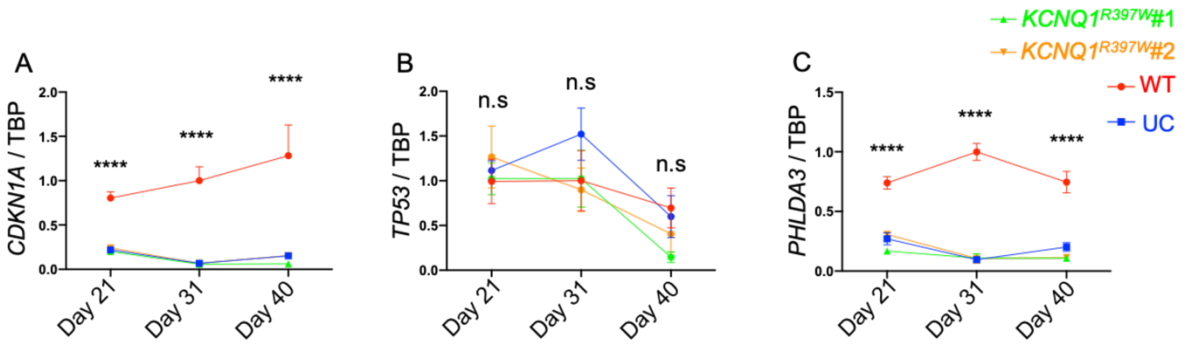

Figure 38. qRT-PCR analysis of *CDKN1A* (A), *TP53* (B), and *PHLDA3* (C) expression in pancreatic organoids of WT, UC, and KCNQ1^{R397W}. The differentiation stages include immature β cells (day 21) and mature β cells (day 32 and day 40). Data were normalized to *TBP*. Data presented as mean ± SD. p values calculated by two-way ANOVA. n.s indicates a non-significant difference, $p < 0.05$ (*), $p < 0.01$ (**), $p < 0.001$ (***), and $p < 0.0001$ (****).

To identify apoptosis as the reason for loss of insulin$^+$ cells, I used a cleaved-caspase 3 antibody to visualize apoptotic cells. Because cleaved-caspase 3 antibody has

unspecific labeling in pancreatic α-cells, I only checked glucagon$^-$ cells. only one cleaved-caspase 3$^+$ cell was found in every samples (Figure 39). Thus, CRISPR-Cas9 could influence the stability of p53-dependent apoptosis.

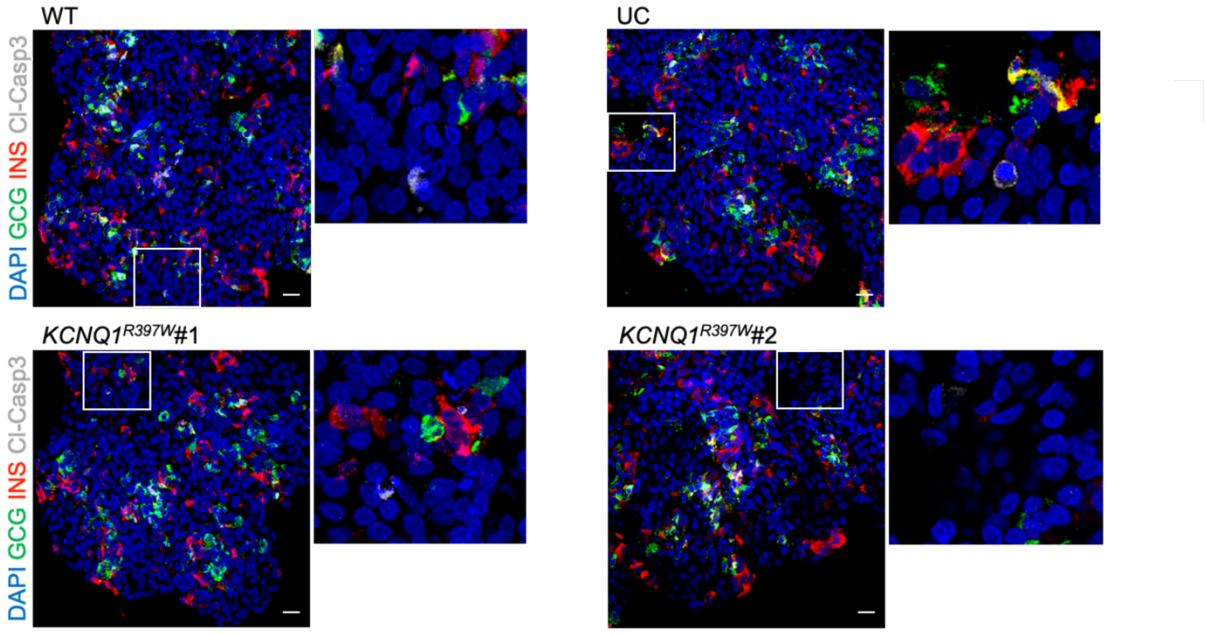

Figure 39. Apoptosis analysis in human β-like cells. Immunostaining for glucagon (green), insulin (red), and cleaved caspase-3 (Cl-Casp3, grey) expressed in mature β-like cells. Scale bar=20 μm.

3.10 Isradipine especially decreased cytoplasmic Ca^{2+} accumulation in KCNQ1^{R397W} β-like cells.

Isradipine (IRP) is an inhibitor of L-type Ca_V channels, which is the main Ca_V channel regulating GSIS[80]. To further confirm the association between cytoplasmic Ca^{2+} accumulation and KCNQ1^{R397W}, IRP was used to analyze Ca^{2+} flux in day 40 β-like cells. Cytoplasmic Ca^{2+} concentration from mutated clone 2 was still significantly higher than the unmodified control (Figure 40). The KCNQ1^{R397W} β-like cells had a lower cytoplasmic Ca^{2+} level under IRP treatment comparing with mutated clone 2 without IRP treatment. Obviously, the cytoplasmic Ca^{2+} concentration of the mutated colonies and unmodified clones under IRP treatment were similar to the unmodified clone without IRP treatment (Figure 40). Thus, IRP could especially decrease cytoplasmic Ca^{2+} accumulation causing by KCNQ1^{R397W}.

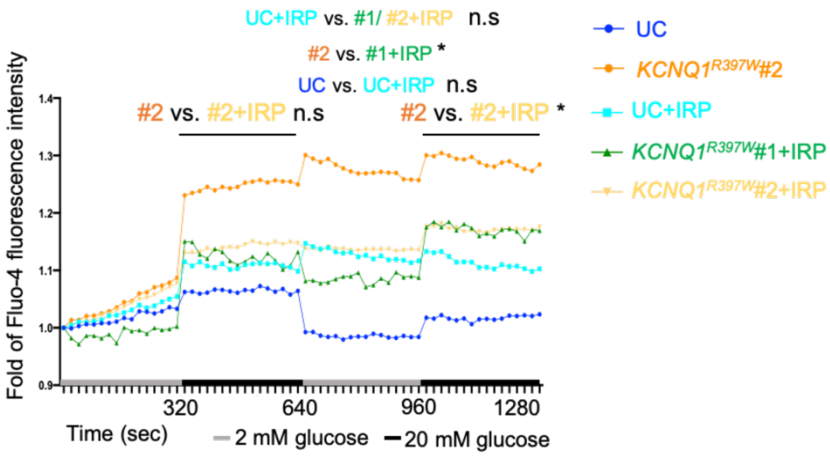

Figure 40. Isradipine decreased intracellular Ca^{2+} concentration in KCNQ1^{R397W} β-like cells. The dynamic Ca^{2+} flux of β-like cells labelled with Fluo-4 AM using cluster analysis. β-like cells were treated with or without isradipine (IRP). Data presented as mean. p values calculated by two-way ANOVA. n.s indicates a non-significant difference, $p < 0.05$ (*), $p < 0.01$ (**), $p < 0.001$ (***), and $p < 0.0001$ (****).Ca^{2+} influx was recorded by Dr. Anca Margineanu and me; the analysis was performed by me.

4. Discussion

Here, I reported that 3D pancreatic differentiation could elucidate the effect of neonatal diabetes candidate mutation on the functional β cell development. KCNQ1^{R397W} and control β-like cells were derived from the same hESCs_H1 cell line, which harbored the same genetic background essential for uncovering the precise role of genes in specific neonatal diabetes. I revealed that KCNQ1^{R397W} increased cytoplasmic Ca^{2+} concentration by affecting the firing frequency of polarization and depolarization without altering β-cell differentiation and proliferation properties. The cytoplasmic Ca^{2+} level forced insulin packaging into insulin granules and increased insulin secretion. Metabolism associated genes were presently down-regulated and impaired GSIS.

4.1 The differentiation of hiPSCs to functional β cells is problematic.

Neonatal diabetes is thought to be mostly related to β-cell dysfunction[34]. However, the access to suitable cadaveric islet donors is currently a bottleneck[2]. An *in vitro* β cell differentiation approach provides an opportunity to study an inaccessible stage of human β cell development and function *in vitro*[45]. hiPSC is a rising star in human disease modeling. However, previous work has pointed out that the reprogramming technique and donor origin could lead to the observed inconsistencies of differentiation using hiPSCs[197-199]. The donor origin's epigenomic and transcriptomic status would influence the differentiation potential and predispose hiPSCs to differentiate to a particular germ layer[42,200]. Thurner and his associates indicated that hiPSCs derived from pancreatic β cells (BiPSCs) retain the signature of epigenetic memory involved in endoderm lineage commitment when compared with hiPSCs from fibroblasts (FiPSCs); the epigenetic memory, such as enhancers and promoters, may pave the pathways involved in pancreatic islet development[42]. It is known that PBMCs originate from the mesoderm. Hence, the retaining epigenetic memory from PBMCs could affect PBMC-derived hiPSCs differentiation toward pancreatic islets, which originates from the endoderm. The EB random differentiation and pancreatic differentiation *in vitro* had shown the bias to convert hiPSCs to ectoderm and mesoderm (Figures 11C and 12). The differentiation property of hiPSCs was different and could limit the understanding of the precise mechanism in diabetes. Taken together, using hiPSCs reliably for pancreatic differentiation is problematic.

4.2 The 3D differentiation allows real-time observation of the generation of neonatal diabetes.

The classical animal models are fast-growing and harbor detailed descriptions of development and physiology[201]. The identification of cellular signaling pathways and potential drug targets in animal models eventually translates to humans[201]. Even though animal models present a traditional alternative for disease research, animal models limit the understanding of the precise function of human genes in diabetes due to certain physiological and metabolic differences. It will be considered that a human patient has diabetes maintaining glucose ≥200 mg/dL in blood. In mice, the value necessary for diabetes definition tends to ≥300 mg/dL[202]. Hugill and his colleagues have shown that mice carrying the same mutation in Kcnj11 (K_{ATP} channel) did not have hyperinsulinemia in contrast to patient[203]. Laboratory rodents are not miniature humans. Age should be taken as a crucial factor when the results of any research in rodents translate to humans[204]. However, there is no precise way to correlate the ages of rodents and humans. It is not acceptable to compare laboratory rat and human age by their life span due to different developing speed in life phases[204]. The physiological characters, musculoskeletal examination and growth of molar teeth, have their specific life phases and limitations in correlating the ages of animals and humans[205,206].

The differentiation of hPSCs in 3D is highly parallel to actual human organs, which can elucidate the mechanisms of human organ regeneration[44,45,207-209]. Therefore, the other limitation is that animal models do not allow real-time observation of the morphology of islet development as in β cell differentiation *in vitro*, which is vital to identify the happening of neonatal diabetes. Unlike the differentiation of hPSCs in 2D, 3D culture allows the exploration of the appropriate cell-cell interactions (Figure 41)[210]. 3D culture (organoids) is much more faithful to elucidate the mechanisms of diseases.

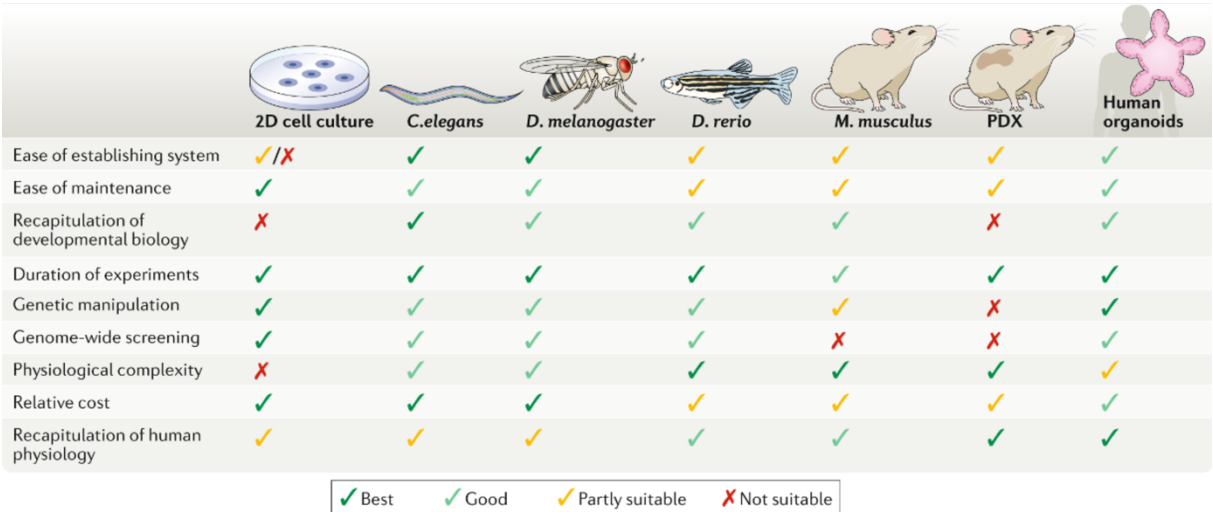

Figure 41. Comparison of the most common model organisms. Figure was taken from published figure 1[201]. The model organisms include *Caenorhabditis elegans* (*C. elegans*), *Drosophila melanogaster* (*D. melanogaster*), *Danio rerio* (*D. rerio*) and *Mus musculus* (M. musculus), patient-derived xenografts (PDX) along with 2D cell cultures and human organoids (3D. culture).

4.3 The proper control for gene editing by CRISPR-Cas9.

A recent report describes that CRISPR-Cas9 induces Tp53 pathway activation and promotes colonies' survival with Tp53-inactivating mutations[174]. It is essential to use appropriate controls to avoid off-target effects from CRISPR-Cas9. The unmodified clone was selected from the fluorescent cell library as controls (Figure 13C). The unmodified hESC was generated together with other KCNQ1^{R397W} hESCs but did not carry KCNQ1^{R397W}.

Data from UC played an important role in eliminating the off-target effects in our experiments (Figure 30). The Tp53 pathway's instability showed inconsistent expression of *CDKN1A* and *PHLDA3* in our CRISPR-Cas9 treated samples (Figure 38). *CNDKN1A* and *PHLDA3* present a Tp53 negative regulator and p53 targeted gene[195,196]. It was suggested that synchronous low expression of *CNDKN1A* and *PHLDA3* could not happen in samples with Tp53-inactivating mutations. No effect, however, was found on activation of caspase 3 dependent apoptosis (Figure 39). It was suggested that some unexpected causal factors inhibited the contribution of PHLDA3 in p53-caspase 3 apoptosis. This instability caused by Cas9-mediated genome editing suggests that Cas9 proteins should be developed for precision genome editing, especially in the Tp53-caspase 3 pathway research.

4.4 Kv7.1 dysfunction contributes to neonatal diabetes.

4.4.1 KCNQ1^{R397W} or the blockade of K_V7.1 channel increase the membrane action potential.

Several mutations at *KCNQ1* are associated with impaired insulin exocytosis[90,211]. Furthermore, knocking out of KCNQ1 in mice and differentiated β cells derived from KCNQ1$^{-/-}$ hESCs have been shown to impair GSIS[165,166]. It should be noted that the forced expression of *KCNQ1* in the insulinoma cell line could impair insulin secretion as well[212]. The KCNQ1$^{-/-}$ mice immunoassay revealed a reduction of insulin+ cells compared to the wild type (Figures 10), being inconsistent with mature KCNQ1$^{-/-}$ β-cell generation in humans[166]. However, the mechanism is unclear behind these conflicting observations.

The extensive versatility of the KCNQ1 channel function might depend on interacting with various auxiliary partners as well[136]. Our patient's mutation caused a change in the amino acid, which was expected to change the structure of helix A of KCNQ1 (Figure 7C). Helix A and helix B form a clamshell-like structure that is essential for CaM binding[154]. CaM regulates the formation of a functional K_V7.1 channel[154]. Thus, our patient's mutation was expected to affect the K_V7.1 channel function. Especially, KCNQ1 and KAT1 have a similar 3D structure presenting by the cryo-electron microscopy[154,160]. Clark and his associates report that S4 and S5 overlaying the C-linker (HA and HB) form a tight packet[160]. In Clark's gating model, the opening or closure of the S6 gate is regulated by S4 coupling or disengaging from C-linker[160]. Unlike regular secondary structure, KCNQ1^{R397W} causing random coil could disrupt the reversible conjunction resulting in the reduced voltage-gated activation, confirmed by our collaborators' Patch-clamp studies (Figures 7C and 8A). K_V channels carry on a delayed outward K^+ current, which is referred to as the outward rectification[3]. Therefore, KCNQ1^{R397W} or blocking K_V7.1 channel could increase the membrane electrical activity of β-like cells as well (Figure 24), being consistent with the blocking K_V7.1 channel by Conkunitzin-S1 in rats[91]. Besides, the increase of membrane electrical activity sustained from day31 until day 40 in KCNQ1^{R397W} β-like cells.

4.4.2 KCNQ1^{R397W} or the blockade of K_V7.1 channel increase the cytoplasmic Ca^{2+} level and insulin secretion.

The K_V channels limit Ca^{2+} influx and subsequently regulate insulin secretion in β cells[88,163]. In the rat, the blockade of K_V7.1 channels increases cytoplasmic Ca^{2+} concentration resulting in hyperinsulinemia[91]. Ca^{2+} influx analysis revealed that both of KCNQ1^{R397W} and blocking K_V7.1 channel disturbed the cytoplasmic Ca^{2+} mobilization, which caused the cytoplasmic Ca^{2+} accumulation in β-like cells (Figures 26A and 26B). The cytoplasmic Ca^{2+} accumulation was also recorded in human islets with chromanol 293B treatment (Figure 26C). The mechanism could be elucidated by the up-regulated genes involved in the oxidative phosphorylation process (Figure 25C).

Glucose rises cytoplasmic Ca^{2+} triggering a cascade of insulin secretion through granule exocytosis in β cells[64]. Insulin, together with a Ca^{2+} ion, forms a hexamer and is crystallized in insulin granules[3,68]. The KCNQ1^{R397W} β-like cells had an increase of cytoplasmic Ca^{2+} level and insulin granules (Figures 26 and 27), which suggested that the elevation of cytoplasmic Ca^{2+} level could increase insulin crystallization. Cytoplasmic free Ca^{2+} level controls the kinetics of insulin release: The cytoplasmic Ca^{2+} elevation is essential for the activation of CaM dependent kinase II[70,71]. CaM kinase II phosphorylates microtubule-associated proteins and accelerates insulin granules transporting to plasma membrane[72,73]. In the next stage, cytosolic Ca^{2+} ions induce the fusion between insulin granules and plasma membrane, resulting in insulin secretion[74,75]. ELISA analysis showed that the KCNQ1^{R397W} β-like cells had an increase in insulin secretion (day 31, figures 28B and 28C). Therefore, the elevation of cytosolic Ca^{2+} ions accelerate the release of insulin granules from the readily releasable pool, which is timely refilled from packaged crystallized insulin granules in KCNQ1^{R397W} β-like cells.

4.4.3 FGFRs mediated GLUT1-dependent negative feedback finally decreases insulin secretion.

FGFs are hormones that regulate lipid and glucose metabolism[96,97]. RNAseq and qPCR analysis showed that *FGFRL1* was firstly down-regulated in mature KCNQ1^{R397W} β-like cells (day 31 and day 32, figures 30B and 31) with an increase in insulin secretion (Figures 22C and 22D). KCNQ1^{R397W} β-like cells decreased the

expression of *FGFR1* and *FGFR3* after culture until day 40 (Figures 30C and 30D). ChiPseq analysis supports that *FGFR1* can target and regulate *PDX1* expression[103]. Overexpression studies of *FGFR1* with PDX1 recognized promoter suggests that *PDX1* is the upstream gene of *FGFR1*[102]. Notablt, both *FGFR1* and *PDX1* were down-regulated in mature KCNQ1^{R397W} β-like cells at day 40 (Figures 30C, 32A, and 32B). It is controversial whether *FGFR1* or *PDX1* is the upstream gene[102,103]. However, the expression of *HNF4α* is regulated by FGFRs in hepatic progenitor cells derived from hiPSC[191]. *HNF4α* is suggested that it indirectly regulate the expression of *PDX1* by *HNF1α*[213,214]. This indicates that FGFRs could be the upstream genes of *HNF4α* and *PDX1*. In human β cells, GLUT1 facilitates glucose transport across cytoplasmic membrane[56]. Both *FGFR1* and *PDX1* have been shown to regulate the expression of *GLUT2* in mouse β cells[102,104-106]. However, qPCR analysis showed that *GLUT1* down-regulated instead of *GLUT2* in human mature β-like cells at day 40. (Figures 33A-33C). The down-regulation of genes related to the cAMP pathway repressed the increase of insulin secretion in KCNQ1^{R397W} β-like cells at day 32 (Figures 34A and 34B). Intriguingly, the down-regulated GLUT1 directly impaired GSIS but not KSIS (Figures 34C and 34D). This suggests that insulin secretion induction by KCl depolarization remit the effect of the loss of GLUT1^{+} and insulin^{+} cells in KCNQ1^{R397W} β-like cells at day 40.

Interestingly, patch-clamp results show the decrease in current densities in KCNQ1^{R397W} and KCNQ1^{G292D} CHO cells (Figure 8A). However, the opposite phenotypes of the hypo- and the hyper-insulinemic patients harboring the *KCNQ1-R397W* and *KCNQ1-G292D* mutations, respectively. This suggests that the different extent of reduction of KCNQ1 activation might cause either hypoinsulinemia or hyperinsulinemia. The patch-clamp and the dynamic insulin secretion ability of KCNQ1^{R397W} β-like cells might implicate that β-cell has some cytoplasmic Ca^{2+} level detectors that mediate the expression of metabolic associated genes to control insulin secretion. FGFRL1 is expressed at the cytoplasmic membrane and in insulin-granule membrane in β cells[108], suggesting that FGFRL1 is closely link to crystalized insulin granules. FGFRL1 is transported to the cytoplasmic membrane and constitutes a heterocomplex with FGFR1 in response to FGF2 stimulation[109], suggesting the heterocomplex forms when insulin granule fuses with cytoplasmic membrane. It suggests that FGFRL1 could be one of these cytoplasmic Ca^{2+} level detectors. However, more data need to be generated to confirm this hypothesis.

Diabetes patients' blood glucose becomes abnormal after a meal, leading to irreversible β-cell deterioration[192]. Our patient had an intrauterine growth retardation with a low birth weight. However, his condition is stable under regular insulin treatment, suggesting that the terminal effects of KCNQ1^{R397W} are the insulin production and/or secretion of β cells. Mature KCNQ1^{R397W} β-like cells were sensitive and became pro-apoptotic (Figure 37). Chronic exposure to high glucose increased KCNQ1^{R397W} β-like cells losing insulin^{+} cells (Figures 35 and 36). The abnormal elevation of cytosolic Ca^{2+} is known to trigger the NLPR3 inflammasome pathway *in vivo*[215,216]. This suggested that the mass disruption of β cells should be much more severe in fetal than the β-like cells *in vitro*. The functional impairment and the loss of β-cell mass could decrease insulin secretion until the blood insulin level underdetermination, which observed in our patient.

4.4.4 Blockade of L-type Ca_V channel could be a candidate treatment for cytoplasmic Ca^{2+} accumulation in β cells.

CACNA1A and *CACNA1C* were down-regulated in day 32 RNAseq assay (Figure 29B). L-type Ca_V channel consists of CACNA1C and CACNA1D that is the most critical Ca_V channel and controls >90% of GSIS in β cells[80,217,218]. However, *CACNA1C* and *CACNA1D* did not reach a statistically significant difference by day 40 (Figure 42). There were no statistically significant differences in the expression of CACNA1H (T-type Cav channel) and CACNA1B (N-type Cav channel) in β-like cells (day 40) as well. Intriguingly, *CACNA1A* (P/Q type Ca_V channel) in KCNQ1^{R397W} β-like cells (day 40) had a significantly lower expression level compared with the control β-like cells (Figure 42). The different expression of P/Q type Ca_V channel did not change the Ca^{2+} accumulation in KCNQ1^{R397W} β-like cells (day 40, figure 40), which confirms the important role of L-type Ca_V channel in β cells.

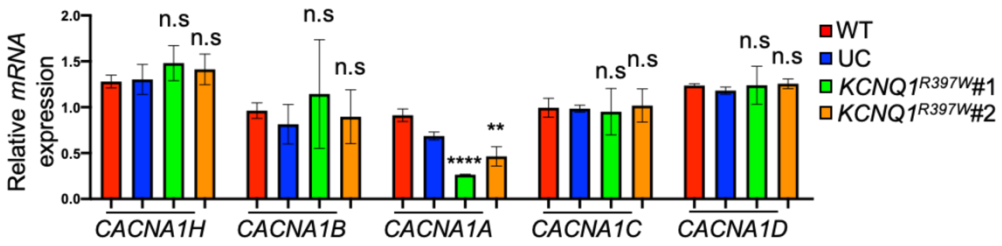

Figure 42. qRT-PCR analysis of *CACNA1H, CACNA1B, CACNA1A, CACNA1C,* and *CACNA1D* expression in pancreatic organoids of WT, UC, and KCNQ1^{R397W} (day 40). Data were normalized to *TBP*. Data presented as mean ± SD. p values calculated by unpaired two-tailed t-test. n.s indicates a non-significant difference, $p < 0.05$ (*), $p < 0.01$ (**), $p < 0.001$ (***), and $p < 0.0001$ (****).

Cytoplasmic Ca^{2+} concentration is regulated by the Ca^{2+} influx across membrane Ca_V channels and efflux/influx of cytosolic Ca^{2+} store, such as ER[10,64-66]. Interestingly, IRP treated β-like cells slightly increased the cytoplasmic Ca^{2+} level, but this increase was not significant (Figure 40). It suggested that the decrease of the Ca^{2+} influx from extracellular media was filled with Ca^{2+} from the cytosolic Ca^{2+} store. Therefore, IRP especially decreased cytoplasmic Ca^{2+} level, which rescued the cytoplasmic Ca^{2+} accumulation caused by KCNQ1^{R397W}. Notably, the substantial elevation of cytoplasmic Ca^{2+} level repressed the expression of metabolism related genes (Figures 29-33). This decrease of expression was irreversible in functional β-cell development. To evaluate the timely IRP treatment, *in vivo* experiment is essential for further test.

5. Summary

KCNQ member 1 (KCNQ1, α subunit) co-assembles with KCNE accessory subunits (β subunit) to generate the $K_V7.1$ channel. K_V channels and K_{ATP} channels interact with voltage-dependent Ca^{2+} channels to trigger and maintain glucose-stimulated insulin secretion of pancreatic β cells. Here, our collaborators (Prof. Dr. K. Raile and Dr. M Gong) reported a diabetes patient with the *KCNQ1* homozygous point mutation who had intrauterine growth retardation with low birth weight and permanent neonatal diabetes. I generated the homozygous point mutation in hESCs_H1 imitating our neonatal diabetes patient by CRISPR-Cas9 homology-directed genome editing. The isogenic mutated hESCs_H1, wild type hESCs_H1, and unmodified control hESCs_H1 were converted into pancreatic islet-like organoids. The KCNQ1 homozygous point mutation β-like cells had a variational phenotype from higher insulin secretion turn into a lower level compared to controls. The KCNQ1 homozygous point mutation and the blockade of $K_V7.1$ channel increased the membrane action potential resulting in cytoplasmic Ca^{2+} accumulation. The increase of insulin secretion as a result of cytoplasmic Ca^{2+} accumulation negatively regulated the expression of metabolic genes of the cAMP pathway, *FGFRs*, *HNF4α* and *PDX1*. *FGFR1* and *PDX1* finally down-regulated *GLUT1* and resulted in a decrease in insulin secretion. Nevertheless, the organoids from the late stage of mature β cells were pro-apoptotic, which could be accelerated by chronic exposure to high glucose resulting in loss of β-cell mass and further decreased β-cell function by lower insulin secretion. Our results expose the critical roles of KCNQ1 in functional β-Cell development.

Zusammenfassung

Das KCNQ-Mitglied 1 (KCNQ1, α-Untereinheit) setzt sich zusammen mit KCNE-Untereinheiten (β-Untereinheit), um den K_V7.1-Kanal zu generieren. K_V-Kanäle und K_{ATP}-Kanäle interagieren mit spannungsabhängigen Ca^{2+}-Kanälen, um die durch Glukose stimulierte Insulinsekretion von Pankreas-β-Zellen auszulösen und aufrechtzuerhalten. Hier berichteten unsere Mitarbeiter (Prof. Dr. K. Raile und Dr. M. Gong) über einen Diabetes-Patienten mit einer homozygoten *KCNQ1*-Punktmutation, der eine Verzögerung des intrauterinen Wachstums mit niedrigem Geburtsgewicht und permanentem Neugeborenen-Diabetes aufwies. Wir haben die homozygote Punktmutation in hESCs_H1 durch homologiegesteuerte CRISPR-Cas9-Genomeditierung erzeugt, welche so unseren neugeborenen Diabetes-Patienten imitiert. Die isogen modifizierten hESCs_H1, Wildtyp-hESCs_H1 und nicht modifizierte Kontroll-hESCs_H1 wurden in pankreasinselzell-ähnliche Organoide umgewandelt. Die β-Zell-ähnlichen Zellen der homozygoten KCNQ1-Punktmutation wiesen, im Vergleich zu Kontrollen, einen abweichenden Phänotyp auf, der von einer höheren Insulinsekretion zu einem niedrigeren Niveau führte. Die homozygote Punktmutation von KCNQ1 und die Inhibition des K_V7.1-Kanals, erhöhte das Membranaktionspotential, was zu einer zytoplasmatischen Ca^{2+}-Akkumulation führte. Die Zunahme der Insulinsekretion als Ergebnis der zytoplasmatischen Ca^{2+}-Akkumulation regulierte die Expression von metabolischen Genen des cAMP-Weges, *FGFRs*, *HNF4α* und *PDX1*, negativ. *FGFR1* und *PDX1* regulierten *GLUT1* schließlich herunter und führten zu einer Verringerung der Insulinsekretion. Nichtsdestotrotz waren die Organoide aus dem späten Stadium der Reifung von β-Zellen pro-apoptotisch, welches durch chronische Exposition von hoher Menge an Glucose beschleunigt werden konnte, was zu einem Verlust der β-Zellmasse und einer weiteren Verringerung der β-Zellfunktion durch eine geringere Insulinsekretion führte. Unsere Ergebnisse zeigen die kritische Rolle von KCNQ1 bei der Entwicklung funktioneller β-Zellen auf.

6. Reference

1 Jennings, R. E., Berry, A. A., Strutt, J. P., Gerrard, D. T. & Hanley, N. A. Human pancreas development. *Development* **142**, 3126-3137, doi:10.1242/dev.120063 (2015).

2 Zhou, Q. & Melton, D. A. Pancreas regeneration. *Nature* **557**, 351-358, doi:10.1038/s41586-018-0088-0 (2018).

3 Rorsman, P. & Ashcroft, F. M. Pancreatic beta-Cell Electrical Activity and Insulin Secretion: Of Mice and Men. *Physiol Rev* **98**, 117-214, doi:10.1152/physrev.00008.2017 (2018).

4 OpenStax College. Anatomy and Physiology, chapter 17.9 The Endocrine Pancreas. Available from: https://legacy.cnx.org/content/col11496/11491.11498/ (2016).

5 Noguchi, G. M. & Huising, M. O. Integrating the inputs that shape pancreatic islet hormone release. *Nat Metab* **1**, 1189-1201, doi:10.1038/s42255-019-0148-2 (2019).

6 Singer, R. A. *et al.* The Long Noncoding RNA Paupar Modulates PAX6 Regulatory Activities to Promote Alpha Cell Development and Function. *Cell Metab*, doi:10.1016/j.cmet.2019.09.013 (2019).

7 American Diabetes, A. Diagnosis and classification of diabetes mellitus. *Diabetes Care* **37 Suppl 1**, S81-90, doi:10.2337/dc14-S081 (2014).

8 Cho, N. H. *et al.* IDF Diabetes Atlas: Global estimates of diabetes prevalence for 2017 and projections for 2045. *Diabetes Res Clin Pract* **138**, 271-281, doi:10.1016/j.diabres.2018.02.023 (2018).

9 Sneddon, J. B. *et al.* Stem Cell Therapies for Treating Diabetes: Progress and Remaining Challenges. *Cell Stem Cell* **22**, 810-823, doi:10.1016/j.stem.2018.05.016 (2018).

10 Fu, Z., Gilbert, E. R. & Liu, D. Regulation of insulin synthesis and secretion and pancreatic Beta-cell dysfunction in diabetes. *Curr Diabetes Rev* **9**, 25-53 (2013).

11 Grunnet, L. G. & Mandrup-Poulsen, T. Cytokines and type 1 diabetes: a numbers game. *Diabetes* **60**, 697-699, doi:10.2337/db10-1782 (2011).

12 Rabinovitch, A. & Suarez-Pinzon, W. L. Role of cytokines in the pathogenesis of autoimmune diabetes mellitus. *Rev Endocr Metab Disord* **4**, 291-299 (2003).

13 Donath, M. Y., Dinarello, C. A. & Mandrup-Poulsen, T. Targeting innate immune mediators in type 1 and type 2 diabetes. *Nat Rev Immunol*, doi:10.1038/s41577-019-0213-9 (2019).

14 You, W. P. & Henneberg, M. Type 1 diabetes prevalence increasing globally and regionally: the role of natural selection and life expectancy at birth. *BMJ Open Diabetes Res Care* **4**, e000161, doi:10.1136/bmjdrc-2015-000161 (2016).

15 Sousa, A. G., Selvatici, L., Krieger, J. E. & Pereira, A. C. Association between genetics of diabetes, coronary artery disease, and macrovascular complications: exploring a common ground hypothesis. *The review of diabetic studies : RDS* **8**, 230-244, doi:10.1900/RDS.2011.8.230 (2011).

16 Skyler, J. S. *et al.* Differentiation of Diabetes by Pathophysiology, Natural History, and Prognosis. *Diabetes* **66**, 241-255, doi:10.2337/db16-0806 (2017).

17 Remedi, M. S. & Emfinger, C. Pancreatic beta-cell identity in diabetes. *Diabetes Obes Metab* **18 Suppl 1**, 110-116, doi:10.1111/dom.12727 (2016).

18 Acosta-Montano, P. & Garcia-Gonzalez, V. Effects of Dietary Fatty Acids in Pancreatic Beta Cell Metabolism, Implications in Homeostasis. *Nutrients* **10**, doi:10.3390/nu10040393 (2018).

19 van der Zijl, N. J. *et al.* Ectopic fat storage in the pancreas, liver, and abdominal fat depots: impact on beta-cell function in individuals with impaired glucose metabolism. *J Clin Endocrinol Metab* **96**, 459-467, doi:10.1210/jc.2010-1722 (2011).

20 Henry, R. R., Wallace, P. & Olefsky, J. M. Effects of weight loss on mechanisms of hyperglycemia in obese non-insulin-dependent diabetes mellitus. *Diabetes* **35**, 990-998, doi:10.2337/diab.35.9.990 (1986).

21 Panunzi, S. *et al.* Determinants of Diabetes Remission and Glycemic Control After Bariatric Surgery. *Diabetes Care* **39**, 166-174, doi:10.2337/dc15-0575 (2016).

22 American Diabetes, A. 2. Classification and Diagnosis of Diabetes: Standards of Medical Care in Diabetes-2019. *Diabetes Care* **42**, S13-S28, doi:10.2337/dc19-S002 (2019).

23 Kim, C., Newton, K. M. & Knopp, R. H. Gestational diabetes and the incidence of type 2 diabetes: a systematic review. *Diabetes Care* **25**, 1862-1868, doi:10.2337/diacare.25.10.1862 (2002).

24 Aroda, V. R. *et al.* The effect of lifestyle intervention and metformin on preventing or delaying diabetes among women with and without gestational diabetes: the Diabetes Prevention Program outcomes study 10-year follow-up. *J Clin Endocrinol Metab* **100**, 1646-1653, doi:10.1210/jc.2014-3761 (2015).

25 Cnop, M. *et al.* Mechanisms of pancreatic beta-cell death in type 1 and type 2 diabetes: many differences, few similarities. *Diabetes* **54 Suppl 2**, S97-107, doi:10.2337/diabetes.54.suppl_2.s97 (2005).

26 Cao, S. S. & Kaufman, R. J. Endoplasmic reticulum stress and oxidative stress in cell fate decision and human disease. *Antioxidants & redox signaling* **21**, 396-413, doi:10.1089/ars.2014.5851 (2014).

27 Ly, L. D. *et al.* Oxidative stress and calcium dysregulation by palmitate in type 2 diabetes. *Experimental & molecular medicine* **49**, e291, doi:10.1038/emm.2016.157 (2017).

28 Thomas, E. R. *et al.* Diagnosis of monogenic diabetes: 10-Year experience in a large multi-ethnic diabetes center. *J Diabetes Investig* **7**, 332-337, doi:10.1111/jdi.12432 (2016).

29 Sanyoura, M., Philipson, L. H. & Naylor, R. Monogenic Diabetes in Children and Adolescents: Recognition and Treatment Options. *Curr Diab Rep* **18**, 58, doi:10.1007/s11892-018-1024-2 (2018).

30 Hattersley, A. T. & Patel, K. A. Precision diabetes: learning from monogenic diabetes. *Diabetologia* **60**, 769-777, doi:10.1007/s00125-017-4226-2 (2017).

31 Kleinberger, J. W. & Pollin, T. I. Undiagnosed MODY: Time for Action. *Curr Diab Rep* **15**, 110, doi:10.1007/s11892-015-0681-7 (2015).

32 Polak, M. & Cave, H. Neonatal diabetes mellitus: a disease linked to multiple mechanisms. *Orphanet J Rare Dis* **2**, 12, doi:10.1186/1750-1172-2-12 (2007).

33 Mohora, R. & Stoicescu, S. M. Congenital Diabetes Mellitus. *Maedica (Buchar)* **11**, 154-157 (2016).

34 Aguilar-Bryan, L. & Bryan, J. Neonatal diabetes mellitus. *Endocr Rev* **29**, 265-291, doi:10.1210/er.2007-0029 (2008).

35 Murphy, R., Ellard, S. & Hattersley, A. T. Clinical implications of a molecular genetic classification of monogenic beta-cell diabetes. *Nat Clin Pract Endocrinol Metab* **4**, 200-213, doi:10.1038/ncpendmet0778 (2008).

36 Forbes, J. M. & Cooper, M. E. Mechanisms of diabetic complications. *Physiological reviews* **93**, 137-188, doi:10.1152/physrev.00045.2011 (2013).

37 Lakey, J. R., Mirbolooki, M. & Shapiro, A. M. Current status of clinical islet cell transplantation. *Methods Mol Biol* **333**, 47-104, doi:10.1385/1-59745-049-9:47 (2006).

38 Hering, B. J. *et al.* Phase 3 Trial of Transplantation of Human Islets in Type 1 Diabetes Complicated by Severe Hypoglycemia. *Diabetes Care* **39**, 1230-1240, doi:10.2337/dc15-1988 (2016).

39 Slack, J. M. Developmental biology of the pancreas. *Development* **121**, 1569-1580 (1995).

40 Takahashi, K. *et al.* Induction of pluripotent stem cells from adult human fibroblasts by defined factors. *Cell* **131**, 861-872, doi:10.1016/j.cell.2007.11.019 (2007).

41 Staerk, J. *et al.* Reprogramming of human peripheral blood cells to induced pluripotent stem cells. *Cell Stem Cell* **7**, 20-24, doi:10.1016/j.stem.2010.06.002 (2010).

42 Thurner, M. *et al.* Genes Associated with Pancreas Development and Function Maintain Open Chromatin in iPSCs Generated from Human Pancreatic Beta Cells. *Stem Cell Reports* **9**, 1395-1405, doi:10.1016/j.stemcr.2017.09.020 (2017).

43 Grabundzija, I. *et al.* Sleeping Beauty transposon-based system for cellular reprogramming and targeted gene insertion in induced pluripotent stem cells. *Nucleic Acids Res* **41**, 1829-1847, doi:10.1093/nar/gks1305 (2013).

44 Rezania, A. *et al.* Reversal of diabetes with insulin-producing cells derived in vitro from human pluripotent stem cells. *Nat Biotechnol* **32**, 1121-1133, doi:10.1038/nbt.3033 (2014).

45 Pagliuca, F. W. *et al.* Generation of functional human pancreatic beta cells in vitro. *Cell* **159**, 428-439, doi:10.1016/j.cell.2014.09.040 (2014).

46 Velazco-Cruz, L. *et al.* Acquisition of Dynamic Function in Human Stem Cell-Derived beta Cells. *Stem Cell Reports* **12**, 351-365, doi:10.1016/j.stemcr.2018.12.012 (2019).

47 Pagliuca, F. W. & Melton, D. A. How to make a functional beta-cell. *Development* **140**, 2472-2483, doi:10.1242/dev.093187 (2013).

48 Vegas, A. J. *et al.* Long-term glycemic control using polymer-encapsulated human stem cell-derived beta cells in immune-competent mice. *Nat Med* **22**, 306-311, doi:10.1038/nm.4030 (2016).

49 Henquin, J. C., Dufrane, D. & Nenquin, M. Nutrient control of insulin secretion in isolated normal human islets. *Diabetes* **55**, 3470-3477, doi:10.2337/db06-0868 (2006).

50 Matschinsky, F. M., Glaser, B. & Magnuson, M. A. Pancreatic beta-cell glucokinase: closing the gap between theoretical concepts and experimental realities. *Diabetes* **47**, 307-315, doi:10.2337/diabetes.47.3.307 (1998).

51 Walker, J. N. *et al.* Regulation of glucagon secretion by glucose: paracrine, intrinsic or both? *Diabetes Obes Metab* **13 Suppl 1**, 95-105, doi:10.1111/j.1463-1326.2011.01450.x (2011).

52 Alcazar, O. & Buchwald, P. Concentration-Dependency and Time Profile of Insulin Secretion: Dynamic Perifusion Studies With Human and Murine Islets. *Front Endocrinol (Lausanne)* **10**, 680, doi:10.3389/fendo.2019.00680 (2019).

53 Muller, T. D. *et al.* Glucagon-like peptide 1 (GLP-1). *Mol Metab* **30**, 72-130, doi:10.1016/j.molmet.2019.09.010 (2019).

54 Thorens, B. GLUT2, glucose sensing and glucose homeostasis. *Diabetologia* **58**, 221-232, doi:10.1007/s00125-014-3451-1 (2015).

55 Sansbury, F. H. *et al.* SLC2A2 mutations can cause neonatal diabetes, suggesting GLUT2 may have a role in human insulin secretion. *Diabetologia* **55**, 2381-2385, doi:10.1007/s00125-012-2595-0 (2012).

56 De Vos, A. *et al.* Human and rat beta cells differ in glucose transporter but not in glucokinase gene expression. *J Clin Invest* **96**, 2489-2495, doi:10.1172/JCI118308 (1995).

57 Mitanchez, D., Doiron, B., Chen, R. & Kahn, A. Glucose-stimulated genes and prospects of gene therapy for type I diabetes. *Endocr Rev* **18**, 520-540, doi:10.1210/edrv.18.4.0307 (1997).

58 Drucker, D. J., Philippe, J., Mojsov, S., Chick, W. L. & Habener, J. F. Glucagon-like peptide I stimulates insulin gene expression and increases cyclic AMP levels in a rat

islet cell line. *Proc Natl Acad Sci U S A* **84**, 3434-3438, doi:10.1073/pnas.84.10.3434 (1987).
59 Ramos, L. S., Zippin, J. H., Kamenetsky, M., Buck, J. & Levin, L. R. Glucose and GLP-1 stimulate cAMP production via distinct adenylyl cyclases in INS-1E insulinoma cells. *J Gen Physiol* **132**, 329-338, doi:10.1085/jgp.200810044 (2008).
60 Idevall-Hagren, O., Barg, S., Gylfe, E. & Tengholm, A. cAMP mediators of pulsatile insulin secretion from glucose-stimulated single beta-cells. *J Biol Chem* **285**, 23007-23018, doi:10.1074/jbc.M109.095992 (2010).
61 Holz, G. G. Epac: A new cAMP-binding protein in support of glucagon-like peptide-1 receptor-mediated signal transduction in the pancreatic beta-cell. *Diabetes* **53**, 5-13, doi:10.2337/diabetes.53.1.5 (2004).
62 Wang, X. *et al.* Glucagon-like peptide-1 regulates the beta cell transcription factor, PDX-1, in insulinoma cells. *Endocrinology* **140**, 4904-4907, doi:10.1210/endo.140.10.7158 (1999).
63 Wang, X., Zhou, J., Doyle, M. E. & Egan, J. M. Glucagon-like peptide-1 causes pancreatic duodenal homeobox-1 protein translocation from the cytoplasm to the nucleus of pancreatic beta-cells by a cyclic adenosine monophosphate/protein kinase A-dependent mechanism. *Endocrinology* **142**, 1820-1827, doi:10.1210/endo.142.5.8128 (2001).
64 Fridlyand, L. E., Jacobson, D. A. & Philipson, L. H. Ion channels and regulation of insulin secretion in human beta-cells: a computational systems analysis. *Islets* **5**, 1-15, doi:10.4161/isl.24166 (2013).
65 Schroder, M. & Kaufman, R. J. The mammalian unfolded protein response. *Annu Rev Biochem* **74**, 739-789, doi:10.1146/annurev.biochem.73.011303.074134 (2005).
66 Wang, R. *et al.* Insulin secretion and Ca2+ dynamics in beta-cells are regulated by PERK (EIF2AK3) in concert with calcineurin. *J Biol Chem* **288**, 33824-33836, doi:10.1074/jbc.M113.503664 (2013).
67 Kang, G. *et al.* Epac-selective cAMP analog 8-pCPT-2'-O-Me-cAMP as a stimulus for Ca2+-induced Ca2+ release and exocytosis in pancreatic beta-cells. *J Biol Chem* **278**, 8279-8285, doi:10.1074/jbc.M211682200 (2003).
68 Dunn, M. F. Zinc-ligand interactions modulate assembly and stability of the insulin hexamer -- a review. *Biometals* **18**, 295-303, doi:10.1007/s10534-005-3685-y (2005).
69 Varndell, I. M., Lloyd, R. V., Wilson, B. S. & Polak, J. M. Ultrastructural localization of chromogranin: a potential marker for the electron microscopical recognition of endocrine cell secretory granules. *Histochem J* **17**, 981-992, doi:10.1007/BF01417947 (1985).
70 Wenham, R. M., Landt, M. & Easom, R. A. Glucose activates the multifunctional Ca2+/calmodulin-dependent protein kinase II in isolated rat pancreatic islets. *J Biol Chem* **269**, 4947-4952 (1994).
71 Norling, L. L., Colca, J. R., Kelly, P. T., McDaniel, M. L. & Landt, M. Activation of calcium and calmodulin dependent protein kinase II during stimulation of insulin secretion. *Cell Calcium* **16**, 137-150, doi:10.1016/0143-4160(94)90008-6 (1994).
72 Malaisse, W. J. *et al.* Role of microtubules in the phasic pattern of insulin release. *Ann N Y Acad Sci* **253**, 630-652, doi:10.1111/j.1749-6632.1975.tb19234.x (1975).
73 Suprenant, K. A. & Dentler, W. L. Association between endocrine pancreatic secretory granules and in-vitro-assembled microtubules is dependent upon microtubule-associated proteins. *J Cell Biol* **93**, 164-174, doi:10.1083/jcb.93.1.164 (1982).
74 Lang, J., Fukuda, M., Zhang, H., Mikoshiba, K. & Wollheim, C. B. The first C2 domain of synaptotagmin is required for exocytosis of insulin from pancreatic beta-cells: action of synaptotagmin at low micromolar calcium. *EMBO J* **16**, 5837-5846, doi:10.1093/emboj/16.19.5837 (1997).

75 Gao, Z., Reavey-Cantwell, J., Young, R. A., Jegier, P. & Wolf, B. A. Synaptotagmin III/VII isoforms mediate Ca2+-induced insulin secretion in pancreatic islet beta -cells. *J Biol Chem* **275**, 36079-36085, doi:10.1074/jbc.M004284200 (2000).

76 Olofsson, C. S. *et al.* Fast insulin secretion reflects exocytosis of docked granules in mouse pancreatic B-cells. *Pflugers Arch* **444**, 43-51, doi:10.1007/s00424-002-0781-5 (2002).

77 Toschi, E. *et al.* Effect of acute hyperglycemia on insulin secretion in humans. *Diabetes* **51 Suppl 1**, S130-133, doi:10.2337/diabetes.51.2007.s130 (2002).

78 Low, J. T. *et al.* Glucose principally regulates insulin secretion in mouse islets by controlling the numbers of granule fusion events per cell. *Diabetologia* **56**, 2629-2637, doi:10.1007/s00125-013-3019-5 (2013).

79 Benninger, R. K., Zhang, M., Head, W. S., Satin, L. S. & Piston, D. W. Gap junction coupling and calcium waves in the pancreatic islet. *Biophys J* **95**, 5048-5061, doi:10.1529/biophysj.108.140863 (2008).

80 Braun, M. *et al.* Voltage-gated ion channels in human pancreatic beta-cells: electrophysiological characterization and role in insulin secretion. *Diabetes* **57**, 1618-1628, doi:10.2337/db07-0991 (2008).

81 Gwiazda, K. S., Yang, T. L., Lin, Y. & Johnson, J. D. Effects of palmitate on ER and cytosolic Ca2+ homeostasis in beta-cells. *Am J Physiol Endocrinol Metab* **296**, E690-701, doi:10.1152/ajpendo.90525.2008 (2009).

82 Barnett, D. W., Pressel, D. M. & Misler, S. Voltage-dependent Na+ and Ca2+ currents in human pancreatic islet beta-cells: evidence for roles in the generation of action potentials and insulin secretion. *Pflugers Arch* **431**, 272-282, doi:10.1007/BF00410201 (1995).

83 Felix-Martinez, G. J. & Godinez-Fernandez, J. R. Mathematical models of electrical activity of the pancreatic beta-cell: a physiological review. *Islets* **6**, e949195, doi:10.4161/19382014.2014.949195 (2014).

84 Yang, S. N. *et al.* Ionic mechanisms in pancreatic beta cell signaling. *Cell Mol Life Sci* **71**, 4149-4177, doi:10.1007/s00018-014-1680-6 (2014).

85 Rorsman, P. & Braun, M. Regulation of insulin secretion in human pancreatic islets. *Annu Rev Physiol* **75**, 155-179, doi:10.1146/annurev-physiol-030212-183754 (2013).

86 Herrington, J. Gating modifier peptides as probes of pancreatic beta-cell physiology. *Toxicon* **49**, 231-238, doi:10.1016/j.toxicon.2006.09.012 (2007).

87 Yang, J. K. *et al.* From Hyper- to Hypoinsulinemia and Diabetes: Effect of KCNH6 on Insulin Secretion. *Cell Rep* **25**, 3800-3810 e3806, doi:10.1016/j.celrep.2018.12.005 (2018).

88 MacDonald, P. E. & Wheeler, M. B. Voltage-dependent K(+) channels in pancreatic beta cells: role, regulation and potential as therapeutic targets. *Diabetologia* **46**, 1046-1062, doi:10.1007/s00125-003-1159-8 (2003).

89 Unoki, H. *et al.* SNPs in KCNQ1 are associated with susceptibility to type 2 diabetes in East Asian and European populations. *Nat Genet* **40**, 1098-1102, doi:10.1038/ng.208 (2008).

90 Yasuda, K. *et al.* Variants in KCNQ1 are associated with susceptibility to type 2 diabetes mellitus. *Nat Genet* **40**, 1092-1097, doi:10.1038/ng.207 (2008).

91 Finol-Urdaneta, R. K. *et al.* Block of Kv1.7 potassium currents increases glucose-stimulated insulin secretion. *EMBO Mol Med* **4**, 424-434, doi:10.1002/emmm.201200218 (2012).

92 Nicholes, K. *et al.* A mouse model of hepatocellular carcinoma: ectopic expression of fibroblast growth factor 19 in skeletal muscle of transgenic mice. *Am J Pathol* **160**, 2295-2307, doi:10.1016/S0002-9440(10)61177-7 (2002).

93 Wu, X. *et al.* FGF19-induced hepatocyte proliferation is mediated through FGFR4 activation. *J Biol Chem* **285**, 5165-5170, doi:10.1074/jbc.M109.068783 (2010).

94 Hutley, L. *et al.* Fibroblast growth factor 1: a key regulator of human adipogenesis. *Diabetes* **53**, 3097-3106, doi:10.2337/diabetes.53.12.3097 (2004).

95 Newell, F. S. *et al.* Characterization of the transcriptional and functional effects of fibroblast growth factor-1 on human preadipocyte differentiation. *FASEB J* **20**, 2615-2617, doi:10.1096/fj.05-5710fje (2006).

96 Jonker, J. W. *et al.* A PPARgamma-FGF1 axis is required for adaptive adipose remodelling and metabolic homeostasis. *Nature* **485**, 391-394, doi:10.1038/nature10998 (2012).

97 Kharitonenkov, A. *et al.* FGF-21 as a novel metabolic regulator. *J Clin Invest* **115**, 1627-1635, doi:10.1172/JCI23606 (2005).

98 Suh, J. M. *et al.* Endocrinization of FGF1 produces a neomorphic and potent insulin sensitizer. *Nature* **513**, 436-439, doi:10.1038/nature13540 (2014).

99 Fu, L. *et al.* Fibroblast growth factor 19 increases metabolic rate and reverses dietary and leptin-deficient diabetes. *Endocrinology* **145**, 2594-2603, doi:10.1210/en.2003-1671 (2004).

100 Wente, W. *et al.* Fibroblast growth factor-21 improves pancreatic beta-cell function and survival by activation of extracellular signal-regulated kinase 1/2 and Akt signaling pathways. *Diabetes* **55**, 2470-2478, doi:10.2337/db05-1435 (2006).

101 Miralles, F., Czernichow, P., Ozaki, K., Itoh, N. & Scharfmann, R. Signaling through fibroblast growth factor receptor 2b plays a key role in the development of the exocrine pancreas. *Proc Natl Acad Sci U S A* **96**, 6267-6272, doi:10.1073/pnas.96.11.6267 (1999).

102 Hart, A. W., Baeza, N., Apelqvist, A. & Edlund, H. Attenuation of FGF signalling in mouse beta-cells leads to diabetes. *Nature* **408**, 864-868, doi:10.1038/35048589 (2000).

103 Narla, S. T. *et al.* Common developmental genome deprogramming in schizophrenia - Role of Integrative Nuclear FGFR1 Signaling (INFS). *Schizophr Res* **185**, 17-32, doi:10.1016/j.schres.2016.12.012 (2017).

104 Waeber, G., Thompson, N., Nicod, P. & Bonny, C. Transcriptional activation of the GLUT2 gene by the IPF-1/STF-1/IDX-1 homeobox factor. *Mol Endocrinol* **10**, 1327-1334, doi:10.1210/mend.10.11.8923459 (1996).

105 Ahlgren, U., Jonsson, J., Jonsson, L., Simu, K. & Edlund, H. beta-cell-specific inactivation of the mouse Ipf1/Pdx1 gene results in loss of the beta-cell phenotype and maturity onset diabetes. *Genes Dev* **12**, 1763-1768, doi:10.1101/gad.12.12.1763 (1998).

106 Brissova, M. *et al.* Reduction in pancreatic transcription factor PDX-1 impairs glucose-stimulated insulin secretion. *J Biol Chem* **277**, 11225-11232, doi:10.1074/jbc.M111272200 (2002).

107 Sleeman, M. *et al.* Identification of a new fibroblast growth factor receptor, FGFR5. *Gene* **271**, 171-182, doi:10.1016/s0378-1119(01)00518-2 (2001).

108 Silva, P. N., Altamentova, S. M., Kilkenny, D. M. & Rocheleau, J. V. Fibroblast growth factor receptor like-1 (FGFRL1) interacts with SHP-1 phosphatase at insulin secretory granules and induces beta-cell ERK1/2 protein activation. *J Biol Chem* **288**, 17859-17870, doi:10.1074/jbc.M112.440677 (2013).

109 Regeenes, R. *et al.* Fibroblast growth factor receptor 5 (FGFR5) is a co-receptor for FGFR1 that is up-regulated in beta-cells by cytokine-induced inflammation. *J Biol Chem* **293**, 17218-17228, doi:10.1074/jbc.RA118.003036 (2018).

110 Henry, G. L. & Melton, D. A. Mixer, a homeobox gene required for endoderm development. *Science* **281**, 91-96, doi:10.1126/science.281.5373.91 (1998).

111 Kroon, E. *et al.* Pancreatic endoderm derived from human embryonic stem cells generates glucose-responsive insulin-secreting cells in vivo. *Nat Biotechnol* **26**, 443-452, doi:10.1038/nbt1393 (2008).

112 D'Amour, K. A. *et al.* Production of pancreatic hormone-expressing endocrine cells from human embryonic stem cells. *Nat Biotechnol* **24**, 1392-1401, doi:10.1038/nbt1259 (2006).

113 Vincent, S. D., Dunn, N. R., Hayashi, S., Norris, D. P. & Robertson, E. J. Cell fate decisions within the mouse organizer are governed by graded Nodal signals. *Genes Dev* **17**, 1646-1662, doi:10.1101/gad.1100503 (2003).

114 Schier, A. F. Nodal signaling in vertebrate development. *Annu Rev Cell Dev Biol* **19**, 589-621, doi:10.1146/annurev.cellbio.19.041603.094522 (2003).

115 Champeris Tsaniras, S. & Jones, P. M. Generating pancreatic beta-cells from embryonic stem cells by manipulating signaling pathways. *J Endocrinol* **206**, 13-26, doi:10.1677/JOE-10-0073 (2010).

116 Uzan, B., Figeac, F., Portha, B. & Movassat, J. Mechanisms of KGF mediated signaling in pancreatic duct cell proliferation and differentiation. *PLoS One* **4**, e4734, doi:10.1371/journal.pone.0004734 (2009).

117 Watanabe, H., Saito, H., Nishimura, H., Ueda, J. & Evers, B. M. Activation of phosphatidylinositol-3 kinase regulates pancreatic duodenal homeobox-1 in duct cells during pancreatic regeneration. *Pancreas* **36**, 153-159, doi:10.1097/MPA.0b013e318157753e (2008).

118 Rosado-Olivieri, E. A., Anderson, K., Kenty, J. H. & Melton, D. A. YAP inhibition enhances the differentiation of functional stem cell-derived insulin-producing beta cells. *Nat Commun* **10**, 1464, doi:10.1038/s41467-019-09404-6 (2019).

119 Morris, K. V. & Mattick, J. S. The rise of regulatory RNA. *Nature reviews. Genetics* **15**, 423-437, doi:10.1038/nrg3722 (2014).

120 Singer, R. A. & Sussel, L. Islet Long Noncoding RNAs: A Playbook for Discovery and Characterization. *Diabetes* **67**, 1461-1470, doi:10.2337/dbi18-0001 (2018).

121 Zhang, H. *et al.* Long noncoding RNA-mediated intrachromosomal interactions promote imprinting at the Kcnq1 locus. *J Cell Biol* **204**, 61-75, doi:10.1083/jcb.201304152 (2014).

122 Arnes, L. & Sussel, L. Epigenetic modifications and long noncoding RNAs influence pancreas development and function. *Trends Genet* **31**, 290-299, doi:10.1016/j.tig.2015.02.008 (2015).

123 Reik, W. & Walter, J. Genomic imprinting: parental influence on the genome. *Nature reviews. Genetics* **2**, 21-32, doi:10.1038/35047554 (2001).

124 Singh, V. B. *et al.* Blocked transcription through KvDMR1 results in absence of methylation and gene silencing resembling Beckwith-Wiedemann syndrome. *Development* **144**, 1820-1830, doi:10.1242/dev.145136 (2017).

125 Asahara, S. *et al.* Paternal allelic mutation at the Kcnq1 locus reduces pancreatic beta-cell mass by epigenetic modification of Cdkn1c. *Proceedings of the National Academy of Sciences of the United States of America* **112**, 8332-8337, doi:10.1073/pnas.1422104112 (2015).

126 Nakano, S. *et al.* Expression profile of LIT1/KCNQ1OT1 and epigenetic status at the KvDMR1 in colorectal cancers. *Cancer Sci* **97**, 1147-1154, doi:10.1111/j.1349-7006.2006.00305.x (2006).

127 Tsai, M. C. *et al.* Long noncoding RNA as modular scaffold of histone modification complexes. *Science* **329**, 689-693, doi:10.1126/science.1192002 (2010).

128 Aylward, A., Chiou, J., Okino, M. L., Kadakia, N. & Gaulton, K. J. Shared genetic risk contributes to type 1 and type 2 diabetes etiology. *Hum Mol Genet*, doi:10.1093/hmg/ddy314 (2018).

129 McMinn, J. *et al.* Unbalanced placental expression of imprinted genes in human intrauterine growth restriction. *Placenta* **27**, 540-549, doi:10.1016/j.placenta.2005.07.004 (2006).

130 Lopez-Abad, M., Iglesias-Platas, I. & Monk, D. Epigenetic Characterization of CDKN1C in Placenta Samples from Non-syndromic Intrauterine Growth Restriction. *Front Genet* **7**, 62, doi:10.3389/fgene.2016.00062 (2016).

131 Schultz, B. M., Gallicio, G. A., Cesaroni, M., Lupey, L. N. & Engel, N. Enhancers compete with a long non-coding RNA for regulation of the Kcnq1 domain. *Nucleic acids research* **43**, 745-759, doi:10.1093/nar/gku1324 (2015).

132 Xie, R. *et al.* Dynamic chromatin remodeling mediated by polycomb proteins orchestrates pancreatic differentiation of human embryonic stem cells. *Cell Stem Cell* **12**, 224-237, doi:10.1016/j.stem.2012.11.023 (2013).

133 Miguel-Escalada, I. *et al.* Human pancreatic islet three-dimensional chromatin architecture provides insights into the genetics of type 2 diabetes. *Nat Genet* **51**, 1137-1148, doi:10.1038/s41588-019-0457-0 (2019).

134 Wrobel, E., Tapken, D. & Seebohm, G. The KCNE Tango - How KCNE1 Interacts with Kv7.1. *Frontiers in pharmacology* **3**, 142, doi:10.3389/fphar.2012.00142 (2012).

135 Wang, M. & Kass, R. S. Stoichiometry of the slow I(ks) potassium channel in human embryonic stem cell-derived myocytes. *Pediatric cardiology* **33**, 938-942, doi:10.1007/s00246-012-0255-2 (2012).

136 Jespersen, T., Grunnet, M. & Olesen, S. P. The KCNQ1 potassium channel: from gene to physiological function. *Physiology (Bethesda)* **20**, 408-416, doi:10.1152/physiol.00031.2005 (2005).

137 Wiener, R. *et al.* The KCNQ1 (Kv7.1) COOH terminus, a multitiered scaffold for subunit assembly and protein interaction. *J Biol Chem* **283**, 5815-5830, doi:10.1074/jbc.M707541200 (2008).

138 Schmitt, N. *et al.* A recessive C-terminal Jervell and Lange-Nielsen mutation of the KCNQ1 channel impairs subunit assembly. *EMBO J* **19**, 332-340, doi:10.1093/emboj/19.3.332 (2000).

139 Maljevic, S. *et al.* C-terminal interaction of KCNQ2 and KCNQ3 K+ channels. *J Physiol* **548**, 353-360, doi:10.1113/jphysiol.2003.040980 (2003).

140 Schwake, M., Jentsch, T. J. & Friedrich, T. A carboxy-terminal domain determines the subunit specificity of KCNQ K+ channel assembly. *EMBO Rep* **4**, 76-81, doi:10.1038/sj.embor.embor715 (2003).

141 Schwake, M. *et al.* Structural determinants of M-type KCNQ (Kv7) K+ channel assembly. *J Neurosci* **26**, 3757-3766, doi:10.1523/JNEUROSCI.5017-05.2006 (2006).

142 Ghosh, S., Nunziato, D. A. & Pitt, G. S. KCNQ1 assembly and function is blocked by long-QT syndrome mutations that disrupt interaction with calmodulin. *Circ Res* **98**, 1048-1054, doi:10.1161/01.RES.0000218863.44140.f2 (2006).

143 Shamgar, L. *et al.* Calmodulin is essential for cardiac IKS channel gating and assembly: impaired function in long-QT mutations. *Circ Res* **98**, 1055-1063, doi:10.1161/01.RES.0000218979.40770.69 (2006).

144 Etxeberria, A. *et al.* Calmodulin regulates the trafficking of KCNQ2 potassium channels. *FASEB J* **22**, 1135-1143, doi:10.1096/fj.07-9712com (2008).

145 Howard, R. J., Clark, K. A., Holton, J. M. & Minor, D. L., Jr. Structural insight into KCNQ (Kv7) channel assembly and channelopathy. *Neuron* **53**, 663-675, doi:10.1016/j.neuron.2007.02.010 (2007).

146 Liin, S. I., Barro-Soria, R. & Larsson, H. P. The KCNQ1 channel - remarkable flexibility in gating allows for functional versatility. *The Journal of physiology* **593**, 2605-2615, doi:10.1113/jphysiol.2014.287607 (2015).

147 Wang, W., Xia, J. & Kass, R. S. MinK-KvLQT1 fusion proteins, evidence for multiple stoichiometries of the assembled IsK channel. *The Journal of biological chemistry* **273**, 34069-34074 (1998).

148 Bendahhou, S. *et al.* In vitro molecular interactions and distribution of KCNE family with KCNQ1 in the human heart. *Cardiovascular research* **67**, 529-538, doi:10.1016/j.cardiores.2005.02.014 (2005).

149 Mao, T. *et al.* [Association of single nucleotide polymorphism of KCNE1 and KCNE4 gene with atrial fibrillation in Xinjiang Uygur and Han population]. *Zhonghua xin xue guan bing za zhi* **41**, 916-921 (2013).

150 Ohno, S. *et al.* KCNE5 (KCNE1L) variants are novel modulators of Brugada syndrome and idiopathic ventricular fibrillation. *Circulation. Arrhythmia and electrophysiology* **4**, 352-361, doi:10.1161/CIRCEP.110.959619 (2011).

151 Abbott, G. W. KCNE1 and KCNE3: The yin and yang of voltage-gated K(+) channel regulation. *Gene* **576**, 1-13, doi:10.1016/j.gene.2015.09.059 (2016).

152 Roepke, T. K. *et al.* Targeted deletion of kcne2 impairs ventricular repolarization via disruption of I(K,slow1) and I(to,f). *FASEB J* **22**, 3648-3660, doi:10.1096/fj.08-110171 (2008).

153 Sachyani, D. *et al.* Structural basis of a Kv7.1 potassium channel gating module: studies of the intracellular c-terminal domain in complex with calmodulin. *Structure* **22**, 1582-1594, doi:10.1016/j.str.2014.07.016 (2014).

154 Sun, J. & MacKinnon, R. Cryo-EM Structure of a KCNQ1/CaM Complex Reveals Insights into Congenital Long QT Syndrome. *Cell* **169**, 1042-1050 e1049, doi:10.1016/j.cell.2017.05.019 (2017).

155 Easom, R. A. CaM kinase II: a protein kinase with extraordinary talents germane to insulin exocytosis. *Diabetes* **48**, 675-684 (1999).

156 Zhao, J. *et al.* In vivo imaging of beta-cell function reveals glucose-mediated heterogeneity of beta-cell functional development. *Elife* **8**, doi:10.7554/eLife.41540 (2019).

157 Zaydman, M. A. *et al.* Kv7.1 ion channels require a lipid to couple voltage sensing to pore opening. *Proceedings of the National Academy of Sciences of the United States of America* **110**, 13180-13185, doi:10.1073/pnas.1305167110 (2013).

158 Thore, S., Dyachok, O., Gylfe, E. & Tengholm, A. Feedback activation of phospholipase C via intracellular mobilization and store-operated influx of Ca2+ in insulin-secreting beta-cells. *J Cell Sci* **118**, 4463-4471, doi:10.1242/jcs.02577 (2005).

159 Hagar, R. E. & Ehrlich, B. E. Regulation of the type III InsP(3) receptor by InsP(3) and ATP. *Biophys J* **79**, 271-278, doi:10.1016/S0006-3495(00)76289-8 (2000).

160 Clark, M. D., Contreras, G. F., Shen, R. & Perozo, E. Electromechanical coupling in the hyperpolarization-activated K(+) channel KAT1. *Nature* **583**, 145-149, doi:10.1038/s41586-020-2335-4 (2020).

161 Hu, C. *et al.* Variations in KCNQ1 are associated with type 2 diabetes and beta cell function in a Chinese population. *Diabetologia* **52**, 1322-1325, doi:10.1007/s00125-009-1335-6 (2009).

162 Jonsson, A. *et al.* A variant in the KCNQ1 gene predicts future type 2 diabetes and mediates impaired insulin secretion. *Diabetes* **58**, 2409-2413, doi:10.2337/db09-0246 (2009).

163 Hou, J. C., Min, L. & Pessin, J. E. Insulin granule biogenesis, trafficking and exocytosis. *Vitam Horm* **80**, 473-506, doi:10.1016/S0083-6729(08)00616-X (2009).

164 Casimiro, M. C. *et al.* Targeted disruption of the Kcnq1 gene produces a mouse model of Jervell and Lange-Nielsen Syndrome. *Proc Natl Acad Sci U S A* **98**, 2526-2531, doi:10.1073/pnas.041398998 (2001).

165 Boini, K. M. *et al.* Enhanced insulin sensitivity of gene-targeted mice lacking functional KCNQ1. *Am J Physiol Regul Integr Comp Physiol* **296**, R1695-1701, doi:10.1152/ajpregu.90839.2008 (2009).

166 Zeng, H. *et al.* An Isogenic Human ESC Platform for Functional Evaluation of Genome-wide-Association-Study-Identified Diabetes Genes and Drug Discovery. *Cell Stem Cell* **19**, 326-340, doi:10.1016/j.stem.2016.07.002 (2016).
167 Cox, D. B., Platt, R. J. & Zhang, F. Therapeutic genome editing: prospects and challenges. *Nat Med* **21**, 121-131, doi:10.1038/nm.3793 (2015).
168 Barrangou, R. & Marraffini, L. A. CRISPR-Cas systems: Prokaryotes upgrade to adaptive immunity. *Mol Cell* **54**, 234-244, doi:10.1016/j.molcel.2014.03.011 (2014).
169 Jinek, M. *et al.* A programmable dual-RNA-guided DNA endonuclease in adaptive bacterial immunity. *Science* **337**, 816-821, doi:10.1126/science.1225829 (2012).
170 Richardson, C. D., Ray, G. J., DeWitt, M. A., Curie, G. L. & Corn, J. E. Enhancing homology-directed genome editing by catalytically active and inactive CRISPR-Cas9 using asymmetric donor DNA. *Nat Biotechnol* **34**, 339-344, doi:10.1038/nbt.3481 (2016).
171 Ran, F. A. *et al.* Genome engineering using the CRISPR-Cas9 system. *Nature protocols* **8**, 2281-2308, doi:10.1038/nprot.2013.143 (2013).
172 Hussain, B., Lucas, S. J. & Budak, H. CRISPR/Cas9 in plants: at play in the genome and at work for crop improvement. *Briefings in functional genomics* **17**, 319-328, doi:10.1093/bfgp/ely016 (2018).
173 Alves-Bezerra, M., Furey, N., Johnson, C. G. & Bissig, K. D. Using CRISPR/Cas9 to model human liver disease. *JHEP reports* **1**, 392-402, doi:10.1016/j.jhepr.2019.09.002 (2019).
174 Enache, O. M. *et al.* Cas9 activates the p53 pathway and selects for p53-inactivating mutations. *Nat Genet* **52**, 662-668, doi:10.1038/s41588-020-0623-4 (2020).
175 Schiroli, G. *et al.* Precise Gene Editing Preserves Hematopoietic Stem Cell Function following Transient p53-Mediated DNA Damage Response. *Cell Stem Cell* **24**, 551-565 e558, doi:10.1016/j.stem.2019.02.019 (2019).
176 Doudna, J. A. The promise and challenge of therapeutic genome editing. *Nature* **578**, 229-236, doi:10.1038/s41586-020-1978-5 (2020).
177 Gu, Z., Eils, R. & Schlesner, M. Complex heatmaps reveal patterns and correlations in multidimensional genomic data. *Bioinformatics* **32**, 2847-2849, doi:10.1093/bioinformatics/btw313 (2016).
178 Wang, J. *et al.* Primate-specific endogenous retrovirus-driven transcription defines naive-like stem cells. *Nature* **516**, 405-409, doi:10.1038/nature13804 (2014).
179 Kassem, S. A., Ariel, I., Thornton, P. S., Scheimberg, I. & Glaser, B. Beta-cell proliferation and apoptosis in the developing normal human pancreas and in hyperinsulinism of infancy. *Diabetes* **49**, 1325-1333, doi:10.2337/diabetes.49.8.1325 (2000).
180 Kaminsky, Z. *et al.* DNA methylation and expression of KCNQ3 in bipolar disorder. *Bipolar Disord* **17**, 150-159, doi:10.1111/bdi.12230 (2015).
181 Chouabe, C. *et al.* Properties of KvLQT1 K+ channel mutations in Romano-Ward and Jervell and Lange-Nielsen inherited cardiac arrhythmias. *EMBO J* **16**, 5472-5479, doi:10.1093/emboj/16.17.5472 (1997).
182 Nishimura, M. *et al.* A novel KCNQ1 nonsense variant in the isoform-specific first exon causes both jervell and Lange-Nielsen syndrome 1 and long QT syndrome 1: a case report. *BMC Med Genet* **18**, 66, doi:10.1186/s12881-017-0430-7 (2017).
183 Schonecker, S. *et al.* Long-term culture and functionality of pancreatic islets monitored using microelectrode arrays. *Integr Biol (Camb)* **6**, 540-544, doi:10.1039/c3ib40261d (2014).
184 Schonecker, S. *et al.* Human Islets Exhibit Electrical Activity on Microelectrode Arrays (MEA). *Exp Clin Endocrinol Diabetes* **123**, 296-298, doi:10.1055/s-0035-1547217 (2015).

185 Haythorne, E. *et al.* Diabetes causes marked inhibition of mitochondrial metabolism in pancreatic beta-cells. *Nat Commun* **10**, 2474, doi:10.1038/s41467-019-10189-x (2019).

186 Deconinck, J. F., Potvliege, P. R. & Gepts, W. The ultrasturcture of the human pancreatic islets. I. The islets of adults. *Diabetologia* **7**, 266-282, doi:10.1007/BF01211879 (1971).

187 Lee, H. Y., Jung, H., Jang, I. H., Suh, P. G. & Ryu, S. H. Cdk5 phosphorylates PLD2 to mediate EGF-dependent insulin secretion. *Cell Signal* **20**, 1787-1794, doi:10.1016/j.cellsig.2008.06.009 (2008).

188 Lee, H. Y. *et al.* Epidermal growth factor increases insulin secretion and lowers blood glucose in diabetic mice. *J Cell Mol Med* **12**, 1593-1604, doi:10.1111/j.1582-4934.2007.00169.x (2008).

189 Sladek, F. M., Zhong, W. M., Lai, E. & Darnell, J. E., Jr. Liver-enriched transcription factor HNF-4 is a novel member of the steroid hormone receptor superfamily. *Genes Dev* **4**, 2353-2365, doi:10.1101/gad.4.12b.2353 (1990).

190 Miquerol, L. *et al.* Expression of the L-type pyruvate kinase gene and the hepatocyte nuclear factor 4 transcription factor in exocrine and endocrine pancreas. *J Biol Chem* **269**, 8944-8951 (1994).

191 Twaroski, K. *et al.* FGF2 mediates hepatic progenitor cell formation during human pluripotent stem cell differentiation by inducing the WNT antagonist NKD1. *Genes Dev* **29**, 2463-2474, doi:10.1101/gad.268961.115 (2015).

192 Robertson, R. P., Harmon, J., Tran, P. O., Tanaka, Y. & Takahashi, H. Glucose toxicity in beta-cells: type 2 diabetes, good radicals gone bad, and the glutathione connection. *Diabetes* **52**, 581-587, doi:10.2337/diabetes.52.3.581 (2003).

193 Della Fazia, M. A., Servillo, G. & Sassone-Corsi, P. Cyclic AMP signalling and cellular proliferation: regulation of CREB and CREM. *FEBS Lett* **410**, 22-24, doi:10.1016/s0014-5793(97)00445-6 (1997).

194 Zhang, W. & Liu, H. T. MAPK signal pathways in the regulation of cell proliferation in mammalian cells. *Cell Res* **12**, 9-18, doi:10.1038/sj.cr.7290105 (2002).

195 Broude, E. V. *et al.* p21 (CDKN1A) is a negative regulator of p53 stability. *Cell Cycle* **6**, 1468-1471 (2007).

196 Kawase, T. *et al.* PH domain-only protein PHLDA3 is a p53-regulated repressor of Akt. *Cell* **136**, 535-550, doi:10.1016/j.cell.2008.12.002 (2009).

197 Balboa, D. & Otonkoski, T. Human pluripotent stem cell based islet models for diabetes research. *Best Pract Res Clin Endocrinol Metab* **29**, 899-909, doi:10.1016/j.beem.2015.10.012 (2015).

198 Rouhani, F. *et al.* Genetic background drives transcriptional variation in human induced pluripotent stem cells. *PLoS Genet* **10**, e1004432, doi:10.1371/journal.pgen.1004432 (2014).

199 Polo, J. M. *et al.* Cell type of origin influences the molecular and functional properties of mouse induced pluripotent stem cells. *Nat Biotechnol* **28**, 848-855, doi:10.1038/nbt.1667 (2010).

200 Bar-Nur, O., Russ, H. A., Efrat, S. & Benvenisty, N. Epigenetic memory and preferential lineage-specific differentiation in induced pluripotent stem cells derived from human pancreatic islet beta cells. *Cell Stem Cell* **9**, 17-23, doi:10.1016/j.stem.2011.06.007 (2011).

201 Kim, J., Koo, B. K. & Knoblich, J. A. Human organoids: model systems for human biology and medicine. *Nat Rev Mol Cell Biol* **21**, 571-584, doi:10.1038/s41580-020-0259-3 (2020).

202 Leiter, E. H. Selecting the "right" mouse model for metabolic syndrome and type 2 diabetes research. *Methods Mol Biol* **560**, 1-17, doi:10.1007/978-1-59745-448-3_1 (2009).

203 Hugill, A., Shimomura, K., Ashcroft, F. M. & Cox, R. D. A mutation in KCNJ11 causing human hyperinsulinism (Y12X) results in a glucose-intolerant phenotype in the mouse. *Diabetologia* **53**, 2352-2356, doi:10.1007/s00125-010-1866-x (2010).

204 Sengupta, P. The Laboratory Rat: Relating Its Age With Human's. *Int J Prev Med* **4**, 624-630 (2013).

205 Kohn, L. A., Olson, P. & Cheverud, J. M. Age of epiphyseal closure in tamarins and marmosets. *Am J Primatol* **41**, 129-139, doi:10.1002/(SICI)1098-2345(1997)41:2<129::AID-AJP5>3.0.CO;2-Z (1997).

206 Razumova, I. V. [Improved method for the histological determination of the physiological age of ixodid ticks (Ixodidae)]. *Parazitologiia* **16**, 209-218 (1982).

207 Fujii, M. *et al.* Human Intestinal Organoids Maintain Self-Renewal Capacity and Cellular Diversity in Niche-Inspired Culture Condition. *Cell Stem Cell* **23**, 787-793 e786, doi:10.1016/j.stem.2018.11.016 (2018).

208 Takasato, M. *et al.* Kidney organoids from human iPS cells contain multiple lineages and model human nephrogenesis. *Nature* **526**, 564-568, doi:10.1038/nature15695 (2015).

209 Turco, M. Y. *et al.* Long-term, hormone-responsive organoid cultures of human endometrium in a chemically defined medium. *Nat Cell Biol* **19**, 568-577, doi:10.1038/ncb3516 (2017).

210 Huch, M. & Koo, B. K. Modeling mouse and human development using organoid cultures. *Development* **142**, 3113-3125, doi:10.1242/dev.118570 (2015).

211 Rosengren, A. H. *et al.* Reduced insulin exocytosis in human pancreatic beta-cells with gene variants linked to type 2 diabetes. *Diabetes* **61**, 1726-1733, doi:10.2337/db11-1516 (2012).

212 Yamagata, K. *et al.* Voltage-gated K+ channel KCNQ1 regulates insulin secretion in MIN6 beta-cell line. *Biochem Biophys Res Commun* **407**, 620-625, doi:10.1016/j.bbrc.2011.03.083 (2011).

213 Kuo, C. J. *et al.* A transcriptional hierarchy involved in mammalian cell-type specification. *Nature* **355**, 457-461, doi:10.1038/355457a0 (1992).

214 Gerrish, K., Cissell, M. A. & Stein, R. The role of hepatic nuclear factor 1 alpha and PDX-1 in transcriptional regulation of the pdx-1 gene. *J Biol Chem* **276**, 47775-47784, doi:10.1074/jbc.M109244200 (2001).

215 Murakami, T. *et al.* Critical role for calcium mobilization in activation of the NLRP3 inflammasome. *Proc Natl Acad Sci U S A* **109**, 11282-11287, doi:10.1073/pnas.1117765109 (2012).

216 Rossol, M. *et al.* Extracellular Ca2+ is a danger signal activating the NLRP3 inflammasome through G protein-coupled calcium sensing receptors. *Nat Commun* **3**, 1329, doi:10.1038/ncomms2339 (2012).

217 Davalli, A. M. *et al.* Dihydropyridine-sensitive and -insensitive voltage-operated calcium channels participate in the control of glucose-induced insulin release from human pancreatic beta cells. *J Endocrinol* **150**, 195-203, doi:10.1677/joe.0.1500195 (1996).

218 Sher, E. *et al.* Voltage-operated calcium channel heterogeneity in pancreatic beta cells: physiopathological implications. *J Bioenerg Biomembr* **35**, 687-696, doi:10.1023/b:jobb.0000008032.49504.48 (2003).

7. List of publications

Zhimin Zhou, Maolian Gong, Amit Pande, Anca Margineanu, Bettina Purfürst, Siqi Jia, Chun Zeng, Han Zhu, Maike Sander, Klemens Raile, Zsuzsanna Izsvak. A Critical Role of KCNQ1 in Human β-Cell Development. *(In process)*

hESCs license: Effekt einer spezifischen Mutation im KCNQ1-Gen auf die Entwicklung und Funktion von aus humanen embryonalen Stammzellen abgeleiteten pankreatischen Beta-Zellen. Robert Koch Institut 155, 08.04.2020.

Poster and Abstract: Characterization of genetic defects of KCNQ1 gene in hiPSC differentiated to pancreatic progenitor and β cells models from neonatal diabetic patients. TransCard Ph.D. Retreat. Germany 2016.

8. Declaration of independence

I, Zhimin Zhou, hereby declare that I developed and wrote the present work independently. The present work was carried out from November 2015 to October 2020 under the scientific direction of Dr. Zsuzsanna Izsvák at the Max Delbrück Center for Molecular Medicine in the Helmholtz Association (MDC), Berlin. This dissertation has not yet been published in any other places.

Berlin, December 2020 Zhimin Zhou

9. Appendix

Abbreviations

Alk5i	Alk5 inhibitor
BiPSCs	hiPSCs derived from pancreatic β cells
CaM	Calmodulin
cAMP	3’,5’-cyclic adenosine monophosphate
CHO	Chinese hamster ovary
Cl-Casp3	cleaved caspase-3
CRISPR	clustered regularly interspaced short palindromic repeats
Cas	CRISPR-associated
DE	definitive endoderm
DMRs	methylated regions
DSBs	double-strand breaks
EB	embryoid body
Epac	exchange protein directly activated by cAMP
ER	endoplasmic reticulum
ERG	ether-a-go-go related genes
FGFs	Fibroblast growth factors
FGFRs	fibroblast growth factor reporters
FGFRL1	FGFR-like 1
FPKM	Fragments Per Kilobase of transcript per Million mapped reads
FiPSCs	hiPSCs from fibroblasts
GCK	glucokinase
GCG	glucagon
GDM	gestational diabetes mellitus
GLP-1	glucagon-like peptide 1
GLUT1	glucose transporter 1
GLUT2	Glucose transporter 2
GM12892	human B-lymphocyte
GO	gene ontology
GSIS	glucose-stimulated insulin secretion
GT	primitive gut tube
HDR	homology-directed repair

hESCs	human stem-cells
hiPSCs	human induced pluripotent stem cells
hPSCs	human pluripotent stem cells
HNF4α	Hepatocyte nuclear factor 4 alpha
INS	insulin
IRP	isradipine
KCNQ1^{G292D}	*KCNQ1-G292D* mutation
KCNQ1^{R397W}	*KCNQ1-R397W* mutation
KCNQ1^{R397W}#1/2	*KCNQ1*^{R397W} hESC line1 or 2
KCNQ1$^{-/-}$	KCNQ1 knock out
KCNQ1$^{wt/wt}$/ KCNQ1^{wt}	Wild type KCNQ1
K562	human myelogenous leukemia
KSIS	30mM KCl-stimulated insulin secretion
IFN-α	interferon-alpha
IL-1β	interleukin-1β
MAP-2	Microtubule-associated protein 2
MODY	maturity-onset diabetes of the young
NHEJ	error-prone non-homologous end joining
PBMCs	peripheral blood mononuclear cells
PCG	Polycomb group proteins
PD	pore domain
PDX1	pancreatic duodenal homeobox-1
PE	pancreatic endoderm
PEP	pancreatic endocrine precursors
PF	posterior foregut
PIP2	phosphatidylinositol 4,5-bisphosphate
PKA	protein kinase A
PLC	phospholipase
PND	permanent neonatal diabetes
PP	pancreatic polypeptide
ROS	reactive oxygen species
sgRNA	single-guide RNA
SNPs	single nucleotide polymorphisms
ssDNA	single-stranded DNA

TMM	weighted trimmed mean of M-values
T1D	type 1 diabetes
T2D	type 2 diabetes
TNF-α	tumor necrosis factor-alpha
VSD	voltage sensor domain
UC	unmodified hESCs
WT	Wild type
293B	Chromanol 293B